

Study of an Austrian Lightning Nano-Satellite (LiNSAT): Space and Ground Segments

by

Ghulam Jaffer, M.Sc.

A dissertation submitted to the Dean of Studies of the Faculty of Electrical Engineering and Information Technology at Graz University of Technology,
in partial fulfillment of the requirements for the degree of

Doctor of Engineering Sciences (Dr. Techn.)

Graz, Austria, 2011

Under the advice and review of:

**Univ.-Prof. Dipl.-Ing. Dr.
Otto Koudelka**

Institute of Communication Networks
and Satellite Communications,
Graz University of Technology

Referee:

**Univ.-Prof. Dipl.-Ing. Dr.
Klaus Torkar**

Space Research Institute,
Austrian Academy of Sciences



Statutory Declaration

I declare that I have authored this thesis independently, that I have not used other than the declared sources/resources, and that I have explicitly marked all material which has been quoted either literally or by content from the used sources.

Place

Date

Signature

Ich erkläre an Eides statt, dass ich die vorliegende Arbeit selbstständig verfasst, andere als die angegebenen Quellen/Hilfsmittel nicht benutzt, und die den benutzten Quellen wörtlich und inhaltlich entnommene Stellen als solche kenntlich gemacht habe.

Ort

Datum

Unterschrift

Abstract

The dissertation describes the spacecraft characteristics and the ground infrastructure in support of a future Austrian lightning nano-satellite (LiNSAT) mission. The LiNSAT mission is suggested to fly as a constellation of up to three nearly identical satellites that will carry out long-term observations of electromagnetic lightning signatures using a HF/VHF broadband radio receiver. A lightning flash is electromagnetically an impulsive wideband process, with a typical duration of about one second. It is comprised of several sub-processes with duration of several milliseconds. Each sub-process causes radiation with specific time-domain characteristics, having maxima at different frequencies. Thus, if the radiation is measured only at a single narrow frequency band, it is difficult to identify the sub-processes. Due to this fact, LiNSAT is proposed to carry a broadband RF detector in the frequency range particularly 20 - 40 MHz. Multiple sub-processes radiate in VLF, HF and VHF bands. Two measurement campaigns for artificial and natural lightning were conducted to simulate the capability of the LiNSAT scientific payload to detect and classify Sferics on-board a nano-satellite. The time-domain signal and integrated energy is used for further analysis. The results of the dissertation will help in the development of the LiNSAT mission. The LiNSAT mission will have practical applications in real-time lightning detection and warning systems thus enhancing our understanding in the climate research.

The second part of the dissertation is dedicated to an online ground segment. An Internet-to-orbit gateway is analyzed for future operations with LiNSAT as a reliably working satellite ground station (GS). The GS has been built by the Ecuadorian Space Agency (EXA) and is operated at costs affordable by universities. For ease of maintenance the GS is located at university campus, so interferences from sources in the urban environment were considered. In the

course of this work it was shown that the interference from mobile radio is present but does not hinder or influence the communication with the satellite. Man-made noise corrupts communication with the satellite at very low elevation angles. The GS operates as a virtual GS by authenticated remote users throughout the world via Internet for operating convenience. Since September 2009 the GS is working in remote - user mode and up to now, there were more than 10,000 passes of many satellites over Guayaquil, Ecuador. From all satellite passes with an elevation angle above 0 degree, successful communication was established with a reliability of 99 % data analyzed in real-time. Among many constraints, synchronization losses and port blocking were resolved and an API solution is worked out as a future task to avoid network latency.

Keywords— Nano-Satellite; Lightning Detection; HF/VHF; Payload; Internet-to-Orbit Gateway; Real-time: Virtual Ground Station; Telemetry; Operational Modes.

Kurzfassung

Diese Dissertation beschreibt die Struktur des Satelliten und die Infrastruktur der Bodenstationen eines zukünftigen österreichischen Nano-satelliten zur Erforschung von Blitzen (LiNSAT). Der gleichzeitige Einsatz von drei nahezu identischen Satelliten für die Langzeitbeobachtung der elektromagnetischen Signale von Blitzen mit HF/VHF Breitbandempfängern ist geplant. Ein Blitz ist elektromagnetisch ein impulsiver Breitbandprozess mit einer typischen Dauer von etwa einer Sekunde. Er besteht aus mehreren Teilprozessen mit Zeitspannen von mehreren Millisekunden. Jeder Teilprozess erzeugt eine elektromagnetische Strahlung mit einer typischen Struktur im Zeitbereich und charakteristischen Frequenzen. Die Erkennung von Teilprozessen mit schmalbandigen Messungen ist daher schwierig. Für LiNSAT wird daher ein breitbandiger Detektor im Frequenzbereich von 20 - 40 MHz vorgeschlagen. Die mehrfachen Teilprozesse strahlen im VLF, HF und VHF Frequenzbereich ab. Um die Eigenschaften des geplanten Nano-satelliten zur Erkennung und Klassifizierung von Sferics besser untersuchen zu können, wurden zwei Messkampagnen mit künstlichen und natürlichen Blitzvorgängen durchgeführt. Die gemessene Gesamtenergie und die Signale im Zeitbereich werden für weiterführende Studien verwendet. Die Ergebnisse der Dissertation tragen zur Entwicklung des Nanosatelliten bei. Das LiNSAT Projekt ist relevant für die Echtzeiterkennung und Vorhersage von Blitzvorgängen und kann daher einen wichtigen Beitrag zur Klimaforschung liefern.

Der zweite Teil der Dissertation beschäftigt sich mit dem Online-Bodensegment (ground station, GS). Eine Internet-zu-Umlaufbahn-Schnittstelle wird analysiert mit Hinblick auf Zuverlässigkeit der Bodenstation für zukünftige Operationen mit LiNSAT. Das Bodensegment wurde von der Ecuadorianischen Raumfahrtagentur

(EXA) speziell unter ökonomischen Gesichtspunkten entwickelt, damit verbunden sind erschwinglichen Kosten für Universitäten. Zur einfachen Wartung und Instandhaltung ist die Bodenstation am Universitätscampus angesiedelt, Interferenzen von Störquellen in einer städtischen Umgebung werden berücksichtigt. Im Zuge dieser Arbeit wird gezeigt, dass Störungen von mobilen Sendern vorhanden sind, diese aber die Kommunikation mit dem Satelliten nicht übermäßig hindern oder beeinflussen. Terrestrische Störsignale verschlechtert die Kommunikation mit dem Satelliten erst bei sehr niedrigen Elevationswinkeln. Die GS arbeitet als virtuelle GS durch entfernte, weltweit verstreute und authentifizierte Nutzer mittels Internet zum operativen Vorteil. Seit September 2009 arbeitet die GS erfolgreich in einem Mode für entfernte Nutzer, bis dato mit mehr als 10.000 Überflügen von unterschiedlichen Satelliten über Guayaquil, Ecuador. Für alle Satelliten-Überflüge mit positiven Elevationswinkeln konnte erfolgreiche Kommunikation mit einer Zuverlässigkeit von 99 % und Datenanalyse in Echtzeit durchgeführt werden. Innerhalb der gegebenen Randbedingungen sind Synchronisationsverluste und Port-Blockierungen behoben worden. Eine API Lösung wurde ausgearbeitet als Maßnahme zur Vermeidung von Latenzzeiten im Netzwerk.

Schlüsselworte – Nanosatellit; Messung von Blitzen; HF/VHF; Nutzlast; orbitale Internetverbindung; Echtzeit; virtuelle Bodenstation; Telemetrie; Operationmoden.

To my parents, loving wife and our daughter Masooma

Acknowledgements

At the outset, I would like to express my gratitude to my supervisor Prof. Dr. Otto Koudelka for his support in every thinkable situation and advice during my doctoral research endeavor for the past four years. It is hard to overestimate his contribution this work simply would not exist without him. As my supervisor, he constantly forced me to remain focused on achieving my goal. His observations and comments helped me to establish the overall direction of the research and to move forward with investigation in depth. I could not have imagined having a better advisor and mentor for my Ph.D.

The thesis is jointly supervised by the members of Institute of Communication Networks and Satellite Communications, Graz University of Technology and Space Research Institute, Austrian Academy of Sciences. I would like to express my sincere thanks to Dr. Konrad Schwingenschuh and Hans U. Eichelberger for generously sharing their time and knowledge in this work and facilitating me at Space Research Institute of the Austrian Academy of Sciences.

It is an honor for me to have Prof. Dr. Klaus Torkar as assessor of my dissertation. I am especially grateful for his time, interest, valuable comments and insightful questions.

I would like to show my gratitude to Prof. Stefan Pack for allowing access to High Voltage Lab to conduct RF measurements with artificial lightning discharges.

It gives me great pleasure in acknowledging the support and help of Prof. Erich Leitgeb for accommodating me during my initial days at my university. I am thankful to Manuela Unterberger for providing me technical documents on TUGSat-1/ BRITE and discussing with me developments of the satellite.

I owe my deepest gratitude to Cmdr. Ronnie Nader of Ecuadorian Civilian Space Agency (EXA), Ecuador, who has made available his support in a number of ways, in particular granting me access to the "Hermes-A/Minotaur", the first Internet-to-orbit gateway for satellite communications and awarded me the first diploma on space operations using the ground system.

I am grateful to Dr. Andrew Klesh of University of Michigan, USA, currently at JAXA, for technical discussions.

I would like to thank administrative and technical staffs who have been kind enough to advise and help in their respective roles.

There are lots of people I would like to thank for a huge variety of reasons. I am thankful to my limited but friendly Graz community. Thanks to my new friends here in Graz and to my old friends in Pakistan.

I am forever indebted to my departed parents who raised me with a love of science and supported me in all my pursuits. They have been an inspiration throughout my life. Many thanks to my wife who has always supported my dreams and aspirations and all she has done for me and our daughter Masooma♥.

Finally, I gratefully acknowledge the funding sources that made my Ph.D. work possible especially, Higher Education Commission (HEC) of Pakistan for funding under the project "HEC-Overseas Scholarship Program".

Table of Contents

Statutory Declaration	ii
Abstract	iii
Kurzfassung	v
Acknowledgements	viii
Table of Contents	x
List of Tables	xiii
List of Figures	xiv
Chapter 1	Introduction 1-1
1.1	Aims and Objectives.....1-1
1.2	Original Contributions to This Work.....1-4
1.2.1	Organization of This Dissertation 1-5
Chapter 2	State of the Art.....7
2.1	Introduction.....7
2.2	Lightning Discharges8
2.3	Lightning Detection.....12
2.4	Lightning Geo-Location16
2.5	Lightning Classification.....19
2.6	Lightning Satellites22
2.7	Lightning Detection Scenarios: Cons and Pros.....26
2.8	Chapter Summary.....28
Chapter 3	LiNSAT: Architecture and Design29
3.1	Introduction.....29
3.2	Space Heritage.....35
3.2.1	CASSINI-HUYGENS 35
3.2.2	TUGSat-1/ BRITE 38
3.3	LiNSAT Constellation, Space and Ground Segments40
3.3.1	Space Segment 40
3.3.2	Constellation: Local and Global Coverage 43
3.3.3	Ground Segment 45
3.4	LiNSAT Modes of Operation47
3.4.1	Experiment Modes (EM) 48
3.4.2	Mode Switching 49
3.4.3	Geo-Location 50
3.5	Payload Instrumentation51

3.5.1	Antennas and Gravity Gradient Boom	51
3.5.2	Data Acquisition System (DAQ)	52
3.5.3	Data Processing Unit (DPU)	53
3.5.4	DAQ Trigger and EMI Filtering	54
3.6	Attitude Control System	59
3.7	Chapter Summary	61
Chapter 4	Experimental Results for Space Segment	62
4.1	Introduction	62
4.2	Lightning Detection Simulation.....	63
4.3	Artificial Lightning Measurement Campaigns.....	66
4.3.1	Electrical Discharges in High Voltage Chamber	66
4.3.2	Acoustic Measurements	82
4.4	Natural Lightning Measurement.....	83
4.5	Data Analysis Conclusions.....	86
4.6	Chapter Summary.....	86
Chapter 5	Architecture of Ground Segment.....	88
5.1	Introduction	88
5.2	Hermes I-2-O Gateway	92
5.3	Operational Modes	94
5.4	Hermes: Implementation	95
5.5	Automated Remote TU Graz GS (AR-TUG).....	99
5.6	AR-TUG Implementation	101
5.7	Amateur License Requirement	103
5.8	Chapter Summary.....	104
Chapter 6	Ground Segment Performance Verification.....	106
6.1	Introduction	106
6.1.1	Virtual GS Implementation	107
6.2	Operational Modes: Results	112
6.2.1	Alpha Mode: Data Receiving Only	112
6.2.2	Beta Mode: Data Transceiving	116
6.2.3	Gamma Mode: Voice Transceiving	117
6.2.4	Delta Mode: Weather Satellite Data Receiving	117
6.3	Online Monitoring of Real-Life Events.....	121
6.4	Constraints	124
6.4.1	VRS-RM/Port Blocking/Firewall	125
6.4.2	Network Latency	125
6.5	Chapter Summary.....	127

Chapter 7	Conclusions and Suggestions for Future Work	129
7.1	Conclusions.....	129
7.2	Suggestions for Further Work.....	131
Appendix: Hermes-A: I-2-O Gateway: Remote Client Station Setup Procedures		132
Mode Alpha: Satellite Tracking and AF Receiving.....		133
HRDv5 Radio Engine		133
HRD Radio Console		134
HRD- Sat Track		134
Audio Stream/VRS Remote Monitor		135
Mode Beta: Satellite Tracking And Data Transceiving.....		135
MixWv2.1x (soft-TNC)		136
Skype		137
HRD- Sat Track		137
Web-Interface/Browser		138
Mode Gamma: Satellite Tracking And Voice /Audio 'HDX' Transceiving.....		139
Mode Delta: Weather Satellite Tracking and APT Data Receiving		139
WxtoImg		139
VRS Remote Monitor		140
List of Acronyms		141
List of Publications		151
Bibliography		157

List of Tables

Table 2-1: Lightning facts, typical values and ranges	10
Table 2-2: Summary of strengths and weaknesses of optical and HF/VHF lightning detection from space. Adopted from (Suszcynsky, Kirkland et al. 2000)	16
Table 2-3: Past/ongoing/future worldwide lightning satellite missions	22
Table 2-4: Trade-offs investigations among LEO, GEO and ground-based systems for lightning detection	27
Table 3-1: NOAA 15 orbital pass minutes, peak azimuth, elevation angles and number of contacts per day per ground station	46
Table 3-2: LiNSAT mission operational (MO) modes	47
Table 3-3: LiNSAT experiment modes closely associated with mission operation modes (Table 3-2)	48
Table 3-4: Matlab code to test Adaptive filter algorithm	57
Table 4-1: RF measurements of high voltage discharges (simulated lightning) in the high voltage chamber	67
Table 4-2: Natural lightning: setup and obtained resultant parameters.	85
Table 5-1: Information about all four modes of satellite operations	103

List of Figures

- Figure 2-1: Global distribution of lightning January 1998 – November 2010 from the combined observation of the NASA OTD and LIS instruments to indicate worldwide average lightning strikes per square km per year. Courtesy: NASA TRMM team 9
- Figure 2-2: Streak camera recording of lightning flash and its time resolved luminous features. The figure is not with uniform scale for the purpose of clarity. Adopted from (Uman 2001). 10
- Figure 2-3: Composite spectra of radiation from lightning normalized to 50 km range. The relationship ($1/\text{distance}$) has been used to convert different receiving distances to the lightning range (50 km) and the ($1/\text{bandwidth}$) has been used to convert peak field measurements to spectrum (Equation 2-1). A major problem faced in interpreting spectra is that the data do not represent radiation from single events (e.g. return strokes) but rather represent a collection of events (sub-processes) in the flash, from (Le Vine 1987). 14
- Figure 2-4: Lightning detection and geo-location mechanism using different techniques for cloud-to-ground lightning 17
- Figure 2-5: Schematic of lightning classification. The return stroke of C-G radiation emits strong LF radiations. Leader processes and the recoil streamer in intracloud lightning generate predominately HF/VHF radiations. All discharges emit optical radiation. 20
- Figure 2-6: Electromagnetic fields in lightning associated different channels, Preliminary Breakdown (PB), Leader (L), Return Stroke (R), Changes in (J, F and K). Adopted from (Le Vine 1987) 20
- Figure 2-7: Lightning taxonomy. The figure indicates signatures associated with different types of lightning discharges. Additionally, power profiles can be seen here. Adopted from (Suszcynsky, Kirkland et al. 2000) 21
- Figure 3-1 :(a): Total received power in the AC frequency range up to 11.52 kHz. A mode change happens at 63 km. The mean and standard deviations of the instrument noise level are red and green, respectively. Blue is the low, green the middle, and red the high frequency range. (b): Maximum number of events in the lightning (LI) data, blue is the low, green the middle, and red the high frequency range. An “event” is defined as an LI value 5 dB or more above the maximum instrument noise level determined from cruise checkout data. The maximum noise

	levels for the low frequency range are -43.68 dBV for the first mode and -38.54 dBV for the second. For the middle and high frequency ranges, they are -59.79/-54.47 dBV and -62.05/-56.88 dBV, respectively. The absolute noise in the second mode increases with the bandwidth of the frequency lines.	37
Figure 3-2:	TUGSat-1 ADCS and antennas configuration	39
Figure 3-3:	LiNSAT structure with antenna configuration of three orthogonal lightning antennas (GGB-LA, LA2 and LA3). GGB is a passive attitude control sub-system to nadir direction. Additionally the multi-purpose boom is integrated as lightning antenna.	41
Figure 3-4:	Block diagram of all subsystems of LiNSAT. The science On-board Computer (OBC), Communication and Power subsystems are interfaced to the main OBC. The Attitude stabilization system is passive using the gravity gradient boom.	42
Figure 3-5:	Geographical locations and satellites footprints over three ground stations	46
Figure 3-6:	Block diagram of the LiNSAT scientific payload.	53
Figure 3-7:	DAQ trigger for lightning detector on-board LiNSAT based on adaptive filters.	55
Figure 3-8:	Acoustic signal (serves as proxy of lightning electromagnetic pulse) measured in high voltage chamber and received using Adaptive filter. Top: Measured lightning signal and reconstructed signal ('error signal') are similar. Middle panel: The error signal is nearly the same, therefore, precise residual between the two signals is shown in the middle panel. Bottom panel: The used noise source and the original lightning signal with a correlated noise (drawn from the noise source via a low pass filter). If the AdF technique is not used, shown in the bottom panel, the second tiny stroke (upper panel) is hidden in the noise floor.	58
Figure 3-9:	TIPP event captured with Adaptive filter. The error signal is close to real input, an advantage of using AdF to trigger on-board memory for saving noise-free lightning transients.	59
Figure 4-1:	Matlab simulated results of the program "lightning detector". In this computation, the threshold level for coarse detection was set to 16 mV to extract all pulses above noise floor. Twenty pulses were detected along with their information about pulse start time (in ms), pulse rise/ fall time (in μ s), amplitude (mV), maximum frequency ($*10^6$ Hz).	65
Figure 4-2:	High Voltage Chamber and Control Room. First part of the measurement setup along with Figure 4-4.	70

Figure 4-3: Lightning event occurrence on a model. Also branched lightning (to ground and air) was observed.	71
Figure 4-4: Lightning electric field captured with electric field probe and oscilloscope. The captured image shows similarities with natural lightning signal shown in Figure 4-23 and Figure 4-24	72
Figure 4-5: The striking phenomenon, upward lightning initiated by sharp objects in the vicinity of chamber ground was observed. In principle, this phenomenon occurs with sharp tips of tall buildings like churches etc. It has similarity with the return stroke phenomenon.	72
Figure 4-6: Color changes (intensity) due to discharges along the rope. The variations indicate current interaction with fibers of the rope under impact of a lightning discharge of ~ 1.8 MV. Post-event inspection revealed no damage in the rope, macroscopically.	73
Figure 4-7: The basic structure of the tent serves as a model for the Faraday cage. There can be arcing if some metal is present inside the tent (no lightning safety)	74
Figure 4-8: Lightning event occurs near the object due to slight movement of the electrode.	74
Figure 4-9: The measured electric field due to arcing (impact) of the lightning discharge on the model of Faraday cage (Figure 4-7). Also, round-trip-time of direct and reflected waves indicates many reflections (in the order of ns) from all walls of the chamber. The measured time indicates the inter-walls distance in meters.	75
Figure 4-10: A nearby object struck by lightning. The model was used to determine the minimum distance from the nearby discharge for using the Faraday cage.	75
Figure 4-11: The waveform of an artificial discharge created with Matlab	76
Figure 4-12: The power spectral density (PSD) of the artificial discharge (Figure 4-11) computed with Matlab	76
Figure 4-13: The waveform of an artificial discharge captured with e-Tek oscilloscope and recreated with Matlab	77
Figure 4-14: The power spectral density (PSD) of the artificial discharge (Figure 4-13) computed with Matlab	77
Figure 4-15: High voltage power supply unit (HV-PSU)	78
Figure 4-16: eTek Oscilloscope display of corona discharge. The captured amplitude is ± 1 mV.	79
Figure 4-17: Artificial lightning: indication of corona and glow discharge	80
Figure 4-18: Glow discharge measurement generated with HV-PSU. The maximum corona sound with glow was generated at 11 - 12 kV and was decaying afterwards. The frequency was observed ~ 118 MHz.	80

Figure 4-19: Artificial lightning, spark discharges on cathode. The maximum frequency observed for the spark was 140 MHz. The spark was produced at 13 kV and higher voltages.	81
Figure 4-20: Spark discharge measurement, the maximum frequency observed for Spark is 140 MHz. The spark was produced at 13 KV and higher and was measured on the oscilloscope.	82
Figure 4-21: The broadband discone antenna used for natural lightning measurements. The antenna was put on the roof of the TU Graz building for better reception and to avoid interferences within the campus.	83
Figure 4-22: Radiations patterns of the discone antenna, indicated by the antenna manufacturer (DA-RP 2011).	84
Figure 4-23: Natural lightning measurement with a digital oscilloscope (Bandwidth = 200 MHz), with a sampling rate of 100 kS/s. It shows two individual strokes within a lightning flash.	84
Figure 4-24: Natural lightning measurement with a digital oscilloscope (Bandwidth = 200 MHz) with a sampling rate of 500 MS/s. A single stroke is indicated along with its reflections.	85
Figure 5-1: Hermes, I-2-O gateway, all modes setup at EXA	94
Figure 5-2: Project Hermes command and control center (CMC) Minotaur engine implementation, Courtesy: EXA.	96
Figure 5-3: Minotaur array implementation, Courtesy: EXA.	97
Figure 5-4: Minotaur antenna radiation patterns	98
Figure 5-5: TUGSat-1/ LiNSAT-GS communication bands	100
Figure 5-6: Block diagram of TU Graz GS (AR-TUG). Adopted from (Koudelka, Egger et al. 2009).	101
Figure 5-7: SatPC32 screenshot	102
Figure 6-1: The communications control using Hermes Web Interface to run/stop, antenna polarity selection and on-board IP camera. An important interface for remote users	108
Figure 6-2: A real-time STK simulation while capturing NOAA-17 in mode delta operation. The simulation shows the orbital data.	109
Figure 6-3: The Minotaur Array on-board and external camera view: Important for VGS user to see live tracking	110
Figure 6-4: VGS for Data RX/TX: Hermes Client station implementation.	111
Figure 6-5: 2-Way Voice RX/TX: Client station implementation	111
Figure 6-6: Hermes Delta mode client station. The APT from NOAA is received and relayed to remote users in real-time through Internet	112
Figure 6-7: Alpha mode with Russian satellite RS-30, Yubiliney, tracked and received TLM beacon, (a): a screenshot of HRD-Sat track, (b): HRD-Radio engine as proxy of Kenwood TS 2000 Trx and (c):	

the received and analyzed telemetry beacon with HRD-DM780 in real-time	113
Figure 6-8: Russian satellite Yubiliney (RS-30) received and decoded in real- time	114
Figure 6-9: February 5th, 2010 a near-miss collision between Iridium- 33/COSMOS 34891 debris and the SwissCube occurred. (a), angle between the two orbiting/approaching bodies ~ 0.09 degree (b), objects approaching (c), post-event	115
Figure 6-10: Mode Beta: Compass-1 tracked, commanded with activation codes and housekeeping data was analyzed in real-time	117
Figure 6-11: Enhancements used at virtual GS: (a): Color palette to differentiate cloud, ground, surface etc, (b): Composite image from NOAA 15, 18 and 19 with Thermal enhancement showing regional temperatures (blue to red), (c): 3D anaglyph to get insight cloud structure, (d): Enhancement showing precipitation	119
Figure 6-12: Multi Spectral Analysis (MSA) - with precipitation enhancement showing cloud charging during high thunderstorm activity in Ecuador. With this enhancement, high cold cloud tops are colored to indicate the probability and intensity of precipitation.	120
Figure 6-13: Tungurahua volcanic eruption captured by NOAA 18 using APT on May 28th 2010, processed with WXtoImg using 'hvct' false color enhancement. The same event monitored by GOES 13 satellite, (Courtesy of NOAA).	122
Figure 6-14: Regional temperatures: received images from NOAA-18 and NOAA-19 using Hermes GS and processed at user virtual GS using WXtoImg.	123
Figure 6-15: High temperature variations (up to 30° C) at Andean mountain region observed on May 15 through May 20, 2010. The image was received from NOAA-18 and NOAA-19 using Hermes GS and processed at user VGS. The after effects in the form of glaciers receding were visually observed.	123
Figure 6-16: Images received and analyzed remotely with WxtoImg at user end, June 2010 (a) Twin-storms in the Pacific ocean (b): Tungurahua volcanic eruption	124
Figure 6-17: The round trip time on July 13, 2010 (Graz to Hermes, EXA).	126
Figure 6-18: The current 'traceroute' as per June 14, 2010 (Graz to Hermes, EXA)	127

Chapter 1 Introduction

This chapter introduces the themes of this dissertation and the motivation behind this research work. The defined goals are discussed for the investigation of the project under study along with the problem statement and the main contributions to this work are outlined in this context. The overall dissertation is summarized and finally, an overview of the dissertation is given on a per-chapter basis.

1.1 Aims and Objectives

The world-wide distribution of thunderstorms sustains the fair weather potential difference around 200 – 500 kV close to the surface of the Earth. This field changes significantly the cloud electric field underneath (~ 10 kV/m) and within (~ 100 kV/m) the cloud (Uman 2001). The fair-weather electric current is a leaking current occurring between two spherical plates (ionosphere and the Earth), the atmosphere being a dielectric between the plates. This net downward transport of positive charge occurs in a current between 1,350 to 1,800 amperes over the entire Earth's surface (Rittner 2003). The lightning causes this fair-weather electric current by bringing negative charge to ground (keeping the spherical capacitor charged). If lightning did not occur continuously, the Earth-ionosphere capacitor would lose its current in less than 10 minutes (Rittner 2003). To maintain the fair weather global

electric current flowing to the surface, 1000–2000 thunderstorms must be active at any given time as 1 ampere of current flows into the stratosphere when a typical thunderstorm is active. Although many space missions have flown in the past, the details of all processes are not yet fully understood, demanding further space-based investigations due to the fact that ground-based radio-frequency (RF) measurements of global rates have significant uncertainties and limitations.

Although lightning location, detection efficiency (DE) and accuracy by GS networks is improved, the main difference in them (GS) is the used detection frequency (LF or VHF) and total lightning detection capability (I-C, C-G and/or both). The majority of the systems are private, thus data access to public is restricted.

Further advantages of the space-based detection are:

- No area coverage restriction to only populated areas, so global coverage is possible
- Lightning detection over tropics and oceans
- Not restricted to cloud to ground (C-G) lightning, but also other types including ionospheric lightning can be detected
- Uniform detection characteristics due to homogeneous sensor systems

Scientific (more data availability), economical launching of one or several satellites for a specific life time is economical for sparsely populated areas) and technical (small and compact design) are a few advantages that space-based lightning detection has over GS networks. Also co-ordinated (space-ground) investigations are complementary to achieve high detection efficiency and accuracy.

Figure 2-1 shows a global map of lightning measurements from space. Although

maps like this exist, we need to develop another lightning mission i.e. LiNSAT. The LiNSAT will provide an opportunity for university students to design, develop and test the payload using COTS components. The scientific requirements of the payload to detect and geo-locate the lightning discharges (in particular at higher latitudes, and geographic poles, if any) can be realized with low budget.

In the past, many macro-satellites (Table 2-3) have flown to detect lightning signatures in radio frequency (RF) and optical domains but few micro-satellites have been developed for this purpose. Due to mass, volume and power constraints, nano-satellites have not been launched for lightning detection in recent times. However, using non-space and commercial-off-the-shelf (COTS) components along with well proven sub-systems and a generic nano-satellite bus (GNB) (de Carufel 2009) from predecessor missions, university-class nano-satellites become feasible for such a scientific payload.

Moreover, a ground station (GS) is an equally important element for the success of the planned space mission. The motivation behind the online remote GS is to use it for a variety of satellites and particularly for a constellation of the Austrian lightning nano-satellite (LiNSAT) as a one-node virtual GS to command, control and collect scientific and engineering data autonomously and analyze them in real-time. This approach not only makes the space operation more reliable by minimizing the human error but also reduces the mission cost considerably.

The work has a major emphasis to perform system studies including space and ground segments. The outcomes of the literature review of the previous missions' e.g FORTE, DEMETER helped to extract parameters for testing of the algorithm. The outcomes of the experiments to measure electric discharges in the lab and the field in the course of this dissertation will support the payload design in the development phase. Realization of the flight hardware is out of the scope of this

dissertation. The LiNSAT subsystems e.g. telemetry and power are based on the TUGSat-1/ BRITE developments (Unterberger 2007; Koudelka, Egger et al. 2009)

1.2 Original Contributions to This Work

The most relevant contributions of this PhD dissertation are concentrated on the preliminary study of the present and future space-based detection of lightning, in particular by university-class nano-satellites. The experimental verification of an online Internet-to-orbit (I-2-O) gateway for future missions such as LiNSAT as potential remote GS using current operational satellites is performed. The specific original developments in this dissertation are listed below and detailed along with this document.

1. Review of present and planned nano-satellite missions. A joint revision gives an insight into the evolution of satellite development by using COTS components to reduce mission cost for making university-class nano-satellites more affordable.
2. A detailed investigation is conducted and documented as well in this thesis to identify potential issues with space and ground segments for the LiNSAT mission.
3. Experimental (simulated and experimental) lightning detection evidence for the planned mission.
4. Design and development of model-based software simulation tool as an emulator for the lightning detector on-board LiNSAT.

5. The I-2-O gateway is well studied and tested with download and translation of housekeeping and telemetry data successfully in real-time of more than 10,000 satellites passes over Guayaquil-Ecuador by the author and authorized remote users.
6. Verification of online GS for current and future missions. The issues of sync loss and port blocking are addressed and the development of an application program interface (API) is planned as future task.

1.2.1 Organization of This Dissertation

The remainder of this dissertation is organized as follows:

Chapter 2 reviews the state-of-the-art in the field of space-based detection of lightning on-board macro and microsatellites. An overview of current nano-satellites is given in context to the LiNSAT mission.

Chapter 3 describes the architecture and design of the project LiNSAT under study.

Chapter 4 details the experimental results of terrestrial lightning measurement campaigns for the feasibility study of LiNSAT which is important for the implementation phase of LiNSAT.

Chapter 5 opens the second part of this dissertation by introducing an online I-2-O gateway for current and future satellites working as remote GS. The ground segment is equally important for the success of the mission.

Chapter 6 elaborates the functional capabilities of the remote GS with many examples and results obtained by using current operational Amateur and university nano-satellites in orbit.

Chapter 7 concludes the dissertation by emphasizing on the key points of the work that was carried out. Finally, future work is proposed with particular focus on space and ground segments of LiNSAT.

Chapter 2 State of the Art

2.1 Introduction

Lightning is one of the most powerful natural displays in the world. This chapter discusses the state-of-the-art of space-based detection of lightning on-board small satellites. The investigation serves a number of purposes: firstly, we identify the feasibility of Sferics detection on-board a nano-satellite and secondly we establish terrestrial measurements as emulation for the on-board detector of LiNSAT (Chapter 4). Thirdly, one of the major challenges of using a nano-satellite for such a scientific payload is to integrate the lightning experiment antenna, receiver and data acquisition unit into the small nano-satellite structure. One of the lightning antennas is proposed to be integrated into the gravity gradient boom (GGB) for stabilization.

The limitations, cons and pros of ground-based detection are highlighted; the need to go for space-based detection is evidenced by looking into scientific, economical, technical aspects, offered services and complementary investigations with ground-based detection networks. The LiNSAT will detect lightning in the HF/VHF range. As the LiNSAT is proposed to fly in a constellation of three nano-satellites, the orbital drift and repetition rate of the satellites in orbit will be used for global coverage.

2.2 Lightning Discharges

Lightning is a hazard, and sometimes a killer, as observed with severe storms and lightning strikes. Worldwide thousands of individual lightning discharges including dramatic bolts occur each day. The map in Figure 2-1 shows the geographic distribution of the frequency of strikes averaged over 8 years (1995 - 2003) of data collected by NASA's Optical Transient Detector (OTD) and by the Lightning Imaging Sensor (LIS) on the Tropical Rainfall Measurement Mission (TRMM). As indicated by the figure, the central part of Africa has been an area with the most lightning strikes and almost all of South America is prone to frequent electrical storm activity (NASA 2011a). A different perspective of worldwide statistical lightning distribution is shown in the same figure: it indicates the number of lightning strikes per square km per year.

Lightning is initiated from thunderclouds known as cumulonimbus. A preliminary breakdown takes place with strong electric field. After this process, a stepped leader moves towards Earth. Before it reaches the Earth, an upward leader released from elevated objects on ground closes the electric discharge (lightning) channel. This initiates the return stroke (RS) which transports current of several 10 kA and subsequently, the temperature reaches 30,000 K (Uman 2001). The rapidly expanding heated air also produces tremendous shock waves, which become audible as the sound of thunder. An optically faint stepped leader discharge is followed by a bright return stroke (RS), with a duration of typically $\sim 100 \mu\text{s}$ (Uman 2001). The successive dart leader process and successive return strokes are typically separated by several tens of ms in time. Around 3.5 negative C-G strokes per flash with a total flash duration ~ 0.3 s are observed (Thomson 1980). From the literature, it is concluded that sometimes people misinterpret the stroke duration (\sim

100 μ s) with flash duration (~ 0.3 s). Some reasons may be strong radiation and the fact that only special streak-cameras can resolve single strokes of a multiple stroke flash. The timelines of other associated successive processes are elaborated in Figure 2-2 and Table 2-1. Other types of lightning are shown in Figure 2-7.

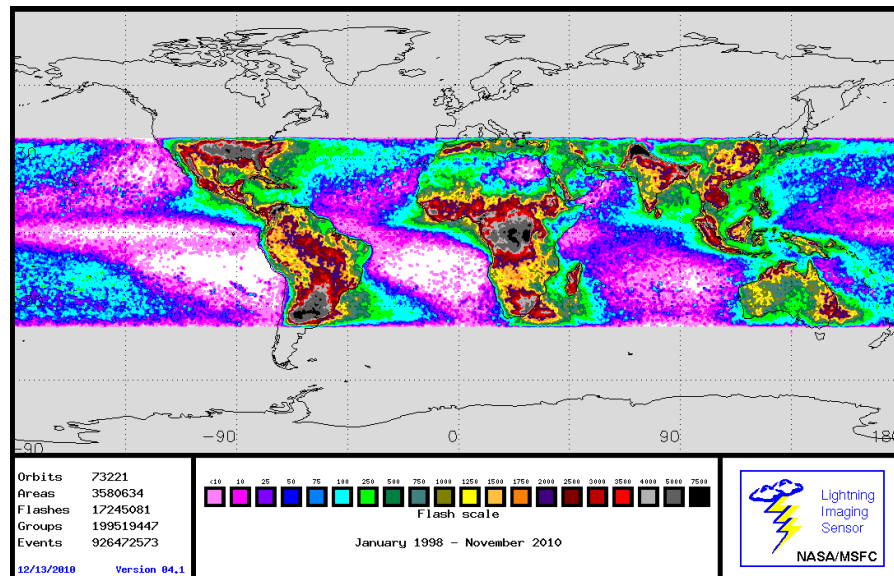


Figure 2-1: Global distribution of lightning January 1998 - November 2010 from the combined observation of the NASA OTD and LIS instruments to indicate worldwide average lightning strikes per square km per year. Courtesy: NASA TRMM team

The main investigation tools and techniques have been photography, spectroscopy, electric and magnetic field and radiation measurements as well as acoustics measurements.

Although the flash and resulting thunder occur at essentially the same time, light travels at 3×10^8 m/s (almost a million times faster than the speed of sound), so obviously a flash can be captured unless obscured by clouds, before the acoustic signal. The classification of lightning is made on the basis of its characteristics and discharge features. Among many types, two major ones are cloud-cloud (I-C) and cloud-ground (C-G) discharges.

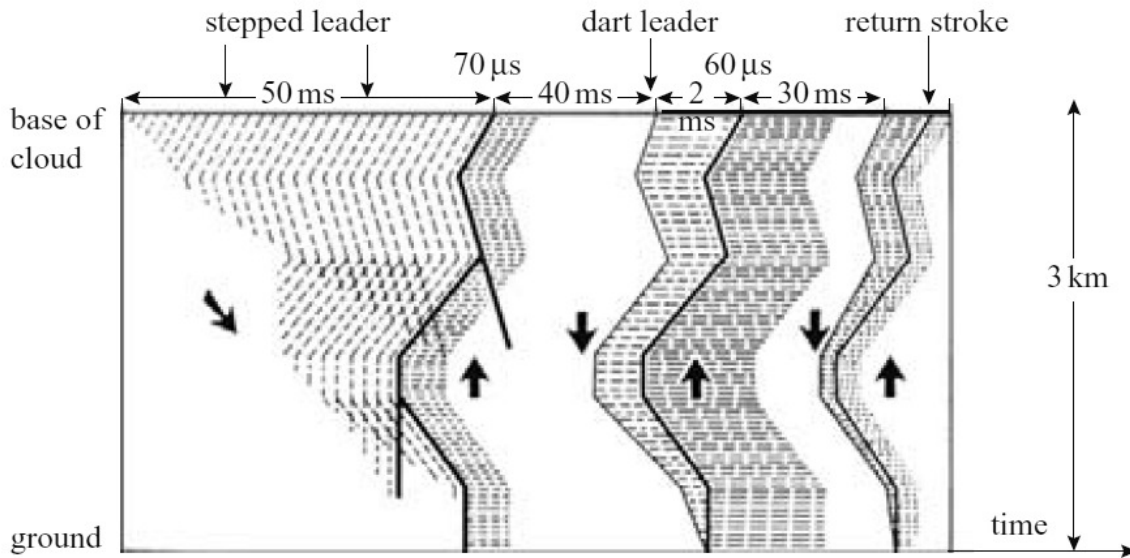


Figure 2-2: Streak camera recording of lightning flash and its time resolved luminous features. The figure is not with uniform scale for the purpose of clarity. Adopted from (Uman 2001).

The Table 2-1 gives data for normal C-G lightning discharges bringing negative charge to Earth. Typical values as well as a range of these values are given. Data were taken from (Rakov and Uman 2003) who in turn obtained the data from a variety of sources.

Table 2-1: Lightning facts, typical values and ranges

	Typical value	Range
Stepped Leader		
Length of step	50 ms	3 - 200 m
Time interval between steps	50 μs	30 - 125 μs
Average velocity of propagation of stepped	150 km/s	100 - 2600 km/s

leader		
Charge deposited on stepped-leader channel	5 C	3 - 20 C
Dart Leader		
Velocity of Propagation	2000 km/s	1000 - 21,000 km/s
Charge deposited on dart-leader channel	1 C	0.2 - 6 C
Return Stroke		
Velocity of propagation	80,000 km/s	20,000 - 160,000 km/s
Current rate of increase	10 kA/ μ s	<1 - >80 kA/ μ s
Time to peak current	2 μ s	<1 - 30 μ s
Peak Current	10-20 A	
Time to half of peak current	40 μ s	10 - 250 μ s
Charge transferred (excluding continuing current)	2.5 C	0.2 - 20 C
Channel Length	5 km	2 - 14 km
Energy dissipated	100 kJ/m	
Lightning Flash		
Number of strokes per flash	3-5	1 - 26
Time interval between strokes	60 ms	3 - 100 ms

Time duration of flash	0.2 s	0.01 - 0.2 s
Charge transferred including continuing current	20 C	3 - 90 C
Energy	10^9 J	$10^9 - 10^{10}$ J

2.3 Lightning Detection

The lightning detection and location is based on the detection of radiation emitted by lightning which is in the form of electromagnetic (RF and optical) radiation and acoustic signals. The radio emissions have transient nature, with a broadband frequency spectrum $\sim 1/f$ (Uman 2001). The thermal radiation of the hot lightning channel produces luminosity lasting up to a few ms. The thunder is generated by shock waves of the expanded hot air.

Lightning detectors receive the electric and/or magnetic components of the radiation field in certain frequency ranges. The frequent bands used most for the detection of lightning are the LF (30 to 300 kHz) and HF/VHF (30 to 300 MHz). The chosen detection frequency (centre and bandwidth) determines the detection range and accuracy. Also the size of the antenna and the sensitivity to the various propagation effects depend on the selected frequency for the lightning detector. LF systems detect the signal from the RS of C-G lightning. The RS is the strongest radio emission (peak at 10 kHz, 100 ms transient) and is generated when the downward leader meets the upward going streamers approximately 100 m above the ground. VHF antennas detect single discharge processes from the stepped leader, recoil streamer and other processes which comprise the inter- and intra-cloud (I-C) lightning. The complete process of the lightning can be visualized by

employing detection and location system in parallel. The ground striking point has to be determined by the data processing.

The detection efficiency (DE) is a function of location of the system and lightning amplitude. The dynamic range of the detector limits the DE of the receiving system. The DE is different for I-C and C-G, also polarity is another limiting factor.

The fact that lightning is a source of interference in amplitude-modulated (AM) radio reception/broadcasting was first shown by (Popov 1896). Radio measurements of lightning were made extensively until the 1960's, although mainly with the purpose of improving radio transmissions (Le Vine 1987) and (Nanevicz, Vance et al. 1987). (Taylor 1973) observed increased radio noise near tornados at 3 MHz, an observation which (Johnson Jr, Hart et al. 1977) extended by studying storm-related radio noise at a wider range of frequencies, from 10 kHz to 74 MHz. (Johnson Jr, Hart et al. 1977) found that noise in the MHz range is the best general indicator of thunderstorm intensity; this is the frequency range that we are considering to use in the on-board lightning detector.

The envelope detector employed in conventional AM radio receivers was used by many researchers to create spectra. In this case, if the input is a single impulse, the spectral amplitude $S(\nu)$ is proportional to the peak value, e_p , of the output. This relationship show that with an ideal band-pass filter of bandwidth B and system gain G , one obtains

$$S(\nu) = e_p/2GB \qquad \qquad \qquad 2-1$$

Data obtained using this technique are shown as the frequency spectra in Figure 2-3. The amplitude of the spectra have been normalized to lightning at 50 km using (1/distance) as the rule for scaling amplitude and (1/bandwidth) as the rule for converting from peak field measurements to spectra when necessary (Equation 2-1) (Le Vine 1987).

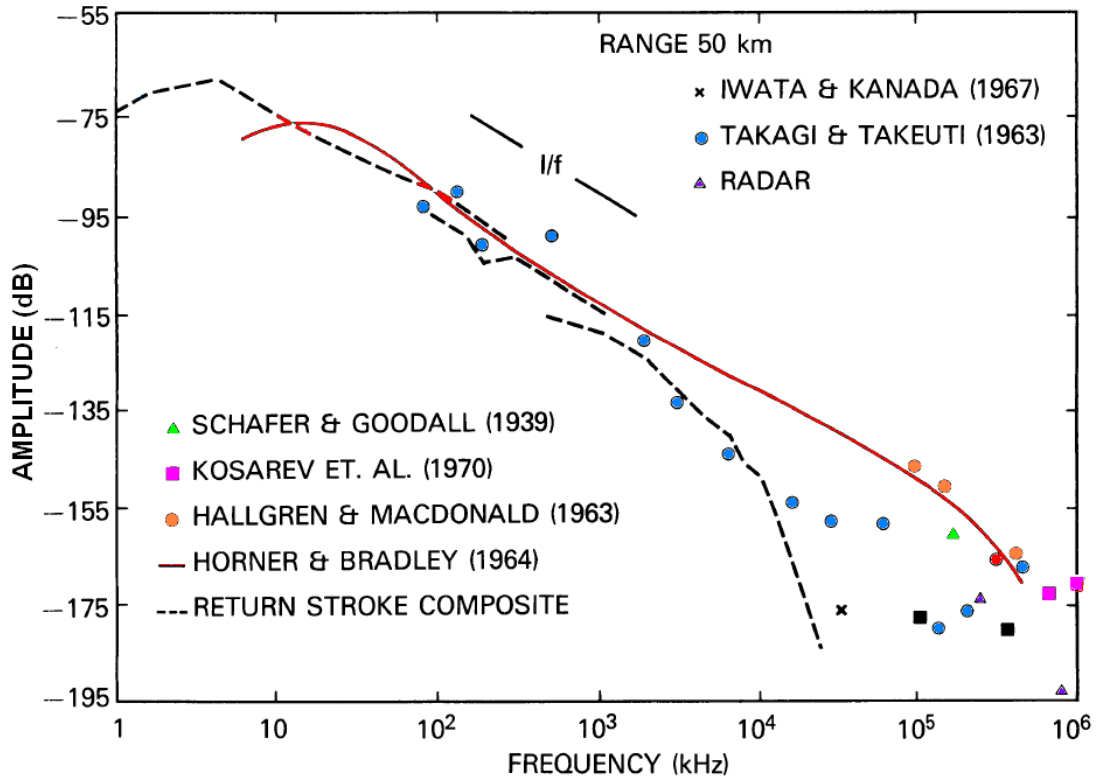


Figure 2-3: Composite spectra of radiation from lightning normalized to 50 km range. The relationship (1/distance) has been used to convert different receiving distances to the lightning range (50 km) and the (1/bandwidth) has been used to convert peak field measurements to spectrum (Equation 2-1). A major problem faced in interpreting spectra is that the data do not represent radiation from single events (e.g. return strokes) but rather represent a collection of events (sub-processes) in the flash, from (Le Vine 1987).

The main advantage of space-based detection of lightning in particular by LEO satellites is the systematic mapping capability of the worldwide lightning distribution based on location (latitude, longitude), seasonal, spatial and temporal variations by the detection in optical and RF domains. The first instrument on-board a LEO satellite, Orbiting Solar Observatory (OSO-2) was reported by (Vorpahl, Sparrow et al. 1970) who used an optical payload to image the lightning flash during midnight, dawn and dusk time only, thus only a fraction of lightning

activity was possible to detect and analyze with a detection efficiency less than 2 %. The main advancement in the optical detection was achieved with the launch of NASA Optical Transient Detector (OTD) on 3 April 1995. As indicated in Table 2-3, OTD detects lightning by looking for a small transient change in the light intensity during both day and night times. (Mackerras, Darveniza et al. 1998) measured lightning variation using C-GR3 (Cloud-Ground Ratio) instruments at sites covering a latitude range from 59.9 degrees N to 27.3 degrees S between 1986 and 1991 inclusive and using satellites, the Defense Meteorological Satellite Program (DMSP) with optical sensors to detect lightning at near local midnight and the Ionospheric Sounding Satellite-b (ISS-b) using RF lightning detection equipment, to obtain the latitudinal variation of total flash density over each major land mass and each major ocean. (Mackerras, Darveniza et al. 1998) estimated the global annual number of total flashes to be 2.05×10^9 /yr, with a mean rate of 65/s. About 54 % of all lightning occurs in the Northern hemisphere. The mean global land total flash density was determined to be about 8.3 /km² yr, about 3.4 times the mean global total flash density over oceans. The LIS on the TRMM satellite unveils an interesting relationship between lightning activity of convective thunderclouds and total amount of cloud volumes: Though TRMM/LIS provides many scientific products; many issues still had to be solved due to the opaqueness of a thundercloud. To overcome this disadvantage Los Alamos science team used VHF observations using the ALEXIS and FORTE satellites. Many scientists conclude that the combination of optical observations and HF/VHF ones is complementary to each other, but the constraints imposed by power, volume, mass and other hinder to achieve all these together on a nano-satellite of 20 cm³ in size and 5 kg of mass with ~ 6 W of power. Some difference between optical and RF detection is elaborated in Table 2-2.

Table 2-2: Summary of strengths and weaknesses of optical and HF/VHF lightning detection from space. Adopted from (Suszcynsky, Kirkland et al. 2000)

	Optical	HF/VHF
Detects:	Light (Current)	RF/HF/VHF (change in current)
Geo-location technique/Required number of satellites:	CCD array/1 Satellite minimum	Time-of-arrival (TOA)/3 satellites minimum
Atmospheric effects:	Scattering/attenuation	Least (Attenuation)
Ionsospheric effects:	No	Frequency dependent dispersion of signal (can be mitigated)
Lightning taxonomy:	Cannot distinguish	Can distinguish C-G vs. I-C, RS, L and TIPP, etc

2.4 Lightning Geo-Location

According to (Cooray 2003a) lightning detection and location systems can be divided into two categories. In the detection systems belonging to the first category the number of lightning flashes striking a given area is obtained without any specific knowledge concerning the actual location of the flashes. Lightning flash counters (LFC) fall into this category. Detection systems that can pin point the point of a strike or the detailed geometry of the lightning channel are the magnetic

direction finding (MDF) systems, time of arrival systems (TOA) and radio interferometric systems (RIM). A detailed review of lightning location system (LLS) was given by (Holle, López et al. 1993) and continued by (MacGorman and Rust 1998).

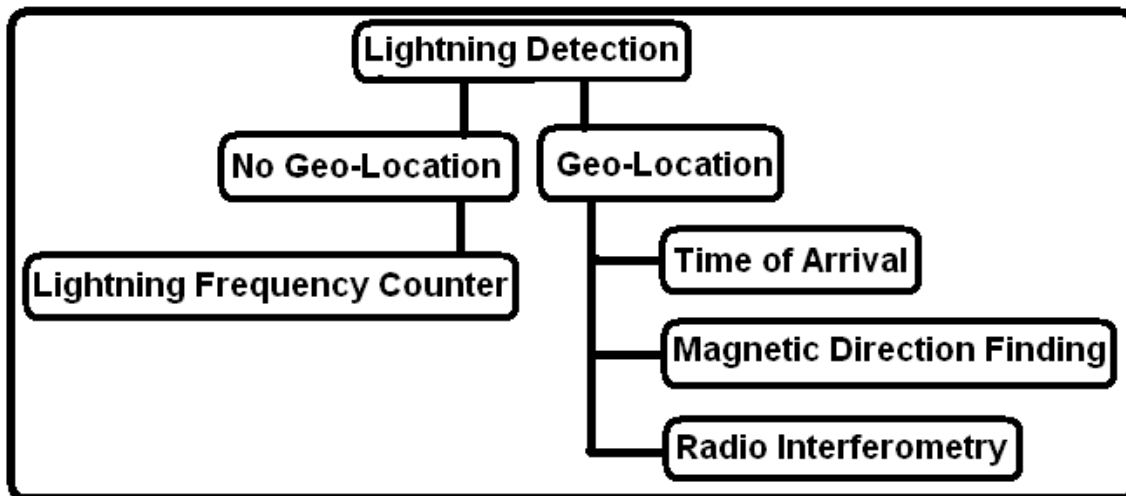
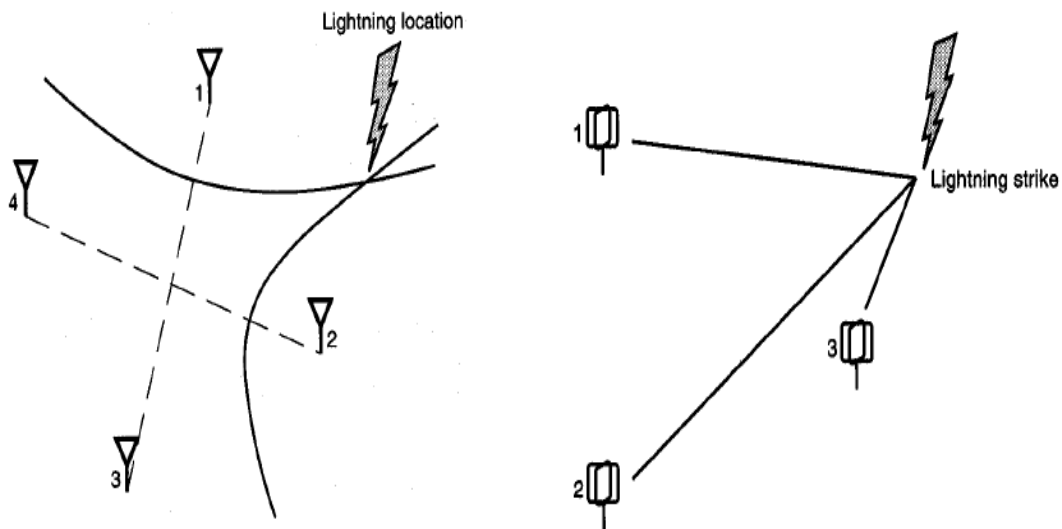


Figure 2-4: Lightning detection and geo-location mechanism using different techniques for cloud-to-ground lightning

An LFC works on a threshold trigger. In order to avoid multiple counts due to subsequent strokes the trigger circuit has a dead time of about one second. In order to achieve a better discrimination between ground and cloud flashes (Anderson, Van Niekerk et al. 1979) developed a counter, called the CIGRE 10 kHz counter, to a frequency response peaked on 10 kHz with a bandwidth of 2.5–50 kHz. The International Council on Large Electric Systems (CIGRE) is an international organization with more than 80 member countries, dedicated to the identification and the development of solutions to technical issues in the power supply sector.

A short rise time in μs can excite systems tuned to the HF/VHF range. When excited by an impulse a receiving system tuned to a central frequency f_0 and bandwidth B generates an oscillating output that decays in a time which is approximately given by $1/B$. If such an antenna system is used to tag the time of

arrival of the impulsive events at several spatially separated satellites the information can be utilized to obtain the location of the discharge events that gave rise to these impulses. The possibility was first suggested by (Oetzel and Pierce 1969). The electrical breakdown process in air gives rise to impulses which can excite systems tuned to HF/VHF, and by mapping the position of a large number of such pulses generated by lightning flashes an image of the lightning flash in three dimensions can be obtained.



Equation 2-2: Schematic for TOA and direction finding. Adopted from (MacGorman and Rust 1998)

VHF RIM was first used for lightning studies by Hayenga and coworkers (Hayenga 1979; Hayenga and Warwick 1981). The technique was further developed and improved by ONERA in France (Richard and Auffray 1985), New Mexico Tech. in USA (Shao 1993; Shao, Krehbiel et al. 1995; Shao, Holden et al. 1996) and Osaka University, Japan (Ushio, Kawasaki et al. 1997). RIM works on measuring the phase difference of the output signal (if lightning is incident on two antennas-system), separated by distance, d , the direction of the incoming wave can

be obtained. The phase difference, φ , of the output signal of the two antennas will be related to the direction of arrival of the wave by:

$$\varphi = 2\pi d \cos \theta / \lambda$$

where λ is the wavelength and θ is the angle between the direction of incidence of the wave and the line joining the two antennas. If the system contains three antennas, one can estimate the azimuth and the elevation of the incoming lightning wave by measuring the phase difference of the output of two independent pairs. In order to obtain a phase measurement it is necessary that the distance between the two antennas or baseline, d , should satisfy the criterion $d/c \leq 1/B$ where c is the speed of light and B is the bandwidth of the antenna system. The central frequency of the antenna system used by the New Mexico group is 274 MHz with a bandwidth of 6 MHz. The system that is in operation in France has a central frequency of 114 MHz with a bandwidth of 1 MHz. The Osaka group utilizes a broadband system having a bandwidth of 10–200 MHz (Cooray 2003a).

2.5 Lightning Classification

Each lightning strike exhibits a unique signature and streak lightning is the most commonly observed in the world. The latter is actually an RS that constitutes the visible part of the lightning stroke. The majority of strokes occur within a cloud (I-C) as indicated by Figure 2-5. Other types are shown in Figure 2-6 and the taxonomy is elaborated in Figure 2-7. The mechanism of a lightning flash is explained by (Cooray, Fernando et al. 2000; Cooray 2003a; Cooray 2003b; Cooray 2007; Cooray 2010).

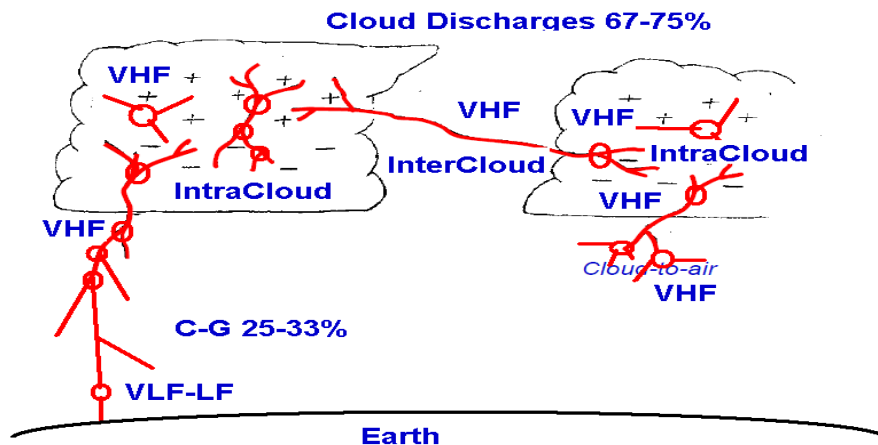


Figure 2-5: Schematic of lightning classification. The return stroke of C-G radiation emits strong LF radiations. Leader processes and the recoil streamer in intracloud lightning generate predominately HF/VHF radiations. All discharges emit optical radiation.

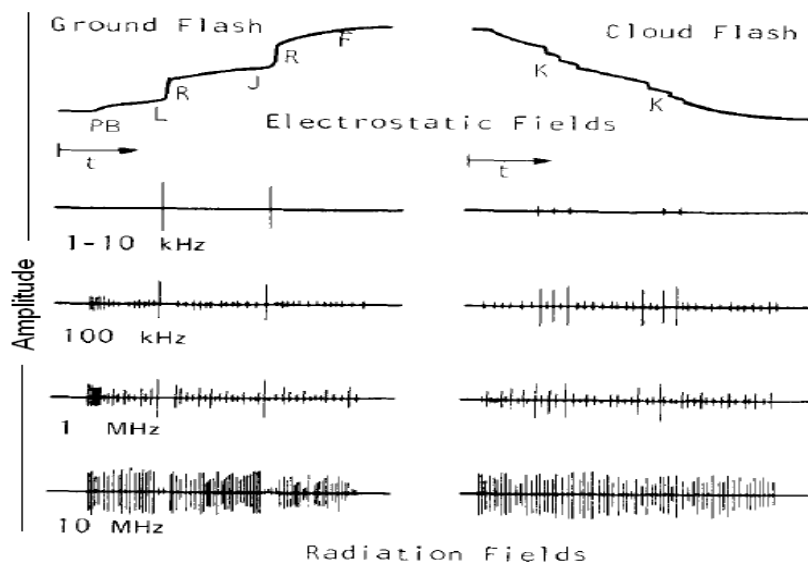


Figure 2-6: Electromagnetic fields in lightning associated different channels, Preliminary Breakdown (PB), Leader (L), Return Stroke (R), Changes in (J, F and K). Adopted from (Le Vine 1987)

Other interesting phenomena in the optical domain are upper atmospheric discharges including elves, jet and sprites.

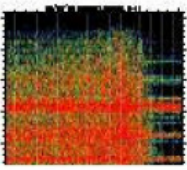
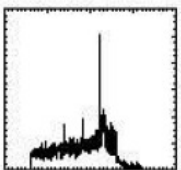
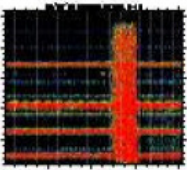
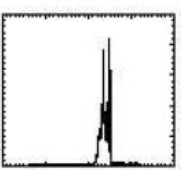
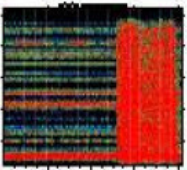
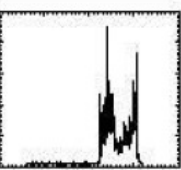
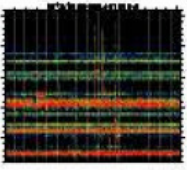
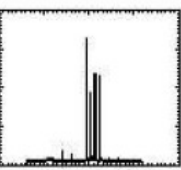
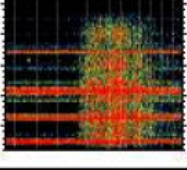
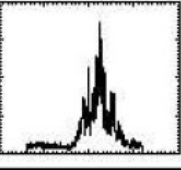
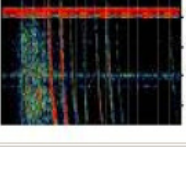
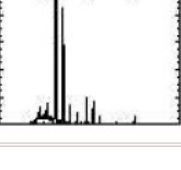
Spectrogram	Power profile	Taxonomy	Features
		1st -RS w/ stepped leader	width > 400 μ S, steady increase, impulse at attachment
		Subseq. -RS w/ dart leader	10 μ S < wid. < 500 μ S sharp fall, impulse at attachment
		1st +RS	10 μ S < wid. < 500 μ S sharp rise, impulse at attachment
		Impulsive in-cloud events, including TIPPS	1 μ S < width < 10 μ S strong
		Non-impulsive in-cloud events including K-events	10 μ S < wid. < 500 μ S slow rise/fall
		Mixed impulsive and non-impulsive in-cloud events	Mixed of impulsive and non-impulsive features

Figure 2-7: Lightning taxonomy. The figure indicates signatures associated with different types of lightning discharges. Additionally, power profiles can be seen here. Adopted from (Suszcynsky, Kirkland et al. 2000)

2.6 Lightning Satellites

The following table provides an overview of space-based lightning detection missions.

Table 2-3: Past/ongoing/future worldwide lightning satellite missions

Satellite	OSO-2/1970/USA	DMSP/1977/USA
Orbit, Altitude, FOV		Alt: 830km, 60° N, 60° S
Payload	Optical	12 PDD each FOV 700*700km ²
Resolutions	S: 100 km	S: 100 km
Detection Efficiency/Error	Detection efficiency < 2 %,	
Constraints	Only night-time detection, Can't distinguish cloud vs. ground discharges	Only 2 % lightning detected within FOV
Results	Total flash density (I-C, C-G), Lightning ratio in geographic locations and seasons	Global distribution of lightning (monthly maps) between 60° N and 60° S. Land to Ocean lightning ratio 5.3 to 10 (7.7 average). Global flash rate, 30/s: 123/s at dusk and 96/s at midnight
Annotations	(Vorpahl, Sparrow et al. 1970; Christian and Latham 1998)	(Turman 1978; Elvidge, Baugh et al. 1997; Mackerras, Darveniza et al. 1998; Beasley and Edgar 2004; Huang and Burke 2004)

ISS-b/ Japan/ 1978	LMS(GEO)/NASA/1990	OTD-Microlab-1, (OV-1)/NASA/1995
	36000 km	735 km, incl. 70° near-polar orbit
RF: 2.5, 5, 10, 25 MHz	CCD	CCD 128*128 pixel, FOV: 100°, 1300*1300km ² ,
	S: 10 km, T: 1 ms	S: 10km, T: 2ms, Detection efficiency: 56-69 %
		Spatial error: 20-40 km, Temporal error < 100 ms
		Can't distinguish C-G vs. I-C, Can't detect lightning discharges confined within 7 km altitude, data averaging (55 to 110 days) require diurnal lightning-cycle bias
Global lightning frequency in N-Hemisphere: 64/s (Spring) and 55/s (Fall) and 54/s (Winter)	Detection efficiency 90 %, Can distinguish I-C and C-G	Total (C-G, I-C), No discrimination
(Miyazaki, Sagawa et al. 1980; Kotaki, Kuriki et al. 1981; Kotaki, Kuriki et al. 1981; Matura, Kotaki et al. 1981; Kotaki and Katoh 1983)	(Christian, Blakeslee et al. 1989; Christian and Latham 1998; Weber, Laboratory et al. 1998; Finke and Kreyer 2002; Christian 2010)	(Boccippio, Koshak et al. 2000; Christian, Blakeslee et al. 2003; Koshak 2010)

LIS-TIRMM/NASA/1997	Alexis/ LANL-USA/ 1993	FORTE/ LANL-USA/ 1997
600*600 km ² , incl: 35°, 350 km		
Optical	VHF (30-300 MHz)	VHF 26-300 MHz, Ant. Aperture: 80°, Optical (PDD)
S: 10 km (~storm), DE: 82%, speed 7 km/s,		22 MHz, (26-48 MHz, 118-140 MHz), Sampling Rate: 50 MHz, Sensitivity 1mV/m/MHz
Error: +-5/s	RF noise corrupted observations/triggering constraints	
Global flash rate: 45/s, Total (C-G, I-C), No discrimination	High-energy, narrow-pulse VHF emissions, TTPs by CID, HF emissions observed on ground. 1 st pulse is in-cloud 2 nd is ground-reflected trace observed at satellite.	TTP, CID, I-C, RF-Optical coincident observations revealed that the light observed by RS is produced in cloud. FORTE-NLDN correlated observations for positive discharges and in-cloud activity associated with ground discharges, I-C Vs. C-G
(Kummerow, Barnes et al. 1998; Ushio, Heckman et al. 2001; Petersen, Nesbitt et al. 2002; Cecil, Goodman et al. 2005; Takayabu 2006; Yokoyama and Takayabu 2008)	(Holden, Munson et al. 1995; Massey and Holden 1995; Russell, Zuelsdorf et al. 1998)	(Jacobson, Knox et al. 1999; Suszcymsky, Kirkland et al. 2000; Roussel-Dupre, Jacobson et al. 2001; Suszcymsky, Light et al. 2001; Tierney, Jacobson et al. 2001; Davis, Suszcymsky et al. 2002; Light and Jacobson 2002; Shao and Jacobson 2002; Jacobson and Light 2003; Lehtinen, Gorham et al. 2004; Burr, Jacobson et al. 2005)

CASSINI-HUYGENS/NASA-ESA/1997	DEMETER/CNES-France/2004	ORAGES/ONERA France/2006
		700 km, incl: 13°
LF-MF	LF-MF	VHF-UHF interferometry as LIS at 200 MHz
		Intense observation of tropics
Lightning on Titan?		
(Molina-Cuberos, Lopez-Moreno et al. 2001; Matson, Lebreton et al. 2004; Molina-Cuberos, Porti et al. 2004; Matson, Lebreton et al. 2005; Coustenis 2006; Ramirez 2006; Lange 2008; Coustenis and Hirtzig 2009)	(Inan, Piddychiy et al. 2007; Parrot, Inan et al. 2008); (Berthelier, Godefroy et al. 2006; Platno, Inan et al. 2006; Inan, Piddychiy et al. 2007; Berthelier, Malingre et al. 2008; Parrot, Berthelier et al. 2008; Parrot, Inan et al. 2008; Parrot, Inan et al. 2009; Fiser, Chum et al. 2010)	(Bondiou-Clergerie, Lalande et al. 2004)

TARANIS/CNES	SwissCube/ Switzerland/ 2009	Maido-1 (Sohla-I)/Japan/ 2009
VHF	Optical	RF, RIM
	Tumbling/High rotation rate	
	Air Glow	
(Blanc, Lefeuvre et al. 2007; Lefeuvre, Blanc et al. 2008; Lefeuvre, Blanc et al. 2009)	(Borgeaud, Scheidegger et al. 2010; SwissCube 2011)	(Morimoto, Kikuchi et al. 2009; Kikuchi, Morimoto et al. 2010)

2.7 Lightning Detection Scenarios: Cons and Pros

Up to now geostationary Earth orbiting (GEO) satellites are restricted to optical detection of lightning; this detection capability is limited by opaqueness of

tropospheric layers and clouds (to differentiate I-C vs. C-G). The signal to noise ratio (SNR) is always high for the satellites in low Earth orbit (LEO). Both optical and RF detection is possible with 1 satellite in polar orbit and with revisit/ repetition and orbital drift for global coverage. The main energy generated by lightning is in the RF range and not in the optical spectrum. The latency is a few ms and lower power requirements, smaller antennas and lower free space loss make the LEO orbit more affordable for scientific investigations. Trade-offs among many factors in LEO, GEO and ground-based detection systems are elaborated in Table 2-4.

Table 2-4: Trade-offs investigations among LEO, GEO and ground-based systems for lightning detection

	GEO	LEO	Ground based
Power	High	Low	N/A
Mass	High	Low	N/A
Cost	High	Low	High
Attitude Control	High	Low (GGB)	N/A
Life Time	High	Low	High
Orbital Coverage	24 hrs, 3 Satellites required for global coverage (no polar regions)	10-15 min*4 (ground contacts) ~ max. 1 hr. contact time per day per satellite per GS, Global (Polar)	Over continents
Ground Antenna	Fixed	Tracking	Fixed
Method	Optical, (RF)	Optical and RF	RF, (Optical, and Acoustic)

Services Exist	Yes	No	Yes
Free Data Access Policy	Yes	No, (LiNSAT-Yes)	No
Direction Finding	No	Yes	Yes
Detection Efficiency, Certainty, Quality,	Table 2-3	Table 2-3	
Sensitivity	Low	High	High
Communication Latency	High (~ 125 ms)	Low (~ 1-5 ms)	Low
Antenna/Sensor complexity	High	Low	High

2.8 Chapter Summary

In this chapter, the state-of-the-art infrastructure of space-based detection of lightning on-board satellites was reviewed that would help significantly during the analysis and design phase of the future mission. The work carried out served a number of purposes for the feasibility study of LiNSAT. Firstly, to find out the relevant payloads (RF and optical) on-board these missions and to extract the outcomes that would help in designing a future mission like LiNSAT. Secondly, lightning taxonomy will help to determine basic parameters for the lightning detector on-board LiNSAT.

Chapter 3 LiNSAT: Architecture and Design

3.1 Introduction

This chapter presents the architecture of a lightning detector on-board LiNSAT in low-Earth-orbit (LEO). The orbit altitude range imposes some constraints on the system. The altitude defines the eclipse and duration time that influences the capacity of recharging the batteries and the duration of their usage. Another disadvantage to scientific investigations with low altitude is less area coverage on ground. At an altitude of ~ 800 km, orbital velocity ~ 8 km/s, and an orbital time is around 90 minutes. The LiNSAT is proposed to be launched in a three satellites constellation for the purpose of time-of-arrival (TOA) (Betz, Schumann et al. 2008) technique to geo-locate the lightning transients.

Our main scientific objective is to investigate lightning events by the observation of HF/VHF electromagnetic signals (Sferics) and to derive the signatures of lightning. One of the important parameters is the lightning flash rate, which can be used as a proxy for locating severe weather activity. Another objective is to discriminate the discharges of lightning events evaluated by the inherent features and to

differentiate cloud discharges (I-C; intercloud and Intracloud) from ground discharges (C-G; cloud-to-ground), return strokes (RS), leaders (L) and trans-ionospheric pulse pairs (TIPP). The discrimination is important because the ratio of the two (I-C/C-G) is a good indicator of convective storm development (Williams, Weber et al. 1989). The TIPP always occur in pulse-pairs. The first pulse is received directly on the satellite and the second one is reflected from the ground and received on satellite with a time delay of 50 – 60 μ s. By using this time delay, the cloud height can be determined.

Other scientific objectives of the planned LiNSAT are the investigation of impulsive electromagnetic signals generated by electrical discharges in terrestrial thunderstorms (lightning), blizzards, volcanic eruptions (McNutt and Williams 2010; Zlotnicki, Li et al. 2010), Earthquakes (Zlotnicki, Li et al. 2010) and dust devils. These electromagnetic phenomena called Sferics cover the frequency range from a few Hertz (Schumann resonances) up to several GHz. Depending on the source mechanism, the wave power peaks at different frequencies, e.g. terrestrial lightning has a maximum power in the VLF and HF range, also TIPPs reaching at LEO and possibly to satellites in GEO peak at VHF. The LiNSAT will be able to discriminate among many discharges if LiNSAT is in the event mode (Table 3-3) by temporal resolution, polarization and unique TIPP characteristics. The TIPP event always occurs as a pair of pulses, the first pulse is directly received at satellite and the second one is reflected from the ground surface. Also, the resulting mixture appears in survey mode (Table 3-3) but with 3 nano-satellites constellation, a coarse location determination can be achieved. The global terrestrial lightning rate is in the order of 50 lightning flashes per second with an average energy per flash of about 10^9 Joule (Rakov and Uman 2003). Only a small percentage of the total energy is converted to electromagnetic radiation. Other forms are acoustic (thunder), optical and thermal, so the whole power of lightning flash is distributed

into many chunks of energies. The signal received by a satellite radio experiment depends on the distance and the energy of a lightning stroke as well as on the orientation of the discharge channel.

Initially the algorithm for the instruments on-board electronics has been developed and verified in Matlab (Mathworks 2011). With the algorithm, the blocks of the lightning receiving chain are simulated individually and as a whole using Matlab functions. To verify the simulations, lab measurements (RF and acoustic) are performed (Chapter 4). The objective of these measurements/ simulations was to find an algorithm which could be implemented on the on-board lightning detector electronics. The requirement is that it must be fast, effective and running with limited resources.

Two terrestrial measurement campaigns were conducted; one for artificial lightning produced in high voltage chambers and the second one for natural lightning recorded in urban environments. We focus mainly on the received time series including noisy features and narrowband carriers to extract characteristic parameters. The chamber inter-walls distance was determined by considering reflections in the first measurements. The results are of great significance for LiNSAT as to determine cloud height and to perform experiments like TIPP reception on-board LiNSAT. The results of these measurements are elaborated in Chapter 4.

The next consideration is to use existing lightning data from the French mission DEMETER (Berthelie, Godefroy et al. 2006; Platino, Inan et al. 2006; Inan, Piddyachiy et al. 2007; Berthelie, Malingre et al. 2008; Parrot, Berthelie et al. 2008; Parrot, Inan et al. 2008; Parrot, Inan et al. 2009; Fiser, Chum et al. 2010) to validate the accomplished results.

The on-board lightning detector has to perform tasks like determination of pulse-width, pulse-count, pulse rise/fall time etc; we get noise possibly from narrowband carriers and artifacts from satellite itself, i.e. electromagnetic interference (EMI) in addition to the lightning signal. Additionally, the HF/VHF band is congested with broadcasting carriers throughout the world. As a contrast to lightning, the carriers are narrow-band, thus easy to distinguish during data analysis. The model will work in experiment modes for the detection of lightning events by employing preset criteria. After successful detection of lightning transients, data will be dumped in available memory for future download. The post-processing on ground will be done to whiten, de-chirp and classify the signals in time and frequency domains.

The LiNSAT is a proposed project for the detection of Sferics in very high frequency (VHF) range in LEO around 800 km. A possible LEO range is $\sim 600 - 1000$ km altitude, and the orbit is selected, 1) in compliance with the TUGSat-1 orbit, 2) as trade off among various parameters i.e. coverage, sensitivity, free space loss. The satellite is a 20 cm^3 in size and weighs ~ 5 kg. During the 2 years mission phase, the nano-satellite project under study could provide the statistics of the spatial and temporal distribution of lightning, but the two parameters cannot be derived simultaneously. The geographical (tropics, land, ocean etc) and seasonal variations of lightning are statistically investigated. In contrast to optical satellite observations the Sferics (electromagnetic signatures produced by lightning strokes) produced by lightning can be observed on the day and night side but with a smaller spatial resolution. The FORTE satellite mission (Jacobson, Knox et al. 1999) found that at an altitude of about 1000 km the impulsive events produced by lightning can reach amplitudes up to 1 mV/m in a 1 MHz band around 40 MHz .

The LiNSAT is based on the design and the bus similar to the Austrian first astronomical nano-satellite TUGSat-1/BRITE-Austria (Unterberger 2008;

Koudelka, Egger et al. 2009) which is scheduled to be launched in summer/ fall 2011. The LiNSAT will carry a broadband radio-frequency receiver payload for the investigation of Sferics. Special emphasis is on the investigation of transient electromagnetic waves in the frequency range of 20 - 40 MHz. The on-board RF lightning triggering system is a special capability of the LiNSAT. The lightning experiment will also observe signals of spacecraft, ionospheric and magnetospheric origin. To avoid false signals detection (false alarm), pre-selectors on-board LiNSAT are part of the Sferics detector. Adaptive filters are formulated and tested using artificial and natural lightning discharges. The filters will be developed in design phase to differentiate terrestrial electromagnetic impulsive signals from ionospheric or magnetospheric signals. The details can be found in (Section 3.5.4).

One of the major challenges of using a nano-satellite for such a scientific payload is to integrate the lightning experiment antenna, receiver and data acquisition unit into the small nano-satellite structure. The optimization in this mission is to use one of the lightning antennas integrated into the gravity gradient boom (GGB) for stabilization of the satellite. The sections 3.3.1 and 3.4 describe the space segment and modes of operation. EMC issues are specially treated. Results of the payload in a simulated environment are presented in Chapter 4.

The lightning emissions are the transient electrical activity of thunderstorms (primarily RS and I-C activity) generating broadband electromagnetic radiation with a spectrum range from ULF to UHF and also visible-light. A typical RS radiation peaks at ~10 kHz, and an I-C stroke produces radiation peaking at a slightly higher frequency at 40 kHz with 2 orders of magnitude less energy than a typical RS (Volland 1995). Electromagnetic radiations at these frequencies propagate through the Earth - ionosphere waveguide, thus can be observed at large distances, thousands of km from the source.

The lightning electromagnetic pulse (LEMP) is a time-varying electromagnetic field that varies rapidly for 10 ns, reaches its maximum and then on its descending way is less fast (\sim a few tens of μ s) and decays to a negligible value. The LEMP is very hazardous due to its ability to damage unprotected electronic devices. LEMPs are powerful radio emissions that radiate across a broad spectrum of frequencies from tens of kHz or lower to at least several hundred MHz as indicated by the inverse of LEMP rise time. For this reason, the payload on-board LiNSAT will be designed as a broadband (20 - 40 MHz) receiver.

LiNSAT will operate in the HF/VHF portion of the electromagnetic spectrum because lower frequency radio emissions (HF and below) often cannot penetrate through the Earth's ionosphere and thus, do not reach LEO. Also, Sferics in higher bands of VHF are less powerful, thus, more difficult to detect. Broadband VHF signals from LEO, if present, complicate the detection and time tagging by the dispersive and refractive effects of the ionosphere. These effects become increasingly severe at lower frequencies in proportion to wavelength squared.

The LiNSAT radio receiver will record waveforms using a fixed-rate 200 MS/s (over-sampling), 12-bit digitizer that takes its inputs from 3-antennas (sub-resonant monopoles) to receive the LiNSAT artifacts (Figure 3-6). The instrument utilizes a coarse trigger based on preset amplitude level and fine triggering to detect transient events.

The radio emissions from natural lightning produce transients which are broadband emissions in the HF/VHF spectrum, a potential source of false alarms for space-based detection of other phenomena in the same band. One of the main challenges of the LiNSAT payload development on-board a LEO nano-satellite is the need to characterize the Earth's radio background. The characterization is necessary for both transient signals, like those produced by lightning and

continuous wave (CW) signals, like those emitted by commercial broadcasting radio and television stations.

Even if a receiver is well-matched to the detection of broadband transients, CW signals can still degrade its sensitivity when many, powerful carriers exist within its bandwidth. Extensive experiments have been performed by the detection of natural and artificial lightning discharges in urban environment to visualize and verify the detectability of transient signals by LiNSAT payload in carrier-dominated radio environments and is discussed by (Jaffer, Koudelka et al. 2008; Jaffer, Koudelka et al. 2010a; Jaffer 2011a; Jaffer and Koudelka 2011b; Jaffer, Koudelka et al. 2011c). These authors showed that terrestrial lightning measurement campaigns are necessary for the LiNSAT hardware developments and to test and verify the algorithm for software improvement.

3.2 Space Heritage

3.2.1 CASSINI-HUYGENS

The LiNSAT research team in Graz is experienced in conducting field and particle experiments for planetary and interplanetary missions (Schwingenschuh, G. J. Molina-Cuberos et al. 2001). A milestone was the participation in an electric field experiment aboard ESA's HUYGENS mission, which for the first time explored the atmosphere of the Saturnian moon Titan. After a 7 years cruise to the Saturnian system and two close Titan encounters NASA's CASSINI orbiter released the HUYGENS probe on 25 December 2004. On 14 January 2005 the atmosphere of Titan was first detected by the HUYGENS Atmospheric Structure Instrument

(HASI) accelerometers at an altitude of about 1500 km. About 5 minutes later at an altitude of 155 km the main parachute was deployed and the probe started to transmit data of the fully operational payload. About 2.5 h later the probe landed near the equator of Titan and continued to collect data for about one hour.

The orbit of the HUYGENS probe has been reconstructed using the data of the entry phase and of the descent under the parachute. The electric field sensor of HASI carried out measurements during the descent (2 hours and 27 minutes) and on the surface (32 minutes). About 3200 spectra in two frequency ranges from DC - 100 Hz and from DC - 11 kHz were collected. The major emphasis of the data analysis is on the detection of electric and acoustic phenomena related to lightning (Fulchignoni, Ferri et al. 2005; Schwingenschuh, Besser et al. 2007), (Schwingenschuh 2006; Schwingenschuh, Hofe et al. 2006; Schwingenschuh, Besser et al. 2007; Schwingenschuh, Lichtenegger et al. 2008b; Schwingenschuh, Tokano et al. 2010).

Three methods are used to identify lightning in the atmosphere of Titan:

- Measurements of the low frequency electric field fluctuations produced by lightning strokes
- Detection of resonance frequencies on the Titan surface - ionosphere cavity
- Determination of the DC fair weather field of the global circuitry driven by lightning

Several impulsive events have been detected by the HASI lightning channel. The events were found to be similar to terrestrial Sferics and are most likely produced by lightning. Large convective clouds have been observed near the South Pole during the summer season and lightning generated low frequency electromagnetic waves can easily propagate by ionospheric reflection to the equatorial region.

The existence of lightning would also be consistent with the detection of signals in the Schumann range and a very small fair weather field, but there is yet no confirmation by the CASSINI orbiter. Figure 3-1 (Schwingenschuh, Lichtenegger et al. 2008b; Schwingenschuh, Tokano et al. 2010) shows some experimental results from CASSINI-HUYGENS.

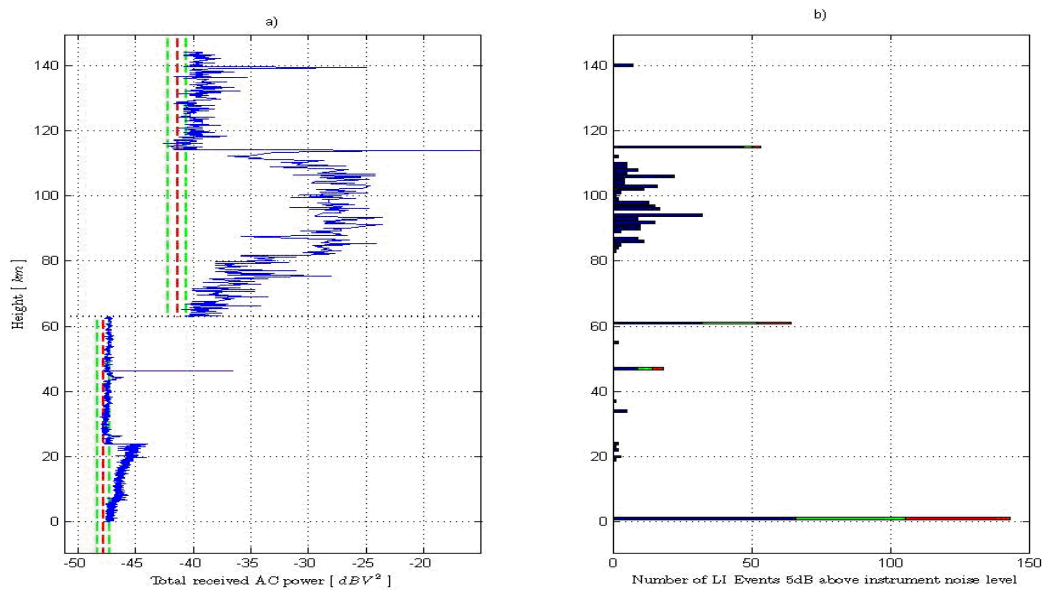


Figure 3-1 (a): Total received power in the AC frequency range up to 11.52 kHz. A mode change happens at 63 km. The mean and standard deviations of the instrument noise level are red and green, respectively. Blue is the low, green the middle, and red the high frequency range. **(b):** Maximum number of events in the lightning (LI) data, blue is the low, green the middle, and red the high frequency range. An “event” is defined as an LI value 5 dB or more above the maximum instrument noise level determined from cruise checkout data. The maximum noise levels for the low frequency range are -43.68 dBV for the first mode and -38.54 dBV for the second. For the middle and high frequency ranges, they are -59.79/-54.47 dBV and -62.05/-56.88 dBV, respectively. The absolute noise in the second mode increases with the bandwidth of the frequency lines.

Only spectral information of the electric field (no waveforms) is transmitted to Earth based on on-board signal processing (Falkner 1999; Hofe 2005). The fast

Fourier transform (FFT) was performed using an on-board signal processor. No triggering scheme was part of the mission. Contrary to the HUYGENS VLF lightning detector, the LiNSAT radio receiver is planned to operate in the HF/VHF range in order to avoid attenuation and signal distortion by the terrestrial ionosphere.

3.2.2 TUGSat-1/ BRITE

The predecessor of LiNSAT is the first Austrian nano-satellite TUGSat-1/BRITE-Austria, being developed by the Graz University of Technology with University of Vienna, Vienna University of Technology and the Space Flight Laboratory of University of Toronto (Canada) as partners. The scientific objective is the investigation of the brightness variation of massive luminous stars of magnitude +3.5. The satellite has a size of 20 cm cube with a mass of about 6 kg and carries a differential photometer as the science instrument. It will fly in a sun-synchronous orbit.

Figure 3-2 shows a mock-up of the satellite. Power is generated by multiple body-mounted strings of triple-junction solar cells. The available power is about 6 W on average. Energy is stored in a 5.3 Ah Lithium-Ion battery. The power subsystem has been designed for direct energy transfer.

A novelty is an advanced attitude determination and control system (ADCS) with three very small momentum wheels and a Star Tracker providing a pointing accuracy at the arc-minute level. Three on-board computers are installed in the spacecraft, one for housekeeping and telemetry, one for the science instrument and one for the ADCS.

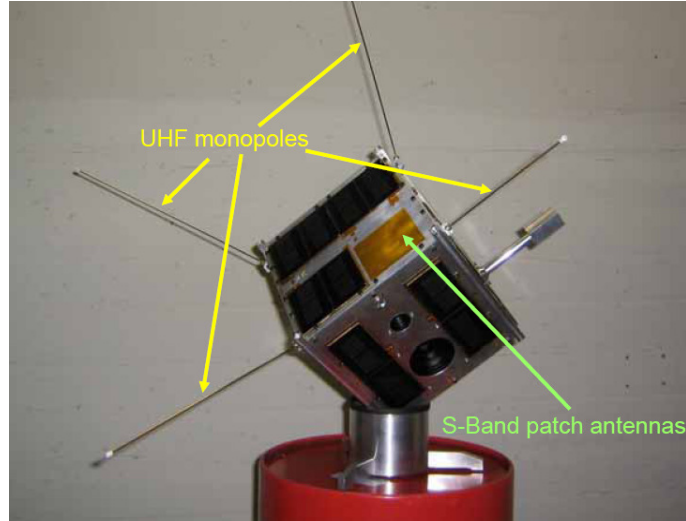


Figure 3-2: TUGSat-1 ADCS and antennas configuration

The telemetry system comprises an S-band transmitter of about 0.5 W. It is capable of transmitting data with a minimum rate of 32 kbit/s. Data rates of up to 512 kbit/s are feasible with existing GSs. The uplink is in the UHF band (437.365 MHz) with 4 kbps speed. A beacon in the VHF band is also implemented (Koudelka, Egger et al. 2009).

Other objectives of TUGSat-1 and LiNSAT are the training of students, hands-on experience in conducting of a challenging space project and synergies between several scientific fields. The investigation of massive luminous stars with a precise star camera opens up new dimension for astronomers as observation of stars without interference by Earth atmosphere can be carried out in LEO with such a small and low-cost spacecraft. Moreover, LiNSAT is a pure student satellite and will contribute in the lightning investigations as a low-cost atmospheric research platform.

3.3 LiNSAT Constellation, Space and Ground Segments

3.3.1 Space Segment

The space segment consists of a constellation of three identical nano-satellites and each satellite is comprised of the following units

- Attitude control through gravity gradient boom (GGB):
- Three orthogonal lightning antennas (GGB-LA, LA2, LA3), one antenna (GGB-LA) is integrated into GGB at nadir direction, Figure 3-3.
- Power subsystem (Solar panels, battery charge and discharge regulator (BCDR) and battery).
- Thermal subsystem
- HF/VHF electronics
- Data processing unit (DPU)
- On-board event detector together with adaptive filtering
- Housekeeping
- Communication UHF/VHF monopole antenna (U-MP/V-MP): 2m and 70 cm frequency bands and S-band patch antenna
- Global Positioning System (GPS)

Other associated sub-systems are mechanical and thermal which are detailed in (TUGSat-1 2011)

All subsystems are shown in Figure 3-4. The components selection criteria for on-board memory, telemetry volume, and power budget are the “cost effectiveness”. Therefore, COTS components will be used.

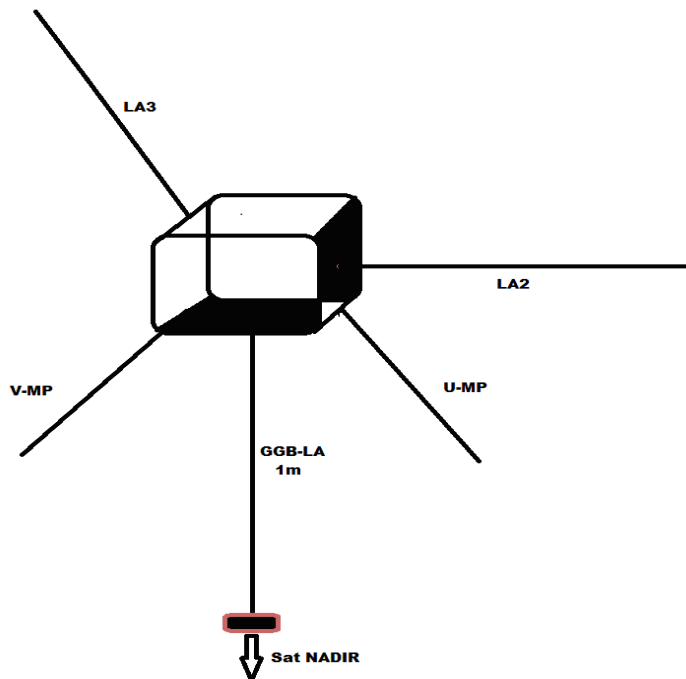


Figure 3-3: LiNSAT structure with antenna configuration of three orthogonal lightning antennas (GGB-LA, LA2 and LA3). GGB is a passive attitude control sub-system to nadir direction. Additionally the multi-purpose boom is integrated as lightning antenna.

The telemetry is based on studies of the TUGSat-1 (Unterberger 2007; Unterberger 2008; Koudelka, Egger et al. 2009). As a heritage from TUGSat-1, the same Generic Nano-satellite Bus (GNB) will be used on LiNSAT with data rate from 32 - 256 kbps. Data volume per day will be ~ 45 MB/GS. For LiNSAT, the actual amount of data is mode-dependent (Table 3-3). The optimum data volume ~ 135 MB/day (3

GS) with 256 kbps data rate is estimated and the on-board commercial solid state memory is available with capacity ~ 500 MB.

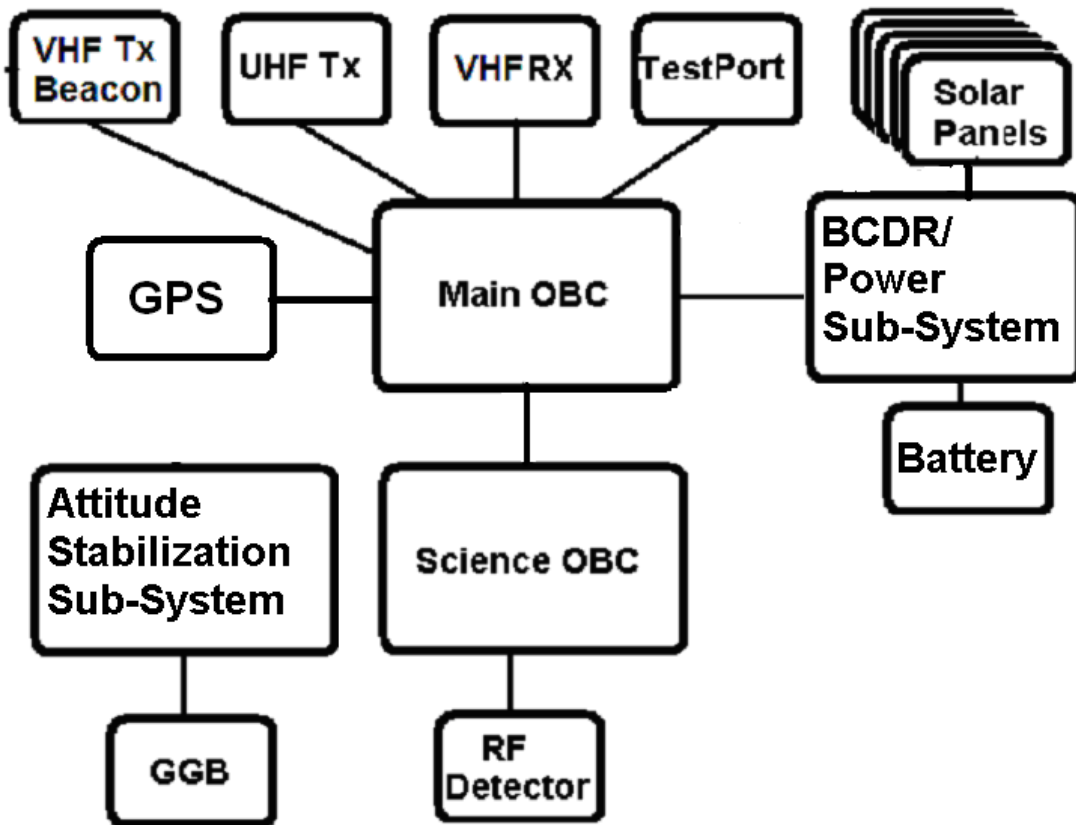


Figure 3-4: Block diagram of all subsystems of LiNSAT. The science On-board Computer (OBC), Communication and Power subsystems are interfaced to the main OBC. The Attitude stabilization system is passive using the gravity gradient boom.

A possible issue can be a single event upset (SEU), caused by a cosmic ray or proton that can change a state in the memory. These are "soft" errors" and can be mitigated by a reset or rewriting of the device for the normal behaviour thereafter. Based on studies done by the SPOT team (Barillot and Calvel 2002), around 8 events upset per year occur in LEO 800 km orbit. The LiNSAT will use commercial memory as contrast to radiation hardened one by the SPOT mission. The nano-satellite will encounter roughly the same number of events. Countermeasures for the memory are necessary and the cold redundancy is considered. An algorithm

for bit flip error correction is an integrated function in a commercial memory. The mechanism uses error detection and correction (EDAC) in order to ensure data reliability. As the current consumption is increased, this may lead to a permanent burn-out. A current limiter is foreseen to reset the experiment and the sub-systems on-board LiNSAT. If the reset is required from one of the three GS, then a data loss of one to two orbits (max. 3 hours) is estimated.

3.3.2 Constellation: Local and Global Coverage

The LiNSAT will be launched in polar orbit due to the requirement of its scientific payload for lightning detection at higher latitudes especially lightning associated with blizzards on poles (if any), ionospheric lightning and trans-ionospheric pulse pairs (TIPPs). Another advantage of the polar orbit is that on-board instruments can be calibrated at the poles due to least/no background noise. Other requirements are

- global lightning detection
- geo-location of the lightning events with time of arrival (TOA) technique
- lightning differentiation (types: bipolar: cloud-ground, intercloud, intracloud and ionospheric discharges (Figure 2-7))

During the commissioning phase, the satellites must be as close as possible in trailing formation for co-incident detection of lightning using angle separations in contrast to time separations. At this stage, there will be no geo-location experiment performed. In the second phase, when the satellites have got enough inter-satellites distances (a few degrees), TOA technique would be used for geo-location. A triangular configuration would be the optimum to measure the direction of the

Sferics for the geo-location purpose. Triangulation will work if all three satellites are located within the field of view (FOV) of the lightning event with maximum 60° separation between the satellites for coincidence mapping of the event. If the angle is higher, the TOA technique cannot be used for geo-location by using triangulation. The spatial resolution depends on the size of the triangular configuration and the accuracy of this triangle can be determined with an accuracy of several km depending on the time synchronization of the satellites. With the Global Positioning System (GPS) accuracy of μs , the spatial resolution would be a few m to 100's of m. In the third phase (approaching end of life (EOL)), the satellites will be used as independent entities (LiNSAT).

To establish a continuous global lightning service, out of this LiNSAT scientific mission, further nano-satellites can be injected into orbit to build a swarm configuration. The failure of one satellite will cause loss of TOA information to geo-locate the event, but one satellite is enough to detect global lightning activity.

In order to determine the time of occurrence and location (latitude, longitude), at least three satellites are required. Knowing the location of the three satellites and measuring the TOA of the Sferics, one can calculate the lightning time of occurrence and geographical latitude and longitude. The satellites are allowed to drift apart later in the mission, but the natural drift (irregularities of the gravitational field, moon, atmospheric drag, etc) limit the life time of the constellation. Moreover, the satellites injection accuracy during the commissioning phase is of crucial importance to have a triangular constellation by using specific mechanism of a dispenser system to have longer time of geo-location experiments during mission life.

3.3.3 Ground Segment

The global coverage emphasizes on the main purpose of ground segment as the distributed GS network (DGSN) to track the satellite and receive housekeeping and scientific data on different geographic locations. DGSN consists of three GS

- Automated remote GS at TU Graz, Austria (AR-TUG) (Jaffer and Koudelka 2011d)
- I-2-O gateway (Hermes-A) in Ecuador (Nader, Carrion et al. 2010a; Jaffer, Klesh et al. 2010c; Jaffer, Nader et al. 2010d)
- One proposed GS at Lahore, Pakistan (LiNSAT-GS)

The first two GS are already functional and the third is proposed and we will pursue its development in near future. Geographical locations and footprints of three satellites over these GS can be found in Figure 3-5.

As indicated in Table 3-1, the satellites in polar orbit have 3 – 4 contacts with GS per day, so a data volume ~ 45 MB/day/GS will be downloaded from the LiNSAT.

From the scientific data reception point of view, the DGSN opens up the mission to a wider range. Therefore, the DGSN would eventually make a difference as compared by the amount of data collected with a single GS. Moreover, the transformation of the DGSN as an autonomously operating network is foreseen. This would ultimately support future nano-satellite experiments effectively. Additionally, its scheduling capability which we pursue in near future will enhance its functionalities. The I-2-O gateway and virtual GS are detailed in Chapter 5 and Chapter 6.

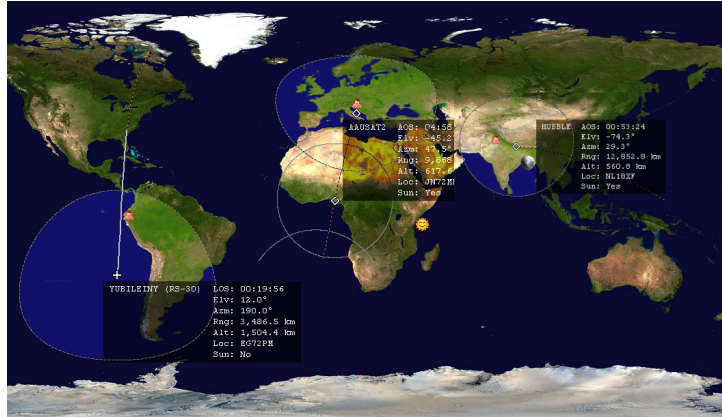


Figure 3-5: Geographical locations and satellites footprints over three ground stations

Table 3-1: NOAA 15 orbital pass minutes, peak azimuth, elevation angles and number of contacts per day per ground station

Date	AOS	LOS	Duration	Peak AZ	Peak EL
10.03.2011	12:12:11	12:23:06	00:10:55	282.6°	8.3°
10.03.2011	21:29:48	21:40:29	00:10:41	77.7°	8.0°
10.03.2011	23:06:58	23:22:31	00:15:33	257.6°	56.0°
11.03.2011	10:06:37	10:21:31	00:14:54	103.9°	29.1
11.03.2011	11:46:50	12:00:31	00:13:41	282.2°	18.1°
11.03.2011	21:09:02	21:13:23	00:04:21	77.3°	1.0°
11.03.2011	22:42:53	22:58:37	00:15:44	80.2°	75.0°
12.03.2011	00:25:48	00:34:41	00:08:53	255.4°	4.9°
12.03.2011	09:43:33	09:56:40	00:13:07	103.8°	15.1°
12.03.2011	1:22:05	1:37:17	00:15:12	282.9°	34.6°
12.03.2011	22:19:11	22:34:20	00:15:09	77.6°	37.7°

3.4 LiNSAT Modes of Operation

LiNSAT provides several mission modes (MO) of operation after successful deployment (Table 3-2). The LiNSAT is planned to perform functions in various modes depending upon task/idle situations.

Table 3-2: LiNSAT mission operational (MO) modes

MO No.	Tasks, Annotation
1	Deployment, <i>Commissioning phase</i>
2	Stabilization, <i>Commissioning phase</i>
3	Lightning Experiment, <i>Scientific Payload</i>
4	Ground Communication, <i>Telemetry</i>
5	Conserve Power/Recharge, <i>in Eclipse</i>
6	Standby

Modes 1 and 2 apply to initial deployment and stabilization of LiNSAT. Mode 3 is the key mode with five experiment mode options (section 3.4.1). Switching to mode 4 occurs for telemetry operations. Mode 5 is applicable when the power subsystem is no longer capable to support normal operations e.g. during eclipse. Mode 6 is the default mode when no other operations are going on. Either telemetry or the lightning experiment will be carried out at a time for efficient use of on-board power.

3.4.1 Experiment Modes (EM)

The scientific payload on-board LiNSAT will perform the detection of lightning events, the measurement of time series, and the data transmission is done by a sub-system to one of the GS within communication window. The sub-categories of the experiment mode, the data transmitted to ground and memory estimation are elaborated in Table 3-3.

The format of the time information from the LiNSAT OBC is a counter with resolution of 1 μ s. To determine the size of the buffer to store the satellite clock time information, first we determine total time in 1 day i.e. 8.64×10^{10} μ s. As the GPS has a clock accuracy of ~ 1 μ s and the events of interest (lightning) have typical duration of ~ 100 μ s. To determine number of bits required to save the time information, we know that to store 2 points, we need 1 bit of memory. So, the time information for one day with μ s accuracy will require ($2^{36.33} = 8.6 \times 10^{10} = 36.33$ bits) ~ 5 bytes. Similarly a memory requirement for other experiment modes can be calculated as follows.

Table 3-3: LiNSAT experiment modes closely associated with mission operation modes (Table 3-2)

Experiment Mode	Tasks, Annotation	Information transmitted	Memory requirement
Survey Mode (Default Mode)	Statistical; Number of lightning events above threshold level (coarse trigger)	Time of the event	5 bytes/event (5 M Events) ~ 25 MB = 10 %
Enhanced Survey Mode	Total power above threshold level	Spectral information	7 bytes/event (5 M events) ~ 35 MB = 10 %
Event Mode	Atmospheric	Waveforms	0.5 MB/event (50

	electromagnetic (Sferics)	(0.1ms - 1 ms)	events) ~ 25 MB
Background/ CW Mode	All events/signals, galactic, interference detected from ionosphere between two lightning events	Spectral information once per orbit	5 % of 45 MB = 2.25 MB =
EMC Mode	Artifacts from satellite itself	Spectral info./ events	2% of 45 MB ~ 1 MB
SGC mode	Co-ordinated LiNSAT and WWLN for total lightning (C-G, I-C) detection	Campaign basis, Events/ Spectral info.	90 % of the memory
Test Mode	Testing of the lightning experiment and the satellite sub-systems	Automatically	1 % of 45 MB, the memory, (occasionally)
Housekeeping Mode	Voltage, temperature, power, EMC etc	Continuously	1 % of 45 MB

3.4.2 Mode Switching

The modes are selected due to geographical location and seasonal variations. Experiment modes are either autonomous or commanded from ground by time, geographical locations, and seasonal information. The basic mode for the LiNSAT is the 'survey mode', but scheduling can be done as required. The LiNSAT gets a time table for the mode transitions. The correlation with latitude is determined on ground. The total download capacity per GS is up to 45 MB by using 256 kb/s data rate and 3 contacts per day. The survey mode is permanently active consuming up to 25 MB/day (~ 5 million events) for obtaining statistics of the worldwide lightning activity. The enhanced mode will be active in lightning activity area (e.g.

Tropics). The major lightning activity area lies within $\pm 65^\circ$ latitude. The Background/CW Mode will detect spectral information of broadcasting carriers and transmit the information once per day. The broadcasting carriers may generate a locally limited interference. By sending the information once per day will help in whiten the lightning data. The data of the EMC mode are produced by the lightning detector too as a correlated noise in the channel. The co-ordinated space-ground mode (CSG) will be performed during special campaigns. The mode will be commanded from ground and special software patches can be uploaded too. The test mode will be used during the commissioning phase and at certain times during mission life. The housekeeping data are transmitted during ground contacts to monitor the health status of the satellite.

3.4.3 Geo-Location

The GPS has an accuracy of at least $1 \mu\text{s}$. Using the TOA information at all 3 satellites, the direction of the lightning occurrence can be inferred. Therefore, if we have same time of occurrence on all 3 satellites in the same FOV, then the lightning event is geo-located (at the centre point between the 3 satellites) above the surface of Earth in terms of latitude, longitude. The altitude of the lightning can be determined together with a ground-based detection network. Lightning as an electromagnetic wave travels with the speed of light ($3 \cdot 10^8 \text{ km/s} \Rightarrow 1 \text{ km} = 3 \mu\text{s} \Rightarrow 1 \mu\text{s} = 333\text{m}$) and with $1 \mu\text{s}$ accuracy of GPS for space applications, the lightning event can be located with a spatial resolution restricted by inter-satellites separation (maximum 60° from the centre of Earth, if two satellites are at horizons and the third one lie within FOV of lightning event) and the accuracy imposed by the GPS system ($\sim 1 \mu\text{s}$). All three satellites must be synchronized with GPS clock and updated frequently for precise geo-location experiments. Also, satellite orbital

elements that in turn feed the satellite tracking program in the form of two line elements (TLE) by NASA NORAD might have some uncertainty in the determination of the exact orbital location that must be considered. As an example, the SwissCube near-miss event with Iridium debris was monitored using one of the GS, Hermes and the inter-distance of the two objects was found to be 1 km in LEO (Section 6.2.1.3). The LiNSAT constellation can help in geo-locating the lightning event if the coincidence mapping is done by the all three satellites within these limitations. Also, by the detection of a TIPP event, the cloud height ($\sim \frac{1}{2}[50 \mu\text{s} * 3*10^5 \text{ km/s}] = 15/2 \text{ km} = 7.5 \text{ km}$) is estimated. As stated earlier, the TIPP occurs in pairs. The first pulse is received directly on the satellite and the second one is reflected from the Earth surface. The time delay between the two is found to be 50 - 150 μs by the ALEXIS and the FORTE missions. The event is helpful to determine the height of the cumulonimbus cloud. The important parameter, namely the time of lightning event can be possibly determined with the 3-satellites constellation using differential TOA. The absolute time of the flash can be compared on all 3 satellites for temporal investigations.

3.5 Payload Instrumentation

3.5.1 Antennas and Gravity Gradient Boom

The voltage V , received at LiNSAT

$$\mathbf{V} = \mathbf{h}_{\text{eff}} * \mathbf{E} \tag{3-1}$$

depends on the lightning electrical field E and the effective length h_{eff} of the antenna. Also,

$h_{\text{eff}} \sim hm/2$ for $h_m \ll \lambda$, where h_m is the mechanical length of the antenna and λ the wavelength.

As no stringent pointing requirements for LiNSAT are foreseen as compared with TUGSat-1, so a simple and inexpensive gravity gradient stabilization (GGS) technique already proven on many missions (ATS 2011) and detailed in (Wertz 1978; Wertz and Larson 1999) which points to the nadir of the satellites is envisaged for satellite attitude control. The GGB is selected due to its economical features like least power consumption (once during deployment) and its low cost. The GGB rod acting as an antenna for lightning detection is deployable with 10 % of the satellite mass (tip mass). In-orbit characteristics depend on several factors, e.g., mechanical forces, non-conservative forces and induced pendulum motions. The boom torque needs to overcome the environmental torque for a maximized stabilization capability. The antenna works in non-resonant mode so the lightning investigation is performed in the same frequency ranges but with reduced efficiency.

3.5.2 Data Acquisition System (DAQ)

As stated earlier, the typical length of a lightning flash is 100 μs . To capture this transient signal at least 1 ms (including pre- and post-trigger) data is required. A low power ADC is selected with sampling rate of 200 MS/s so the transient signal can be reconstructed well for signature analysis. The time of 1 sample with this sampling rate is 5 ns. The ADC has 12 bit resolution. Therefore 1 ms stroke data needs memory to be 400 kB (~ 0.5 MB). The lightning annual flash rate is 50 - 70 flashes per second (high latitudes to equator) that becomes on the average, 5 million flashes a day (2 million flashes on the average with high latitudes). The data acquisition system (DAQ) is capable of retriggering a new record within a few

microseconds of the end of the previous record. Data of many lightning events will be stored in a cyclic memory. The memory is capable to be overwritten all the times. A significant number of events can be stored in a solid-state mass memory before downloading via telemetry to the ground segment. The Sferics data will be identified with their pulse width and sharply rising amplitude with pulse rise time. The records will then be analyzed on ground to investigate HF/VHF signatures in time and frequency domains. The payload configuration is shown in Figure 3-6.

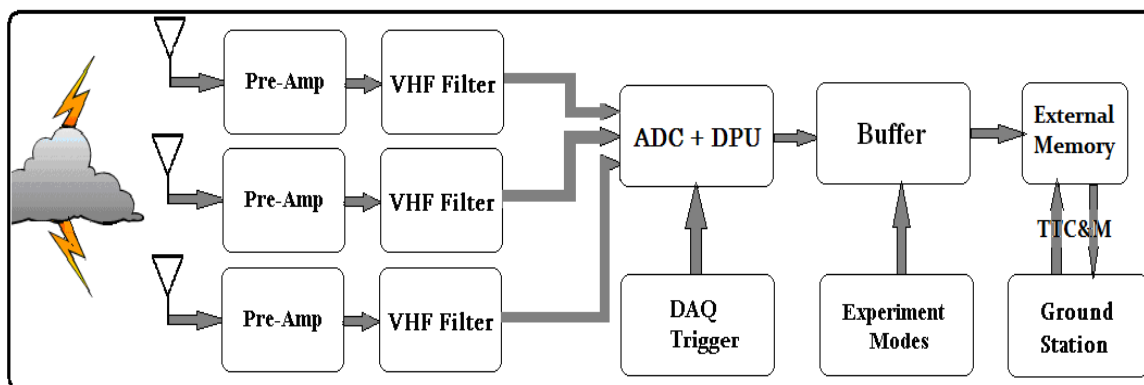


Figure 3-6: Block diagram of the LiNSAT scientific payload.

Three inputs from the antennas are fed to a low power ADC with four input channels synchronous sampling to avoid a multiplexer that complicates the inputs by time shifts. The ADC contains 4 'Sample and Hold' (S/H) circuits synchronized with one clock, so parallel and synchronized sampling is performed. The power consumption is up to 500 mW with such an ADC.

3.5.3 Data Processing Unit (DPU)

The signal from the antennas are fed to the data processing unit (DPU) through a pre-amplifier prior to analog/digital conversion and further processing. As

mentioned earlier, the maximum lightning electric fields at 1000 km altitude have an amplitude of 1mV/m at 40 MHz, 1 MHz bandwidth (Jacobson, Knox et al. 1999). After filtering and amplification, the 200 MS/s ADC will over-sample the received signals and the digitized signals are dumped into the commercially available memory (~ 500 MB) with the help of two levels of event detection (coarse and fine). Data acquisition captures a waveform record. A triggering unit helps in elimination of unwanted signals stemming from other origins and artifacts from the satellite itself.

3.5.4 DAQ Trigger and EMI Filtering

The event detector is an important part of the detection system; a signal processing subsystem performing various signal processing functions is used to classify the signals into distinct categories.

The adaptive filtering (AdF) structure shown in Figure 3-7 is based on and draws heritage from adaptive noise cancellation (ANC) (Haykin 1996). The input signal $d[k]$ is a lightning transient pulse that is contaminated with artifacts $a_d[k]$ from LiNSAT. The co-efficients for the reference signal $x[k]$ can be derived from two sources, either by ground-based EMC investigations as a preliminary estimation as preselector co-efficients for AdF (GPC) or the output from the lightning sensor on-board the nano-satellite. The goal is to detect natural lightning spikes, so finally we will have to rely on an on-board sensor for updating the co-efficients of AdF. The reason behind updates could be

- Slightly shifting of the subsystems emissions curve within the scientific payload measurement range
- Cancellation of disturbances generated by LiNSAT or subsystems, $a_x[k]$.

Electric field emissions in the measurement range 20-40 MHz from on-board subsystems have an emission curve of the artifacts generated by LiNSAT. It can happen that the frequency of the emission curve shifts within the measurement range, therefore, the filter co-efficients need to be updated to track the movement in a robust manner.

The coarse trigger is a threshold level. Also, the adaptive filtering approach will be used as fine trigger on-board the satellite (DAQ Trigger, Section 3.5.2).

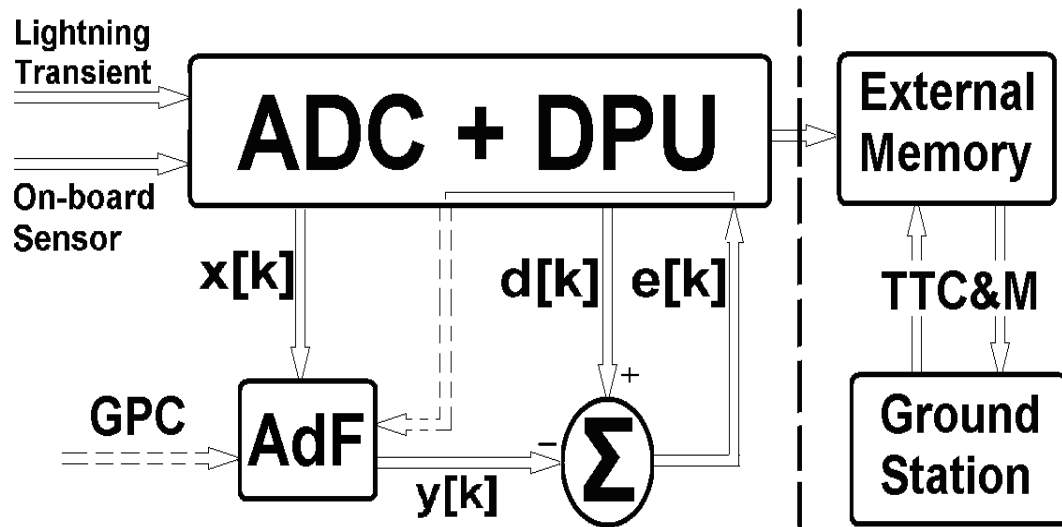


Figure 3-7: DAQ trigger for lightning detector on-board LiNSAT based on adaptive filters.

The orbital footprint of the LiNSAT will be scanning the whole Earth during several orbits but the lightning flash rate varies along the orbit from the poles to equator as shown in Figure 2-1. This is valuable statistical environmental input for the $d[k]$ channel for precise triggering and to avoid false alarms.

$x[k]$ is a digitized output of the sensor on-board which detects artifacts in terms of electric field emissions from LiNSAT itself. This could be broadband or narrowband, e.g. a clock signal or harmonics of the digital electronics

$$\mathbf{x}[k] = \mathbf{a}_x[k] \quad 3-2$$

$d[k]$ is the digitized signal of the lightning transient after passing through antenna, HF/VHF filter and pre-amplification including noise picked up in this receiving channel,

$$\mathbf{d}[k] = \mathbf{s}[k] + \mathbf{a}_d[k] \quad 3-3$$

where $a_d[k]$ and $a_x[k]$ are correlated noise sources.

AdF is an FIR filter while the initial co-efficients for the filter are derived from ground-based investigations (GPC) during the development phase.

$y[k]$ is the output of the AdF that sums up with $d[k]$ to produce error signal $e[k]$ that ultimately is used for

1. Trigger purpose for the on-board lightning detector to dump the ring buffer/cyclic memory contents into external memory for future download using telemetry, tracking, command and monitoring (TTC&M) by one of the ground stations through visibility/communication window
2. To modify the coefficients of the AdF accordingly using least mean square (LMS) algorithm.

The filter is in the digital domain and is application dependent. The filter co-efficients must be updated regularly so that the residual goes to zero. The output is a noise-removed lightning signal which will trigger the memory to store the transients.

To determine the capability of the filter, we tested it with real life signals i.e. artificial discharges in high voltage chamber (Section 4.3) and natural signals (Section 4.4) in particular a TIPP event recorded by the ALEXIS satellite (Massey, Holden et al. 1998; Jacobson, Knox et al. 1999). The outputs were found to be

similar to the noise-free real lightning transients and correlated noise in the lightning channel was removed (Jaffer, Koudelka et al. 2011c). The major advantage of the output (error signal) is that it would trigger the memory (on-board LiNSAT) with a lower threshold level. Therefore, lightning pulses with even small peaks will be captured using the adaptive filter fine trigger, otherwise would be hard to capture due to higher noise floor. The outputs are shown in Figure 3-8 and Figure 3-9.

The pseudo code to generate such signals using AdF through Matlab function is elaborated in Table 3-4.

Table 3-4: Matlab code to test Adaptive filter algorithm

```
function [E,Y,noise,sig_plus_filterednoise]=anc_lightning(signal,filterorder,cutoff_frequency)
%
[E,Y,noise,sig_plus_filterednoise]=anc_lightning(b23(1.18*10^6:1.28*10^6,1),4,0.4);
noise=0.1*randn(length(signal),1); ..... % noise modeling
nfilt=fir1(filterorder,cutoff_frequency)'; ...% filter order LP
fnoise=filter(nfilt,1,noise); .....% correlated noise data
sig_plus_filterednoise=signal+fnoise; .....% input plus noise
coeffs=nfilt-0.01; .....% filter initial conditions
mu=0.05; .....% step size for algorithm updating
S=initlms(coeffs,mu); ..... % Init LMS FIR filter
[Y,E,S]=adaptlms(noise,sig_plus_filterednoise,S);....% Y=filtered data,
E=Prediction Error
```

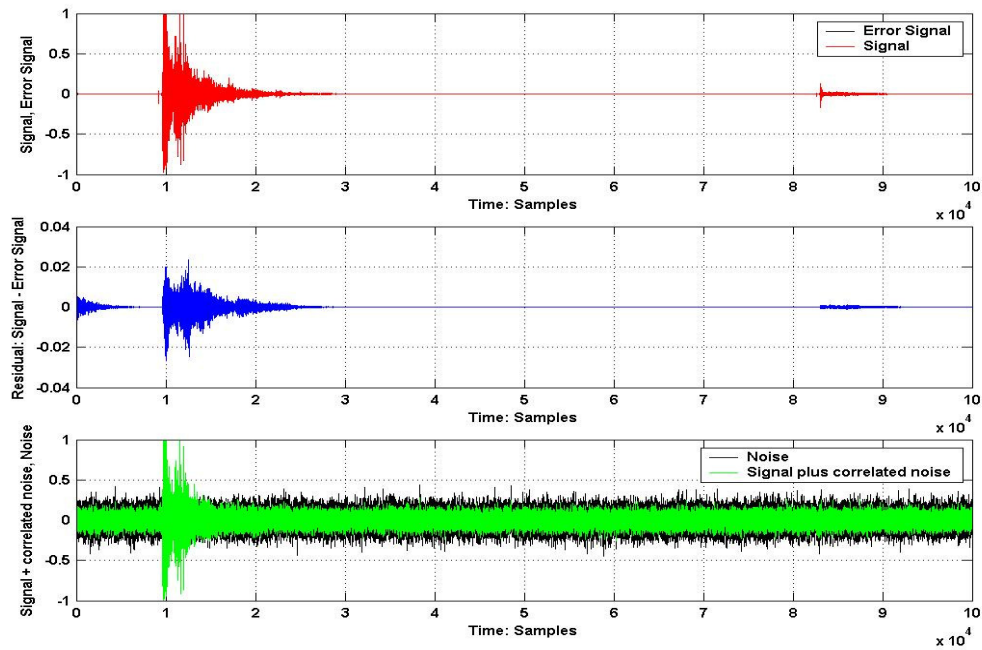


Figure 3-8: Acoustic signal (serves as proxy of lightning electromagnetic pulse) measured in high voltage chamber and received using Adaptive filter. Top: Measured lightning signal and reconstructed signal ('error signal') are similar. Middle panel: The error signal is nearly the same, therefore, precise residual between the two signals is shown in the middle panel. Bottom panel: The used noise source and the original lightning signal with a correlated noise (drawn from the noise source via a low pass filter). If the AdF technique is not used, shown in the bottom panel, the second tiny stroke (upper panel) is hidden in the noise floor.

The other signal of interest to test AdF is natural lightning (i.e. TIPP) captured with ALEXIS satellite. Again, the noise-removed signal can be seen Figure 3-9 (upper panel).

Based on previous experiments using engineering models and the TUGSat-1 study, the DAQ Power estimations are ~ 3 W on average up to 5 W (peaks) for short time. The power consumption is mainly determined by the consumption of the digital electronics. Among several requirements, e.g. robustness, tracking speed and

stability of the AdF, the on-board computational power of the DPU is one of the constraints in space. A technique to overcome this deficiency on-board is power aware computing (Graybill and Melhem 2002) and one case-study for the FORTE mission is discussed in (Shriver, Gokhale et al. 2002).

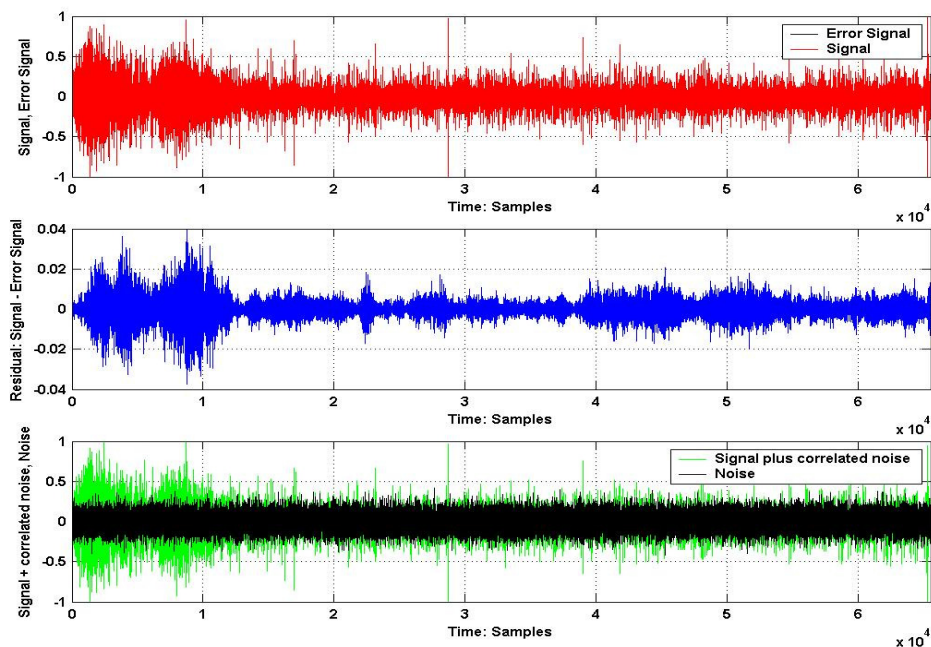


Figure 3-9: TIPP event captured with Adaptive filter. The error signal is close to real input, an advantage of using AdF to trigger on-board memory for saving noise-free lightning transients.

3.6 Attitude Control System

Unlike TUGSat-1/BRITE-Austria which is three-axis stabilized, LiNSAT will use the widely used and inexpensive gravity gradient stabilization (GGS) technique for its attitude control. The deployable GGB has a length of 1m. The vector of the boom and its counterweight will be rotating around a vector pointing directly

towards the center of the Earth. If this oscillation can be dampened, it is possible to control the attitude of the satellite such that the nadir surface points towards the Earth within limits of ± 5 degrees (Taylor-Univ 2011; Taylor-University 2011). This is sufficient for antenna pointing.

The setup from Figure 3-3 benefits from the RF noise survey (Burr, Jacobson et al. 2004; Burr, Jacobson et al. 2005) and enables investigations of all types of lightning (Figure 2-7) including TIPP (Holden, Munson et al. 1995; Massey and Holden 1995; Massey, Holden et al. 1998; Tierney, Jacobson et al. 2002) and compact intracloud discharges (Smith 1998; Nag and Rakov 2010; Nag and Rakov 2010).

A redundant approach (passive magnetic and GGB attitude control) is being used by Quakesat (Quakesat 2011). It used a GGB back in 2003 and is still operating. The attitude determination and control system (ADCS) of this satellite is primarily a magnet, but it extends a magnetotorquer out on a boom providing more than the average effects from the gravitational gradient. As there is no large tip mass, the gravity gradient effect is reduced, thus magnets are needed to reduce damping effects and ultimately stabilizing the pointing accuracy

A recently proposed technique for a nano-satellites ADCS is the aerodynamic drag method discussed in (Rawashdeh and Lumpp Jr 2010). Aerodynamics drag is not sufficient in LEO with an altitude of ~ 1000 km, as it gets a little bit weak, since drag is a function of altitude based on density.

The tip mass is comparable to total mass of the satellite (10%). In principle the GGB works for imaging payload with a pointing accuracy of $\sim \pm 5^\circ$, but roll of the satellite must be taken into account. The dipole antenna has coarse detection (no stringent directional/ pointing requirement), also the FOV at 800 km altitude with $\pm 5^\circ$ (nutation of the axis) is compared to thunder-cloud size. The roll angle assumption of the antenna can be as large as 360° and is important to be

considered. The rolling and nutation can affect each of three channels. By looking at all three channels we will have sufficient information about these effects.

3.7 Chapter Summary

A feasibility study of LiNSAT for lightning detection and characterization as part of climate research with a low-cost scientific mission was presented that was carried out in the framework of this dissertation. In order to overcome the mass, volume and power constraints of the nano-satellite, it is planned to use the gravity gradient boom as a receiving antenna for lightning Sferics and to enhance the satellite's directional capability.

The Architecture of a lightning detector on-board LiNSAT in LEO was described. The LiNSAT will be a follow-up mission of TUGSat-1/BRITE and use the same generic bus and mechanical structure. As the scientific payload is a lightning detector and it has no stringent requirement on the ADCS to be three axis stabilized, so the GGS technique is more suitable for this mission.

To avoid false signals detection (false alarm), pre-selectors on-board LiNSAT are part of the Sferics detector. Adaptive filters are formulated and will be developed to differentiate terrestrial electromagnetic impulsive signals from ionospheric or magnetospheric signals. The noise-removed signal was found to be similar to the real lightning signal. Therefore, the signal will be used for fine trigger on-board the LiNSAT.

The next consideration is to use existing lightning data from previous missions to validate the accomplished results.

Chapter 4 Experimental Results for Space Segment

4.1 Introduction

It is important to perform all necessary experiments to simulate the scientific payload in feasibility studies before the development and implementation phase. The results obtained are the basis for this design phase. This chapter presents results of simulation and two terrestrial measurement campaigns to geo-locate and discriminate lightning types in the presence of noise sources.

Our main scientific objective is to investigate lightning events by the observation of HF/VHF electromagnetic signals (Sferics) and to derive the signatures of lightning. One of the important parameters is the lightning flash rate, which can be used as a proxy for identifying severe weather activity. Another objective is to discriminate the discharges of lightning events evaluated by the inherent features and to differentiate cloud discharges (I-C; intercloud and Intracloud) from ground discharges (C-G; cloud-to-ground), return strokes (RS), leaders (L) and trans-ionospheric pulse pairs (TIPP). The discrimination is important because the ratio of the two (I-C/C-G) is a good indicator of convective storm development (Williams, Weber et al. 1989; Williams 2005; Williams 2009), Figure 2-6.

Two measurement campaigns were conducted; one for artificial lightning produced in high voltage chambers and the second for natural lightning recorded at urban environments. We focus mainly on the received time series including noisy features and narrowband carriers to extract characteristic parameters. The chamber inter-walls distance was determined by considering reflections in the first measurements.

Initially the algorithm for the instruments on-board electronics has been developed and verified in Matlab. The next consideration is to use existing lightning data from the previous French mission DEMETER to validate the accomplished results.

The LiNSAT team has participated in various space missions investigating electromagnetic phenomena. The data of these missions will be used to test the hard- and software of the lightning experiment before the launch.

4.2 Lightning Detection Simulation

In Austria, the lightning flash density is between 0.5 and 4 flashes per square km per year, depending on terrain (Diendorfer, Schulz et al. ; Schulz and Diendorfer 1999; Diendorfer, Schulz et al. 2002; Schulz and Diendorfer 2004; Schulz, Cummins et al. 2005). The lightning flash duration is about half a second. The simulated signals are evaluated with coarse and fine triggered detection using the "lightning detector" program written in Matlab. The blocks of the receiving chain are simulated individually and as a whole using Matlab functions. To verify the simulations, lab measurements (RF and Acoustic) are performed (Chapter 4). The objective of these measurements/ simulations was to find an algorithm which could be implemented on the on-board lightning detector electronics, (requirements: must be fast, effective and running with limited resources)

A second data set of lightning strokes for simulation using the program was analyzed. The program computes the pulse width, pulse rise time, number of detected pulses, frequency and pulse-amplitude and stores all the information in a resultant matrix; in an emulation of cyclic memory. The algorithm is mode dependent and basically captures lightning signals above a certain threshold level. It classifies and characterizes the pulses. A standard class of lightning transients was used to test the algorithm and possible working of experiment modes Table 3-2.

For coarse detection, the whole window was divided into one thousand 1 ms sub-windows for computing mean and standard deviation (power) in each sub-window above threshold level. This procedure will help us in pre-selecting the data and to switch the experimental modes while the satellite is above Equator, Poles etc with the lightning detector on-board the LiNSAT. Telemetry using coarse trigger will be downloaded for ground-based analysis. The resultant matrix of the program is shown in Figure 4-1.

```
PULSE=>No.   Start-Time  Widthth  thLevel  AmplitudeRMS  Rise-Time  Max-Frequency
```

```
resultantMatrix =
```

1.0000	4.0000	2.0000	16.0000	17.3449	17.8759	0.0196
2.0000	7.0000	2.0000	16.0000	17.9203	21.3362	0.0164
3.0000	13.0000	2.0000	16.0000	19.1966	28.3573	0.0123
4.0000	19.0000	3.0000	16.0000	18.0037	33.4029	0.0105
5.0000	27.0000	1.0000	16.0000	17.6707	41.1366	0.0085
6.0000	31.0000	1.0000	16.0000	22.0093	48.6074	0.0072
7.0000	34.0000	1.0000	16.0000	21.3789	51.1032	0.0068
8.0000	37.0000	2.0000	16.0000	21.6722	54.3378	0.0064
9.0000	40.0000	1.0000	16.0000	16.7201	53.3761	0.0066
10.0000	47.0000	1.0000	16.0000	22.8012	65.2410	0.0054
11.0000	50.0000	12.0000	16.0000	134.4105	157.5284	0.0022
12.0000	64.0000	2.0000	16.0000	19.4476	79.5581	0.0044
13.0000	70.0000	1.0000	16.0000	21.2800	87.0240	0.0040
14.0000	74.0000	2.0000	16.0000	18.5694	88.8555	0.0039
15.0000	78.0000	2.0000	16.0000	17.2528	91.8023	0.0038
16.0000	81.0000	1.0000	16.0000	19.4400	96.5520	0.0036
17.0000	84.0000	1.0000	16.0000	21.9625	101.5700	0.0034
18.0000	88.0000	1.0000	16.0000	20.0368	104.0295	0.0034
19.0000	92.0000	1.0000	16.0000	21.6809	109.3447	0.0032
20.0000	98.0000	1.0000	16.0000	18.6548	112.9238	0.0031

Figure 4-1: Matlab simulated results of the program "lightning detector". In this computation, the threshold level for coarse detection was set to 16 mV to extract all pulses above noise floor. Twenty pulses were detected along with their information about pulse start time (in ms), pulse rise/ fall time (in μ s), amplitude (mV), maximum frequency ($\times 10^6$ Hz).

4.3 Artificial Lightning Measurement Campaigns

4.3.1 Electrical Discharges in High Voltage Chamber

In these measurement campaigns, artificial lightning was produced in a laboratory at Space Research Institute, Austrian Academy of Sciences, Graz and in the high voltage facility of the Institute for High voltage Technology and System Management of the Graz University of Technology (TU Graz) high voltage chamber. The voltage of the artificial lightning discharge in the high voltage facility was from 700 kV to ~ 1.8 MV under normal pressure and temperature conditions. The system has selectable positive and negative polarity and electrodes' inter-distance. The measurement setup in the TU Graz facility consisted of an electric field probe (60 Hz to 100 MHz) and digital oscilloscope (bandwidth = 500 MHz) with external and manual trigger (pre-, post-trigger) option. All the relevant information can be found in Table 4-1.

We focus mainly on the received time series including noisy features to extract characteristic parameters. The chamber inter-walls distance was determined by considering reflections in the measurement. Round-trip-time of direct and reflected waves indicates many reflections from walls of the chamber. The captured image shows similarities with the natural lightning signal shown in Figure 4-23 and Figure 4-24. These measurements are important for training the algorithm for TIPP

detection and for the cloud height determination on LiNSAT. All experimental results are shown in the following figures.

Table 4-1: RF measurements of high voltage discharges (simulated lightning) in the high voltage chamber

S. No.	RF Signature	Measurement Polarity, Comments, Structure	Setup
01	3 * (pre-discharges)	Negative polarity flash, slow increase of voltage	
02	3 Lightning	Negative polarity	
03	3 Lightning	Positive. polarity	
04	8 Flashes	Positive. polarity, (3, pipe cut, 1, pipe cut, 1, pipe cut, 1, pipe cut 1, cut pipe, 1)	Catch Rod
05	7 Lightning strokes	Positive. Polarity	Catch Rod
06	3 Lightning strokes	Positive. Polarity	Catch Rod + Model Model closer to Catch Rod
07	3 Lightning strokes	Positive. Polarity	Catch Rod + Model Model closer to Catch Rod
08	2 Lightning strokes	Positive. Polarity	Catch Rod + Model
09	3 Lightning strokes	Positive. Polarity	Model polarity closer to the Catch Rod

10	3 Lightning strokes	Positive. Polarity	1.6 MV Model on mat
11	3 Lightning strokes	Positive. polarity, branching 1 Stroke, 2 Stroke 3'er branching, branching Stroke 3	Model without mat
12	6 Lightning strokes	Positive. polarity, 1 - Wood 2 - Wood, grounding point => Plastic plate (4 and 5), 6 - Overturning shoe left	Model with wooden shoes and isolation
13	6 Lightning strokes	Positive. Polarity, all metal parts are part of the arc	Model + Tshirt + shoes + + Cap safety pin
14	5 Lightning strokes	Positive. polarity	Model + Tshirt + cap (2 - Stroke) + wire (necklace) + 1 euro to cap (1 Stroke), electrode , 1 Stroke. Electrode up, 1 Stroke
15	2 Lightning strokes	Positive. polarity	Model + Tshirt + cap + necklace + clasp
16	4 Lightning strokes	Positive. polarity, 1-2, Ground strap off, 3 - Strong arc ie full Lightning discharge 4	Faraday hole
17	6 Lightning strokes	Positive. polarity, 160 kV, 190 kV (overturning)	lead-loop corner
18	4 Lightning strokes	Positive and negative polarity, 190 kV (Positive. Pol, no overturning), 190 kV (negative pol., no overturning), 190 kV (negative polarity, no overturning), 200 kV (Negative Pol. overturning)	lead-corner loop shortened

19	8 Lightning strokes (2 pre-discharges)	Positive. Polarity, 180 kV, 180 kV, 170 kV, 160 kV, 150 kV, 140 kV, 1 pre-discharges, 120 kV loop pre-discharges	Head, separation distance ~ 1cm
20	7 Lightning strokes (2 * pre-discharges)	Positive. Polarity, 120 kV (overturning), closer, 100 kV (overturning), 80 kV (overturning), 1 over, 1 over, 1 pre-discharges, 70 kV conductor pre-discharges	loop separation distance ~ 1cm
21	5 Lightning strokes	Positive. Polarity, 180 kV, 180 kV, insulated tent moving, down electrode, 180 kV (branching), 180 kV (Earth), 180 kV	tent
22	3 Lightning strokes (1 * Discharge along the rope)	Positive. Polarity, 180 kV (in ladder), 180 kV (in ladder), 180 kV Discharge along rope; (clapping at the end)	rope
23	2 Lightning strokes	Positive. Polarity, 180 kV (antenna steering), 180 kV (antenna steering and power-out cable)	radio, cable grounding rail
24	2 Lightning strokes	Positive. Polarity, 180 kV, to Model, 180 kV	Radio, power cable
25	3 Lightning strokes	Positive. Polarity, 180 kV, tube down, 180 kV, 180 kV, Positive. Polarity, 180 kV, 180 kV	Umbrella, beer cane Model
26	4 Lightning strokes	Positive. Polarity, 180 kV, 180 kV, 180 kV, 180 kV	Car
27	2 Lightning strokes	Positive. Polarity, 180 kV, 180 kV	Car

Note:

Electric Field Probe: DC to 100 MHz

Digital Phosphor Oscilloscope: TDS3054B, 5GS/s

Sample Time: $1/5 \cdot 10^9$ samples/s \Rightarrow 0.20 ns

Bandwidth: 500MHz

Record Length: 500 points (Fast Trigger), 10000 points (Normal Trigger)

The oscilloscope has two trigger modes. When compared to Matlab 500 (Fast Trigger Mode) and 10,000 (Normal Mode), the 500 points correspond to 100 ms (1 point is 20 μ s) and the 10,000 points correspond to 10ns (1 point is 1 ps).

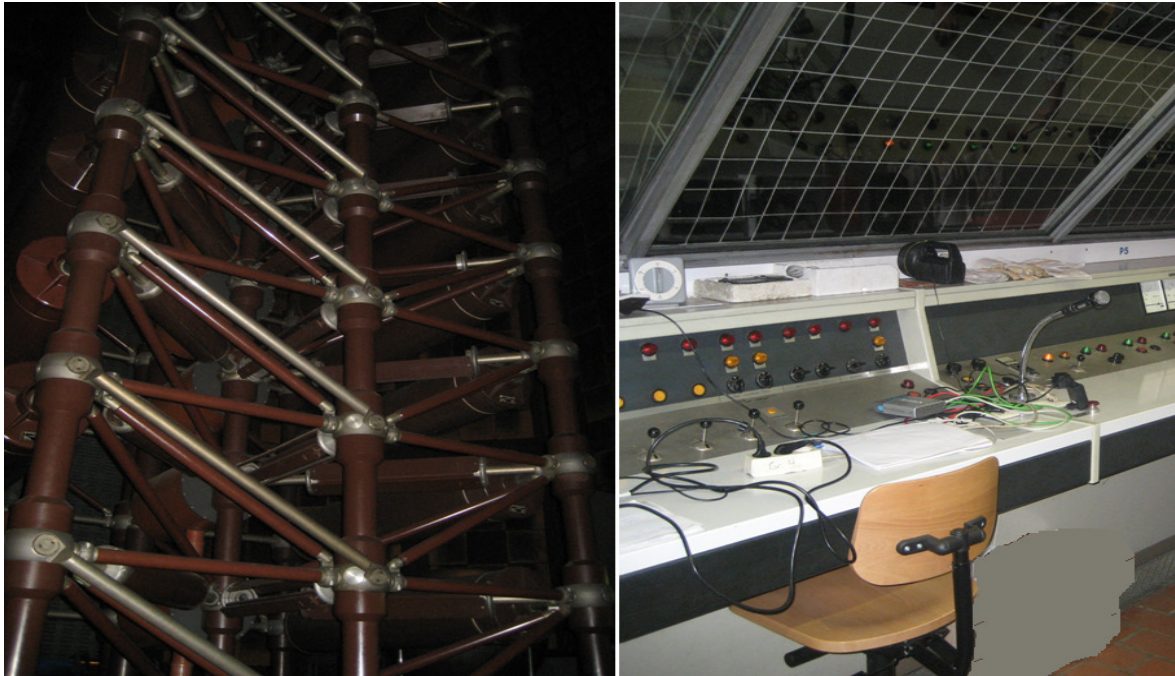


Figure 4-2: High Voltage Chamber and Control Room. First part of the measurement setup along with Figure 4-4.



Figure 4-3: Lightning event occurrence on a model. Also branched lightning (to ground and air) was observed.

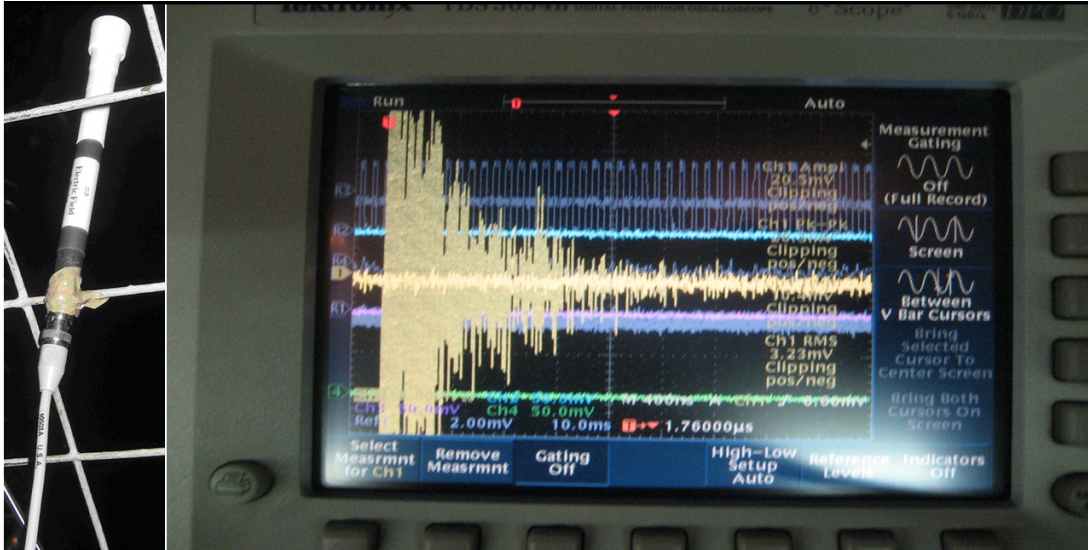


Figure 4-4: Lightning electric field captured with electric field probe and oscilloscope. The captured image shows similarities with natural lightning signal shown in Figure 4-23 and Figure 4-24



Figure 4-5: The striking phenomenon, upward lightning initiated by sharp objects in the vicinity of chamber ground was observed. In principle, this phenomenon occurs with sharp tips of tall buildings like churches etc. It has similarity with the return stroke phenomenon.

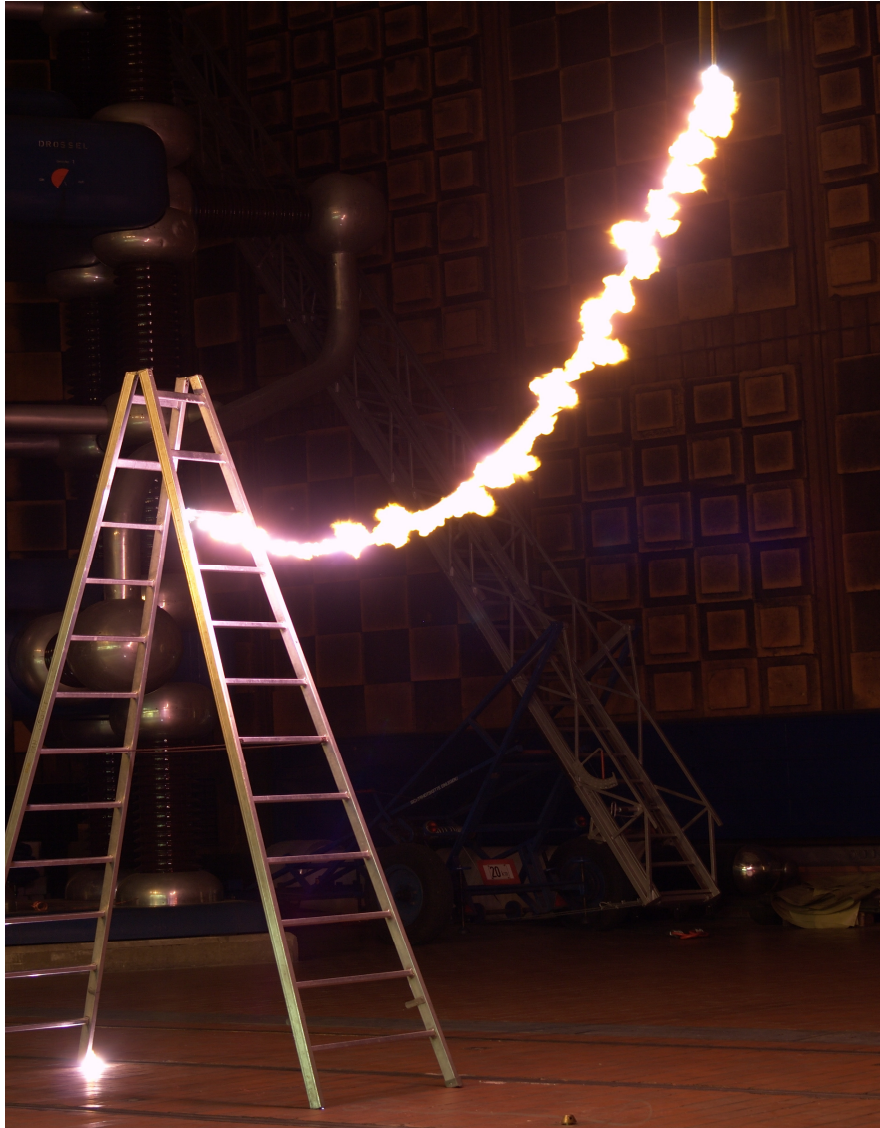


Figure 4-6: Color changes (intensity) due to discharges along the rope. The variations indicate current interaction with fibers of the rope under impact of a lightning discharge of ~ 1.8 MV. Post-event inspection revealed no damage in the rope, macroscopically.



Figure 4-7: The basic structure of the tent serves as a model for the Faraday cage. There can be arcing if some metal is present inside the tent (no lightning safety)



Figure 4-8: Lightning event occurs near the object due to slight movement of the electrode.

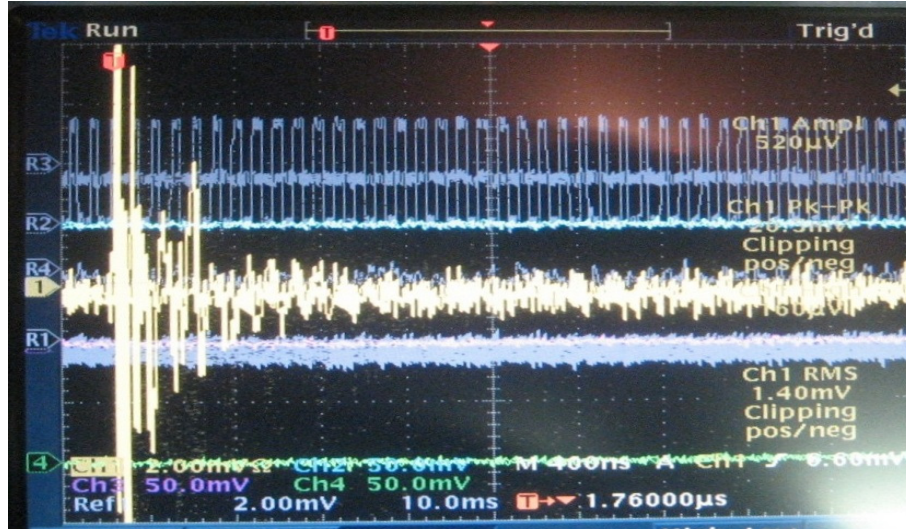


Figure 4-9: The measured electric field due to arcing (impact) of the lightning discharge on the model of Faraday cage (Figure 4-7). Also, round-trip-time of direct and reflected waves indicates many reflections (in the order of ns) from all walls of the chamber. The measured time indicates the inter-walls distance in meters.

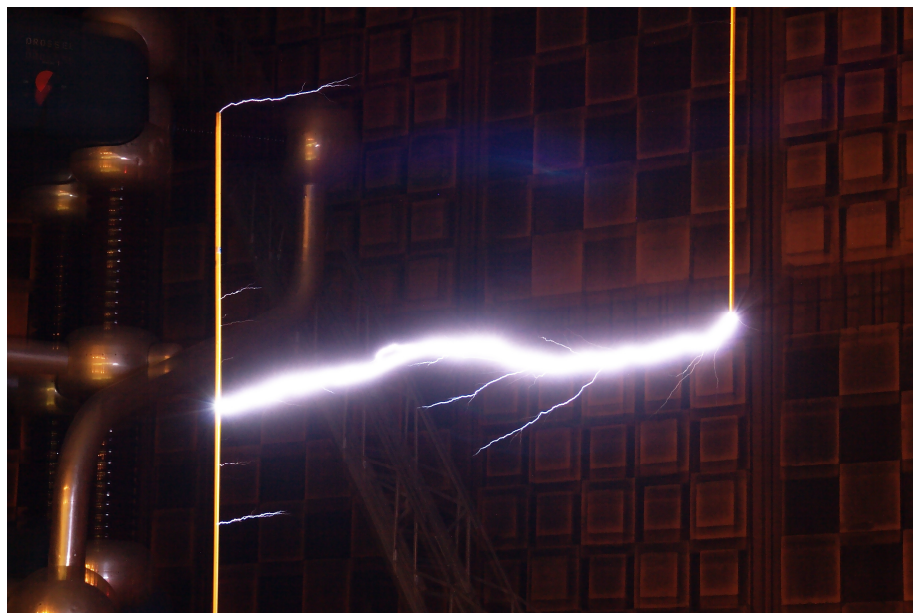


Figure 4-10: A nearby object struck by lightning. The model was used to determine the minimum distance from the nearby discharge for using the Faraday cage.

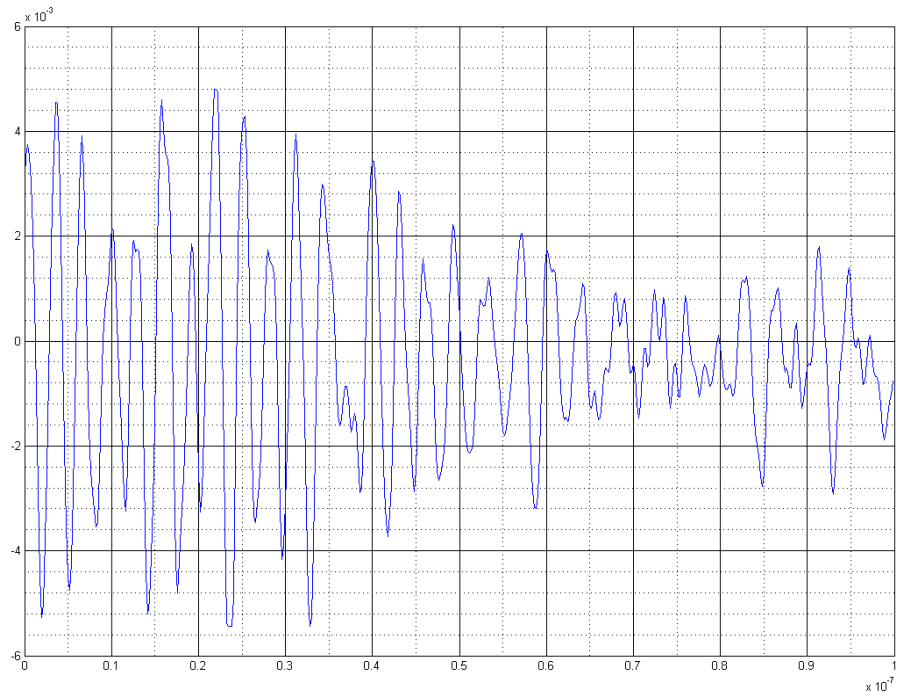


Figure 4-11: The waveform of an artificial discharge created with Matlab

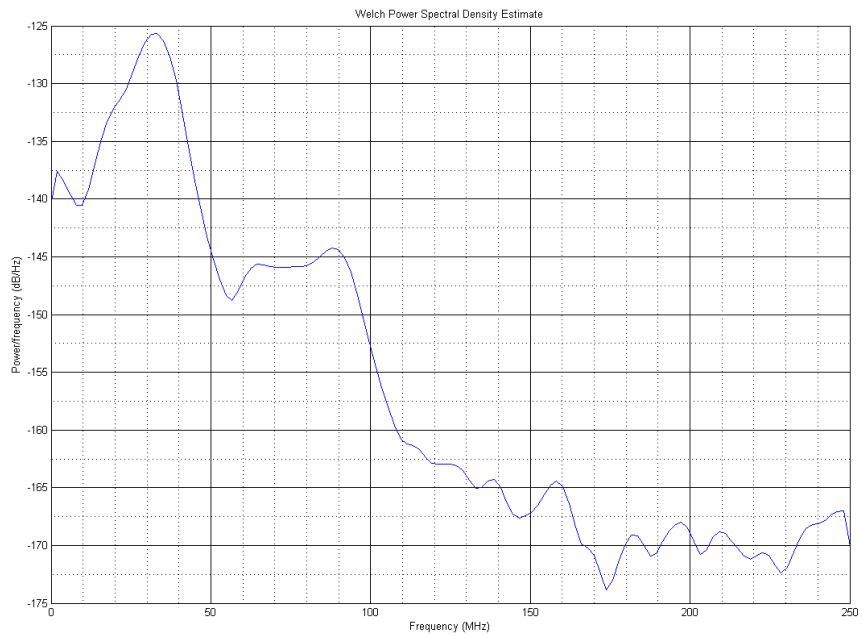


Figure 4-12: The power spectral density (PSD) of the artificial discharge (Figure 4-11) computed with Matlab

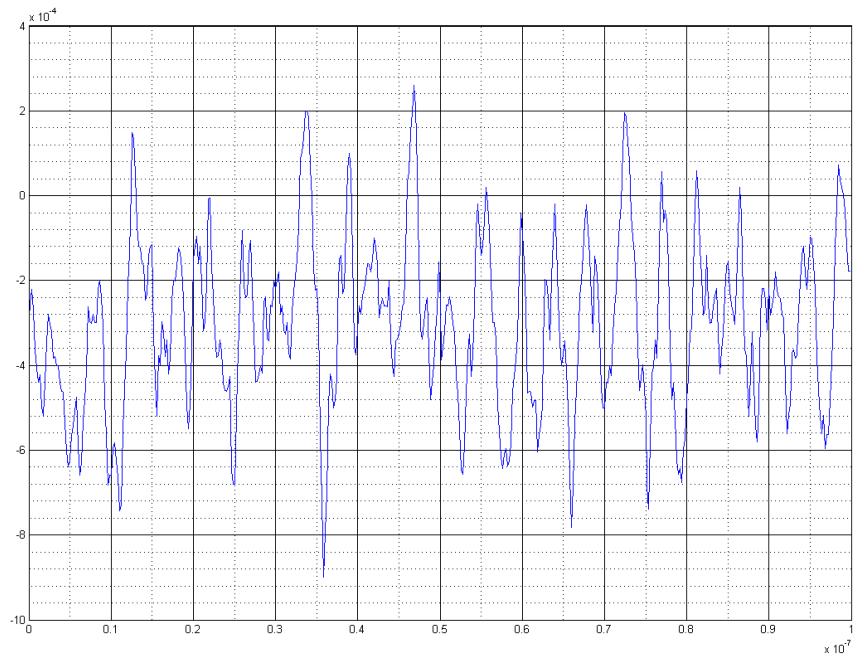


Figure 4-13: The waveform of an artificial discharge captured with e-Tek oscilloscope and recreated with Matlab

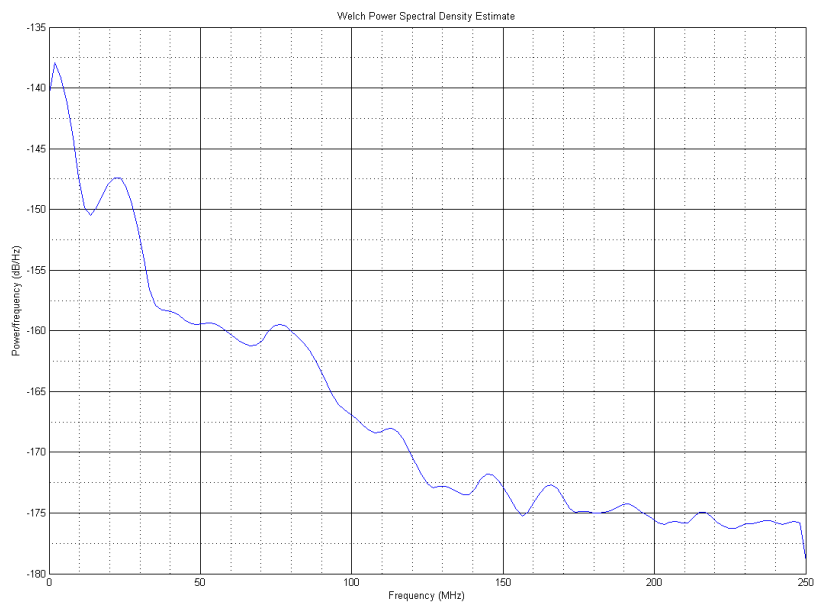


Figure 4-14: The power spectral density (PSD) of the artificial discharge (Figure 4-13) computed with Matlab

4.3.1.1 Electrical Discharges in a Lab

Besides the measurements from the previous section, we wanted to determine all associated phenomena with natural lightning e.g. corona discharges, glow and sparks. Moreover, these phenomena were easily produced in the lab due to controlled setup. Thus it was not necessary to perform these measurements in the high voltage chamber. This setup helps to investigate distinct features of all three mentioned discharge types and the transition among all these phenomena related to voltage in a pre-defined setup.

The setup comprises of

- High voltage power supply unit (HV-PSU)
- Electrodes: a metal plate (anode) and screw (cathode) combination with inter-distance of 1 inch (2.54 cm)
- Electric field probe (60 Hz to 100 MHz); uncalibrated
- Digital Oscilloscope (eTek, 500 MHz bandwidth)



Figure 4-15: High voltage power supply unit (HV-PSU)

4.3.1.2 Corona Discharges

The very first broadband phenomenon occurs with a hissy sound due to increase in the voltage. The maximum corona acoustic along with glow was observed at 11 - 12 kV using HV-PSU..

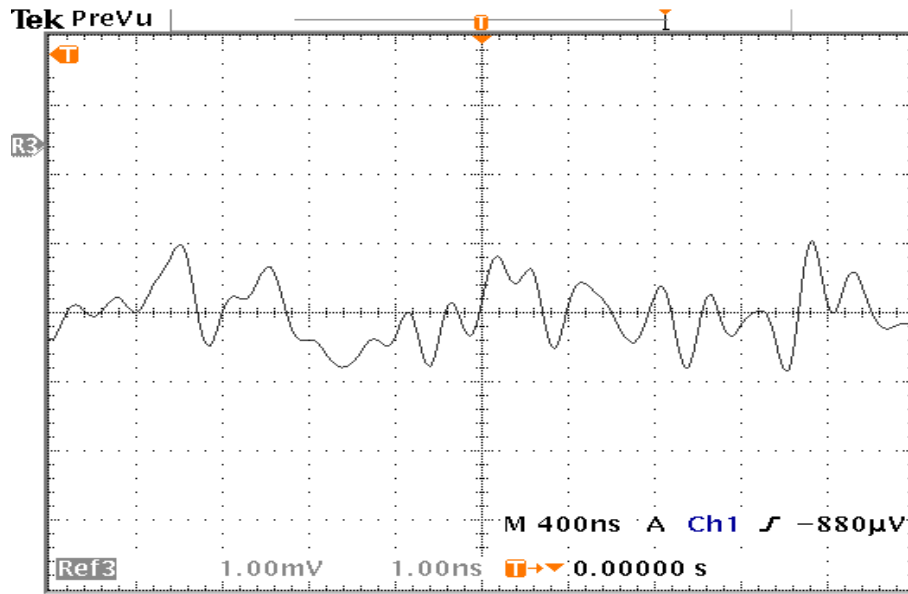


Figure 4-16: eTek Oscilloscope display of corona discharge. The captured amplitude is ± 1 mV.

4.3.1.3 Glow Discharges

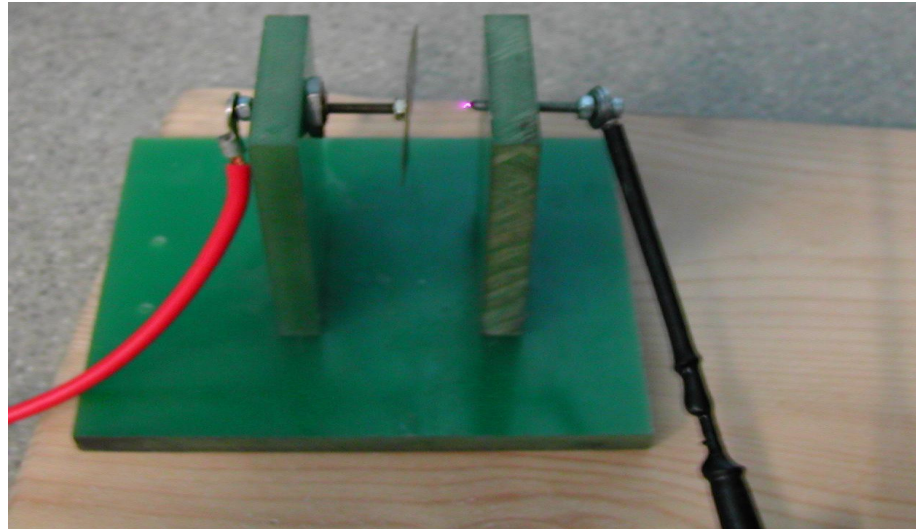


Figure 4-17: Artificial lightning: indication of corona and glow discharge

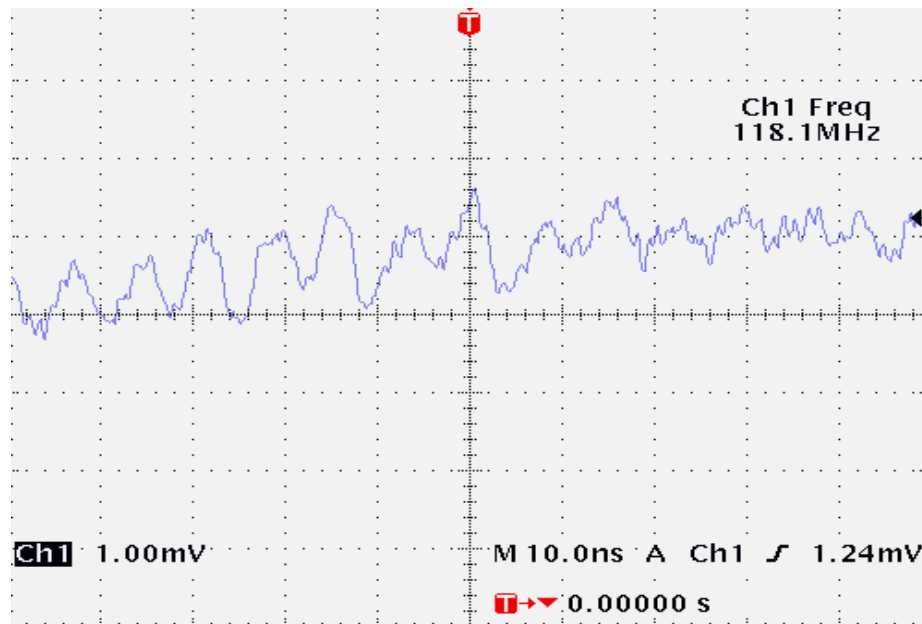


Figure 4-18: Glow discharge measurement generated with HV-PSU. The maximum corona sound with glow was generated at 11 - 12 kV and was decaying afterwards. The frequency was observed ~ 118 MHz.

4.3.1.4 Spark Discharges

The HF and VHF radiations associated with initial breakdown pulse in cloud flashes were studied by (Krider, Weidman et al. 1979) who found that radiations at 3 MHz, 69 MHz, 139 MHz and 259 MHz tend to peak during the initial half cycle of the pulse.

The same feature was observed in the lab at 139.6 MHz shown in Figure 4-19 and Figure 4-20

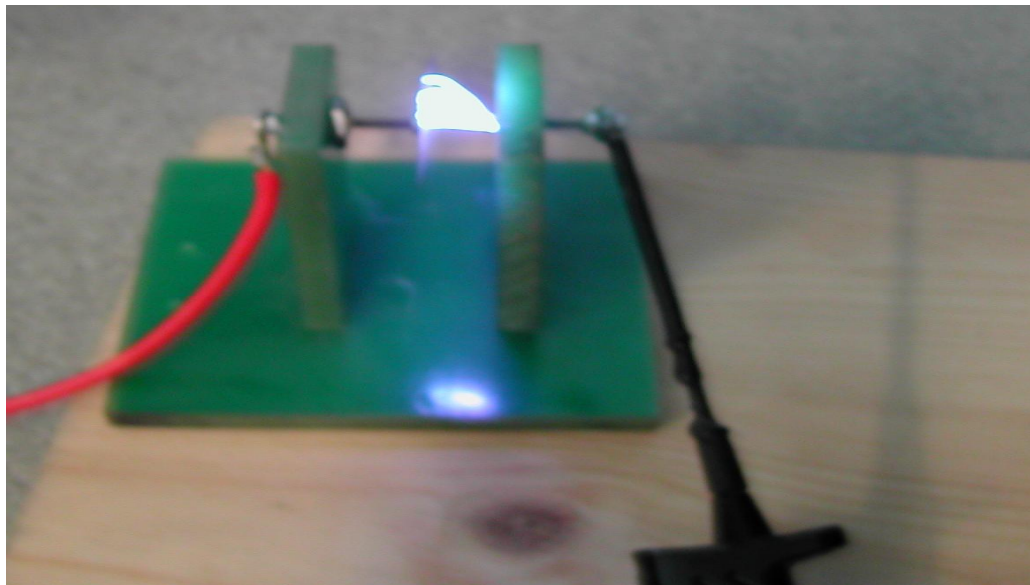


Figure 4-19: Artificial lightning, spark discharges on cathode. The maximum frequency observed for the spark was 140 MHz. The spark was produced at 13 kV and higher voltages.

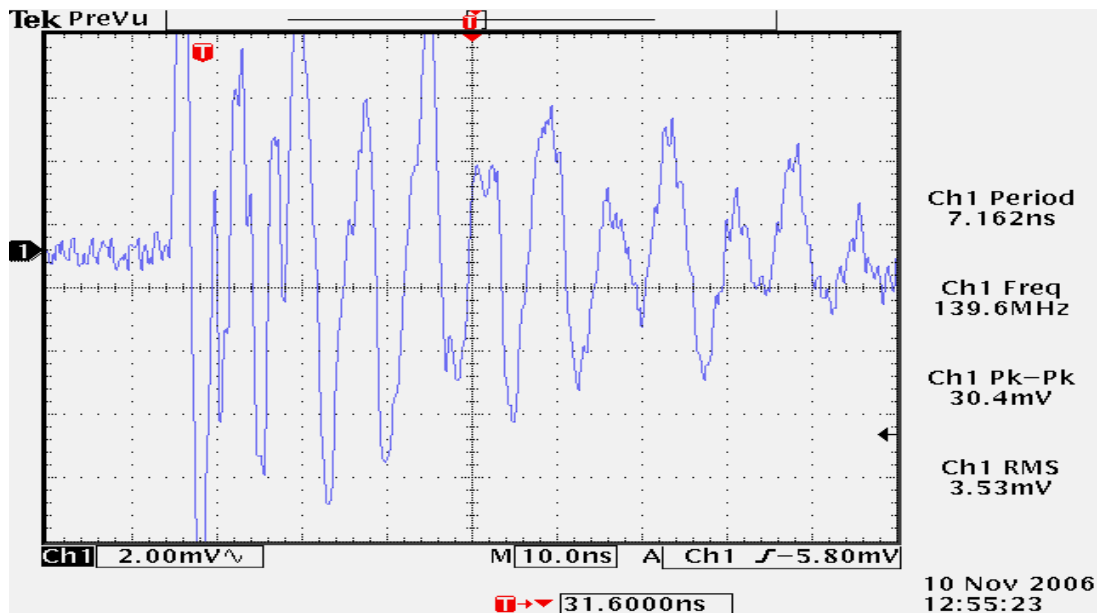


Figure 4-20: Spark discharge measurement, the maximum frequency observed for Spark is 140 MHz. The spark was produced at 13 KV and higher and was measured on the oscilloscope.

4.3.2 Acoustic Measurements

Thunderclaps are important to estimate the distance between the lightning and terrestrial observer. This method can be used during co-ordinated space-ground mode (CSG) campaigns of the LiNSAT in one of the experiment modes (Table 3-3). Acoustic measurements were performed in parallel to RF detection of artificial lightning in the high voltage chamber (Eichelberger, Prattes et al. 2010; Eichelberger, Prattes et al. 2011). The outcomes helped to correlate RF signatures of the artificial discharges. Additionally, the acoustic signal was used as an input for the adaptive filter (as a lightning signal) to test the algorithm.

4.4 Natural Lightning Measurement

During intense thunderstorm activity on June 30, 2010, in urban area of Graz, Austria, natural lightning measurements were performed using a broadband discone antenna, 15 m shielded cable and a digital oscilloscope (Bandwidth = 200 MHz) to correlate with artificial lightning discharges measured in the high voltage chamber (section 66). The radiation pattern of the antenna is shown in Figure 4-22.



Figure 4-21: The broadband discone antenna used for natural lightning measurements. The antenna was put on the roof of the TU Graz building for better reception and to avoid interferences within the campus.

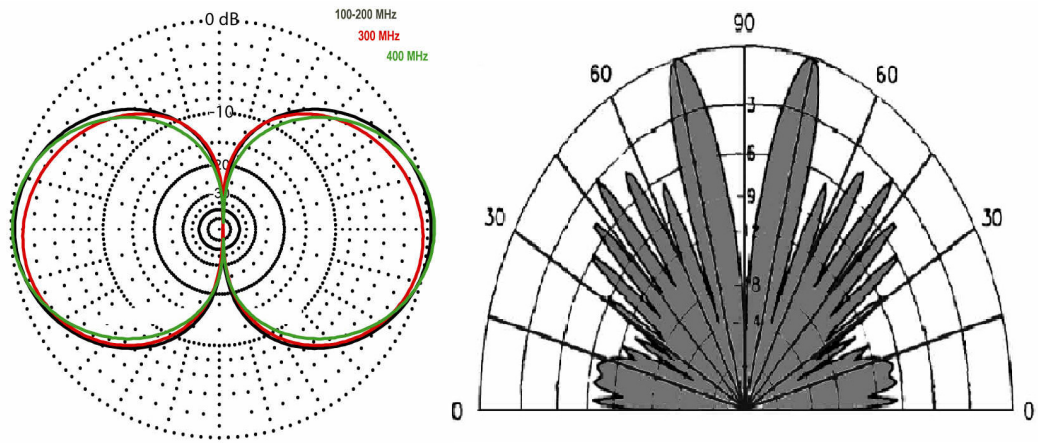


Figure 4-22: Radiations patterns of the discone antenna, indicated by the antenna manufacturer (DA-RP 2011).

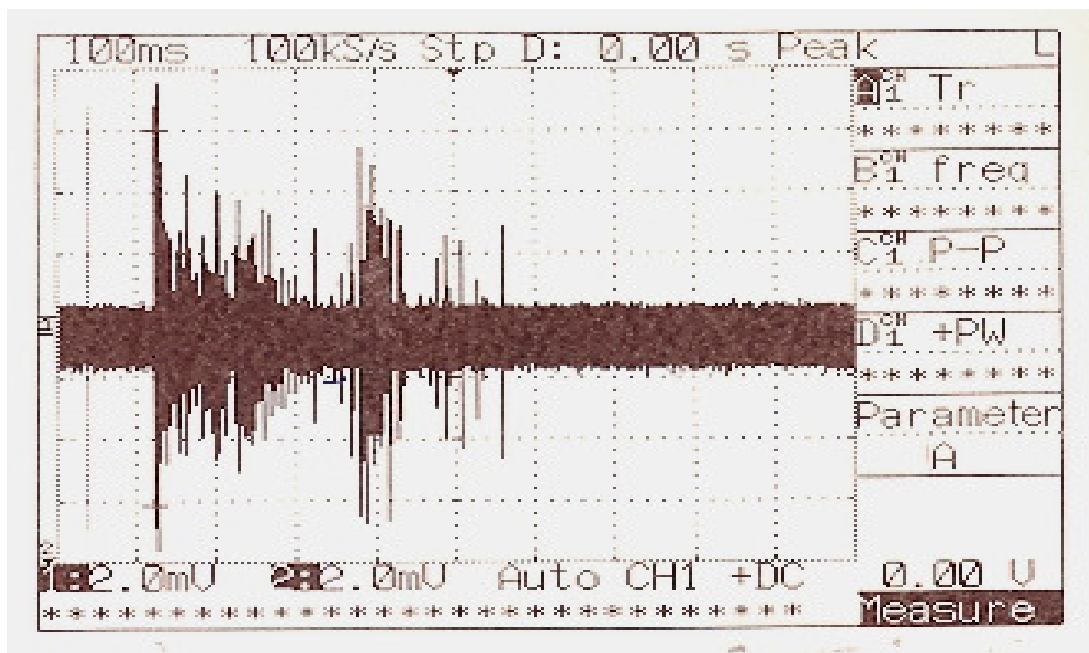


Figure 4-23: Natural lightning measurement with a digital oscilloscope (Bandwidth = 200 MHz), with a sampling rate of 100 kS/s. It shows two individual strokes within a lightning flash.

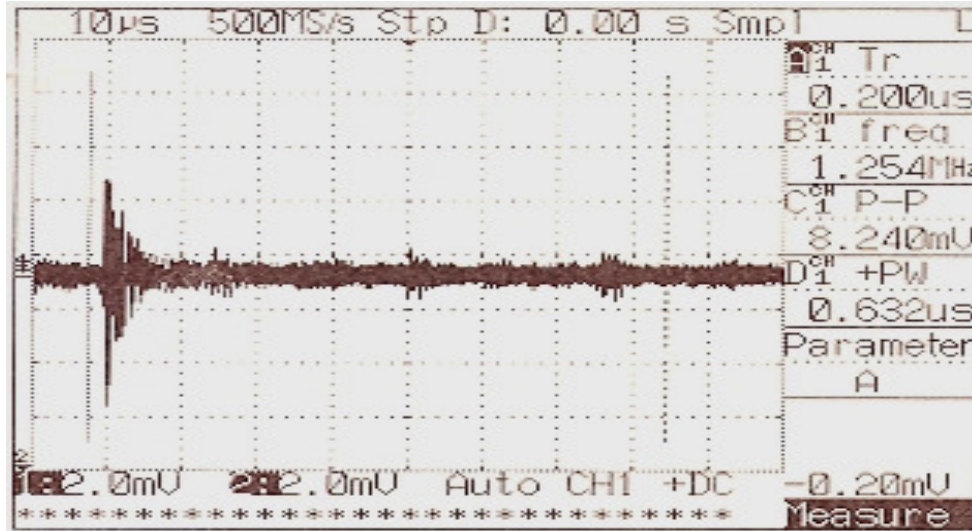


Figure 4-24: Natural lightning measurement with a digital oscilloscope (Bandwidth = 200 MHz) with a sampling rate of 500 MS/s. A single stroke is indicated along with its reflections.

Table 4-2: Natural lightning: setup and obtained resultant parameters.

	f_{sampling}	$V_{\text{p-p}}$	V_{noise}	t_{rise}	t_{fall}	$t_{\text{inter-pulse}}$
Figure 4-23	100 kS/s	18 mV	2 mV	10 ms	200 ms	250 ms
Figure 4-24	500 MS/s	6 mV	1 mV	1 μs	5 μs	15 μs

f_{sampling}	Sampling frequency of the oscilloscope
$V_{\text{p-p}}$	Peak-to-peak voltage
V_{noise}	Noise floor
t_{rise}	Pulse rise time (10-90% of the peak voltage)
t_{fall}	Pulse fall time (90-10% of the peak voltage)
$t_{\text{inter-pulse}}$	Time between two pulses (reflections, TIPP etc)

4.5 Data Analysis Conclusions

The measurements from the HV chamber and in natural environment have been evaluated in the time domain. We also determined statistically that the rise/fall time for each stroke (Table 4-2) is different and that it is relevant to indicate the unique signature of each sub-process of the lightning event. The envelope of the signal is analyzed as follows

- Events: by correlating the size of the HV chamber (reflections) with the signal trace
- By analyzing the ambient noise (and carrier) properties in these measurements

Out of these results the requirements for the lightning electronics of the LiNSAT (sample rate, buffer size, and telemetry rate etc) were deduced (Section 3.4.1). From the literature, the lightning is found to require the sensitivity of 1 mV/m/MHz. Down-scaling of ground-based detection of lightning comes up with nearly the same value.

4.6 Chapter Summary

In this chapter the results of two measurement campaigns were elaborated; one for artificial lightning produced in the high voltage chamber and in the lab, and the second for natural lightning recorded in an urban environment. We focused mainly on the received time series including noisy features and narrowband

carriers to extract characteristic parameters. The chamber inter-walls distance was determined by considering reflections in the first measurements.

The algorithm for the instruments on-board electronics has been developed and verified in Matlab. The time and frequency domain analysis helped in deducing all the required parameters of the scientific payload on-board LiNSAT.

Chapter 5 Architecture of Ground Segment

5.1 Introduction

Students pursuing scientific and technological research in space/satellite communications, want to communicate with the International Space Station (ISS), download live satellite images, and receive telemetry, housekeeping and scientific/engineering payload data from nano-satellites and larger spacecrafts. To meet this need, the Ecuadorian Space Agency (EXA) has recently provided the civilian world with an I-2-O gateway, Hermes-A/Minotaur Space Flight Control Center (SFC) (EXA 2011) available for public use. This gateway virtually connects participating clients around the world with the capability to access LEO satellites remotely both with data and voice transmissions providing a broad community for multinational cooperation. The goal of the GS is to lower financial and engineering barriers that hinder access to science and telemetry data from orbit. Hermes can also be automated by the user to track LEO satellites via a schedule, an advantage for long term operations.

In this chapter, technical details of the I-2-O gateway, its implementation for remote clients and current developments in this context are discussed. The GS has

a range up to 22,000 km with Molnya satellites. Since this GS is located in an urban area, the communication at low elevation angles can be hindered through natural barriers and/or man-made noise.

Hermes is capable of detection, tracking, command, control and receive/transmit data and voice from spacecrafts within its range. Most importantly, Hermes is the first GS to be publicly available, can be controlled and operated completely over the Internet for space operations, sending spacecraft signals over the network to authorized entities.

The Hermes-A GS is also a powerful laboratory that allows us to experiment and learn for ourselves about satellite technology from first-hand experience. It also serves other international institutions abroad like the Japan Aerospace Agency (JAXA), University of Michigan, the Graz University of Technology, the Swiss Ecole Polytechnique Fédérale de Lausanne (EPFL) and it is sometimes used for national safety purposes when monitoring possible spacecraft collisions on its range of 6000 km, like the event of February 5, 2010 between Iridium-33 debris and the EPFL SwissCube, section 6.2.1.3 (Jaffer, Nader et al. 2010d). The incident could be monitored only with Hermes due to its location. The novel use of Hermes is to pass along the signal of weather satellites to entities that would decode the signal and use it for disaster warning, prevention and mitigation, helping save properties and possibly lives.

Because Hermes-A is only the first of a series of GS, the data collected regarding automatic operations will be critical for future use. With several stations operating automatically, a user anywhere in the world can connect, monitor and control a formation of satellites from their single laptop, a capability that has not been realized by the satellite community so far.

Experiments were carried out to verify the technical capabilities of the Hermes GS by testing it for all four modes of Hermes operations (Alpha, Beta, Gamma and Delta) remotely (synchronous round-the-world test) to verify its capabilities to use as potential command GS for near-future university class nano-satellite missions, University of Michigan's Radio Aurora Explorer (RAX) (RAX-UoM 2011), Graz University of Technology, Graz, Austria's TUGsat1/BRITE (Launch: mid of 2011) (Koudelka, Egger et al. 2009) and the successor AusTriAn Lightning Nano-Satellite (LiNSAT) (Jaffer, Koudelka et al. 2008; Jaffer, Koudelka et al. 2010a; Jaffer 2011a; Jaffer and Koudelka 2011b; Jaffer, Koudelka et al. 2011c). Results are obtained by simultaneously downloading data and voice on four continents: North America (Michigan), South America (Ecuador), Europe (the author of this dissertation at TU Graz, Austria) and Asia (Japan). This demonstration serves to illustrate the cooperative efforts and ability of the virtual GS in the tracking of satellites and education of students. The satellites tracked include HO-68, ITUpSAT1, UWE-2, BEESAT, SwissCube, SO-67, CO-57, 58, 65, 66, RS22, RS30, AO51 and COMPASS1 (AMSAT 2011) and these coordinated studies are presented in Chapter 6 to inform the community about latency effects and the advantages that automatic operations may provide and can be utilized for formation satellite communications.

The basic design of the virtual GS (VGS) on the user side is based on a suite of free software namely, Ham Radio Deluxe (HRD, -Radio, -Sat Track, -DM 780) (HRD 2011) and VRS-Remote Monitor (VRS-RM) (VRS-RM 2011). The HRD functions as proxy of the real GS located at EXA and VRS-RM (central server) over the Internet using TCP/IP connection. There are four channels on the VRS-RM. Ch-1 and Ch-2 are the main and sub transceiver audio frequency (AF) respectively. The Ch-3 is for the reception of weather satellites. Ch-4 will be used for AF reception of video transmission from the Ecuadorian's first satellite, Pegasus, in development phase and launch expected around mid-2011. Optionally, Google Earth (GE) (GE 2011)

can also be integrated with HRD to enhance the results and virtual tours to GS area and satellite footprints. Using these and other software tools, along with Amateur radio equipment and a low-cost antenna, the GS is able to provide access to orbit for a multitude of users without each having to go through the costly setup. The design and implementation of the virtual GS in satellite research, development and space operations settings are discussed in Chapter 6.

The Amateur radio community has been involved with all these modes of communication over many decades and is responsible for standards in communication protocols, as well as packet radio, satellite development, and operations. The most common protocol being used for university built nano-satellite communication is AX.25 (AX.25 2011). By using their freely available satellites and co-operated university nano-satellites, along with Hermes becomes a great platform to learn more and more about these interesting and most practical applied fields. Many university student designers have worked closely with this group in order to benefit from existing design and operations standards, and to learn from past experiences.

The learning technique developed is "Hands-on-Space-Communications-Training." The big advantage of VGS is that no physical interaction with real equipment required to accomplish all operations; one remote user at a time with full control of Hermes. Among other GS networks are Global Educational Network for Satellite Operations (GENSO), initiated by European Space Agency (ESA) and many universities worldwide are taking part in this project. Currently it is in system testing phase and second release of open source software is expected to be March - June 2011 (GENSO 2011). Other GS of the same breed is Mercury GS Network (MGSN) of the Space Systems Development Laboratory at Stanford University. It supports two methods of controlling GS resources: an HTTP-based graphical user

interface (GUI), and a TCP-based session message server. Further details can be found on (MGSN 2011).

The satellites in LEO ~ 800 -1000 km have a communication window with GS around 12 - 18 minutes per pass providing only brief communication possibilities throughout the day. The university class small satellites are usually expected to remain operational for two years. Satellite tracking, telemetry/data decoding and checking health status of satellites using VGS is a great opportunity that benefits both experienced and novice satellite operators in post-launch space operations for the success of their mission.

5.2 Hermes I-2-O Gateway

An I-2-O gateway is a machine that acts as a connecting interface between computers or other devices connected to the Internet and computer systems orbiting the Earth, like satellites or even manned spacecrafts. Such connection is made when the I-2-O establishes a stable link between the spacecraft and a computer or a network of computers on the Internet, Hermes has no Terminal Node Controller (TNC), as its main job is to convert protocols from one network on the ground (Internet) to another network or device in orbit by routing and translating the radio signal received to a protocol that can be understood by a user-end TNC. It also has full remote GS operation capabilities. Hermes will serve transport, session and presentation layers, application layer will remain on the user side. The client station is implemented in Figure 5-1 using a software TNC, HRD- DM780 (HRD 2011) or MixW (MixW 2011). MixW has an advantage to use its notch filter feature to enhance the data reception.

The only one of the four Hermes modes (Delta) does not need a control interface to track the satellite for data reception. But optionally, Minotaur can be used for NOAA reception by controlling and tracking the satellites of NOAA series.

Contrary to a standalone normal GS, Hermes receives the telemetry and other data from LEO satellites and the audio frequency (AF) signal is relayed in real-time to remote users all over the world through Internet. The received AF is post-processed by a TNC: a software HRD-DM 780 or MixW on VGS as the decoding program at the user end. For online reception of the AF feed, the only requirement is VRS-RM running on the user PC having broadband Internet access. The user must have a public IP address authenticated by EXA to access Hermes, track the current operational satellites and receive telemetry signals live throughout the world. In that way the Hermes project transforms a simple laptop computer located anywhere in the world, into a full space-qualified GS. The gateway is shown in Figure 5-1.

The low-cost infrastructure, along with open source software for setup of VGS support future scientific missions as demonstrated with many examples mentioned above. The setup can accomplish many useful scientific investigations particularly, ash, cloud and lightning detection. Such a setup can be used for scientific missions in real-time data reception using the Internet to control the satellites remotely. The main emphasis is on low-cost GS infrastructure that can be used for university class nano-satellites. Hermes is the decoding and computing system. Minotaur can receive from 50 MHz to 2.4 GHz and Hermes can decode these signals. Hermes/Minotaur together forms an I-2-O gateway that is publicly available to universities.

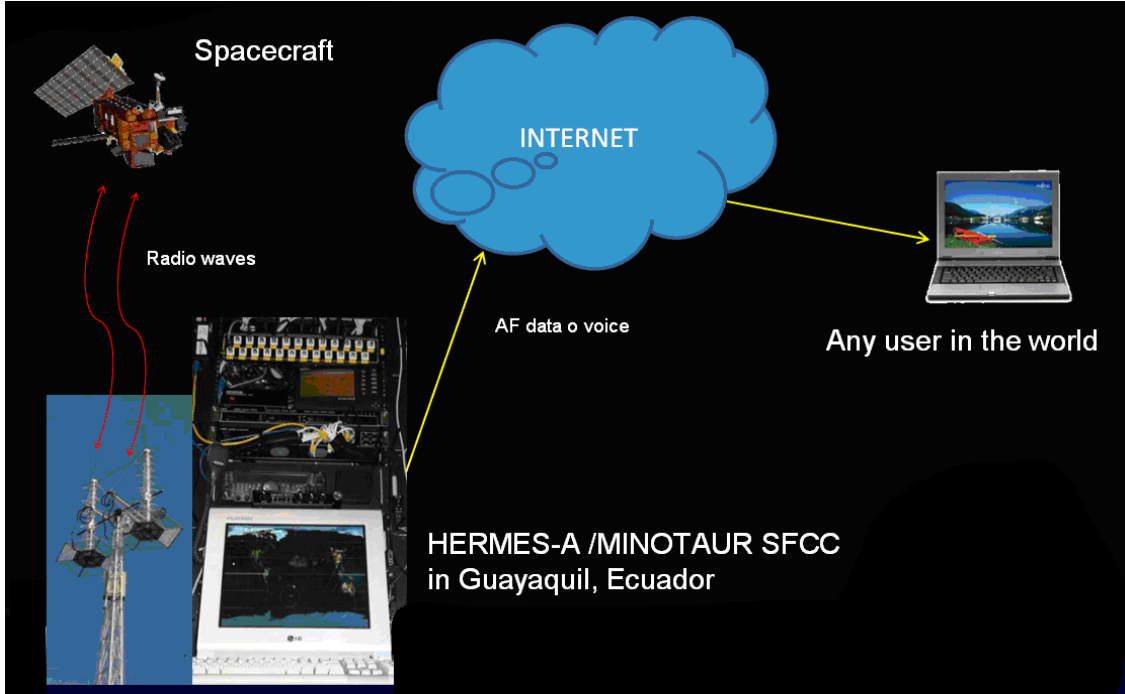


Figure 5-1: Hermes, I-2-O gateway, all modes setup at EXA

5.3 Operational Modes

The gateway can operate in four modes of analog and digital space operations.

MODE A (Alpha): Reception of data from orbit and relay through Internet

MODE B (Beta): Half/full duplex connection between computers on the Internet and orbiting satellites

MODE C (Gamma): Half duplex voice conversation between any computer on the Internet and manned spacecrafts

MODE D (Delta): APT/HRPT (High Resolution Picture Transmission) signal relay from weather satellites to any computer on the Internet

The Hermes is capable to handle four modes of operation. The voice mode is not within the scope of LiNSAT mission. The details along with obtained results of other three modes are explained in Chapter 6, 6.2.

5.4 Hermes: Implementation

Hermes-A/Minotaur is based in the coastal city of Guayaquil, is a command center and a control office. It is composed by the command and control centre (CMC) shown in Figure 5-2 and the Minotaur antenna array in Figure 6-3. All received information from satellite will pass through Hermes (Gateway) in the form of AF and received by VGS anywhere in the world (Figure 5-1). The Hermes-A/Minotaur works in broad ranges of frequency bands like VHF, UHF, 900 MHz and 2.4 GHz. Hermes-A server matrix processes the signal and serves the Internet gateway functions to relay the AF to the destined remote user. TNC transforms this AF into data from the satellite, telemetry, housekeeping, scientific, engineering etc therefore a remote user connected to university node authorized to access Hermes will serve as a VGS and can schedule the Hermes to transform it into an online and real-time automated remote virtual GS.

The CMC houses the

- Hermes-A radio engine
- Audio processing module
- AF Internet server
- Database server
- Firewall and

- 2- Control stations

The first control station manages the radio engine and the antenna array tracking for the target spacecraft (Figure 5-3)

The second control station manages the data decoding process and the target's space flight simulation and orbital prediction

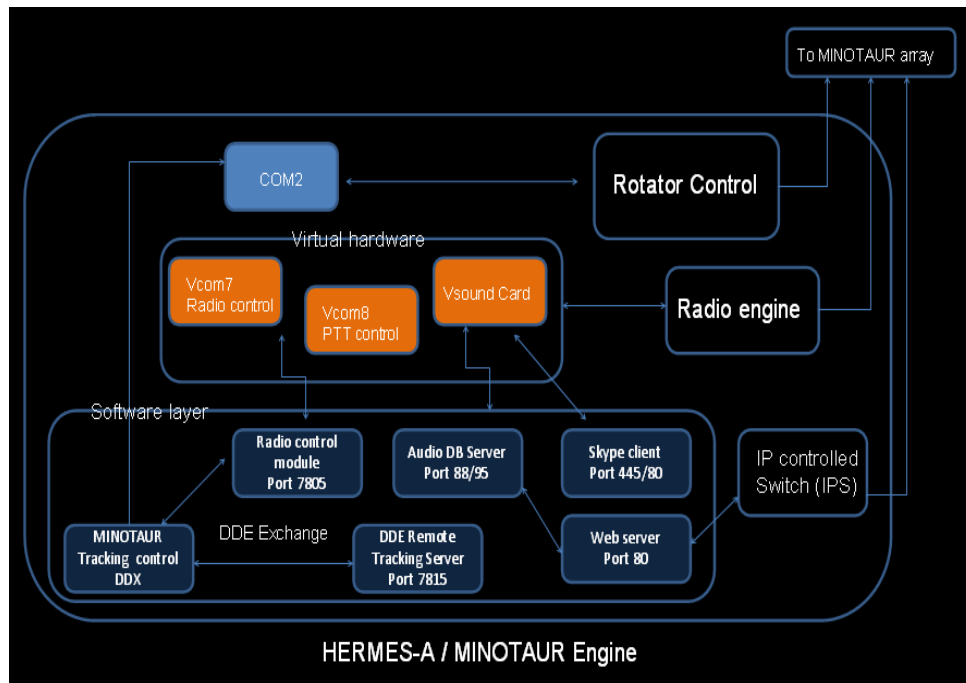


Figure 5-2: Project Hermes command and control center (CMC) Minotaur engine implementation, Courtesy: EXA.

Due to location of Hermes, the system has 0 to 178 deg view from North to South.

Hermes can handle the following range of frequencies with GS gain

2m:	180 to 172 MHz RHCP/LHCP	70 dB
70cm:	320 to 500 MHz RHCP/LHCP	75 dB
33cm:	830 to 950 MHz RHCP/LHCP (max. sensitivity on 913 MHz)	

23cm:	2.2 to 2.6 GHz RHCP	70 dB
QHA/APT:	137 MHz (NOAAs)	20 dB
Range:	22,000 km (Molnya Sat.)	
Radio Horizon:	Barriers, almost none. Hermes can receive signals from satellite 0 to 178° (AOS to LOS).	
Antenna:	Helical with Right Hand Circular Polarization (RHCP) and Left Hand Circular Polarization (LHCP) online switching capability	

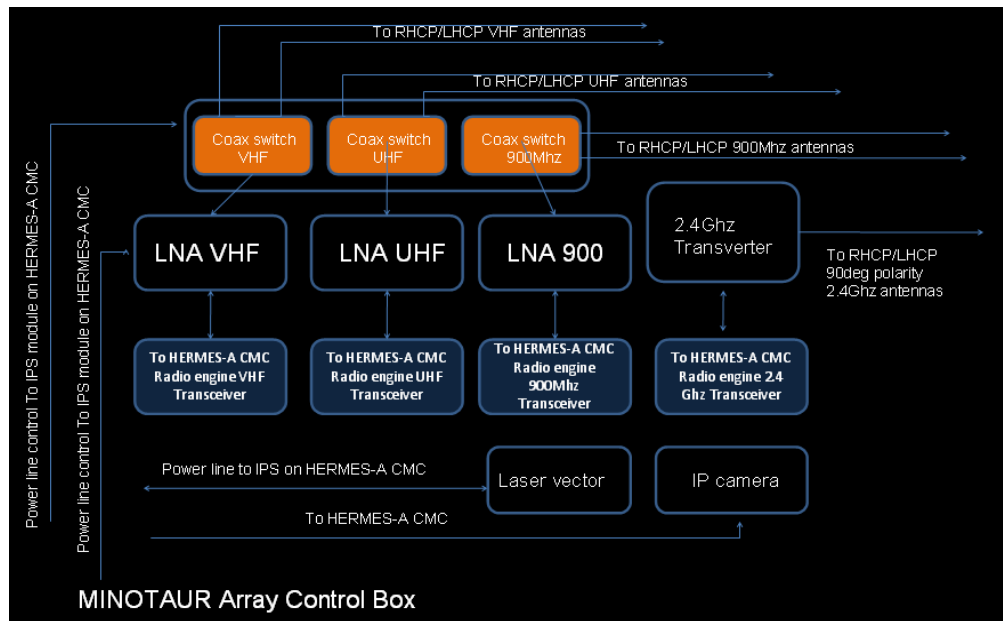


Figure 5-3: Minotaur array implementation, Courtesy: EXA.

The Minotaur is the high gain and highly directional antenna and its radiation patterns are shown in Figure 5-4.

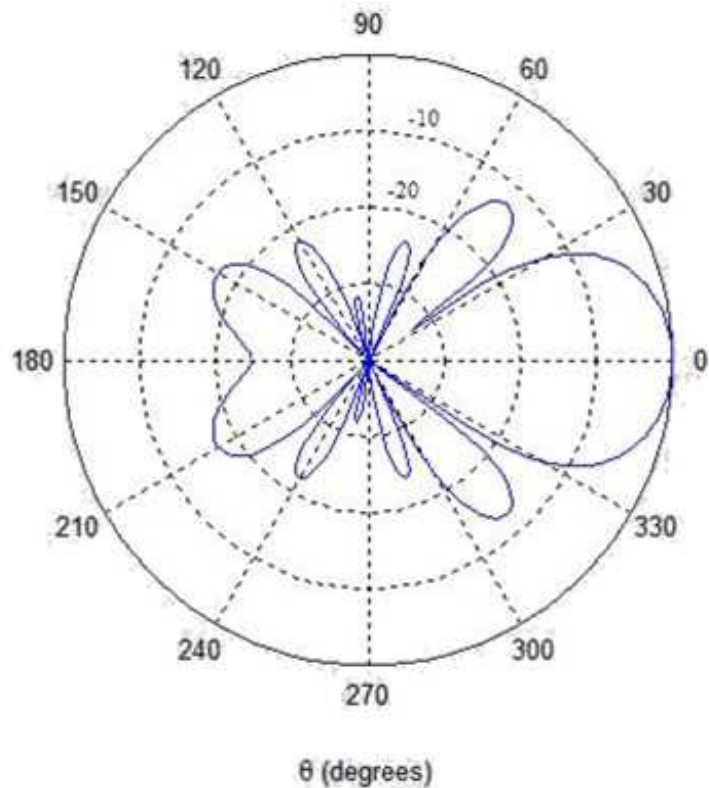


Figure 5-4: Minotaur antenna radiation patterns

Hermes-A is the first SFCC of a planned network of 5 SFCC. Hermes-B will be installed in the Galápagos Islands. Hermes-C and Hermes-D are proposed to be installed on Tacna, Peru and in Puerto Montt, Chile. Hermes-E will be installed on the Ecuadorian Antarctic research base Pedro Vicente Maldonado. Hermes expansion in Europe, UAE, India and Pakistan is under development. In its final configuration, the network can offer more than an hour of uninterrupted connection between Internet users and the satellite in orbit, representing a significant advantage for long term multi-satellite communications.

5.5 Automated Remote TU Graz GS (AR-TUG)

The cost is a major factor in the satellite development at universities. This can be reduced up to 10 % (Wertz and Larson 1996; Wertz and Larson 1999; Sandau 2006) by automating ground-satellite operations as these are routinely for limited times per satellite pass in LEO. Use of COTS components designed for non-space applications is one of the driving philosophies of university class satellite design for fast and inexpensive construction. Another paradigm growing faster is to reduce GS operation cost by automating the GS and to operate it remotely whenever required. The mission requires extensive but short time usage like determining position of spacecraft in space (updating TLEs frequently), receiving and executing commands from GS to receive specific data (science, engineering payload, telemetry beacon etc), and to switching a subsystem on/off and/or uploading configuration/new software and many more. Among many other requirements is the Doppler compensation with a computer program along with tracking and updating TLEs. Many of the above mentioned requirements do not need personnel presence the whole day, as the communication window of LEO satellite depending on maximum elevation (MEL) is 10 - 20 minutes a satellite pass.

The basic design of the automated GS on the user side is based on free software suites. The design and implementation of the automated GS can be used for current operational and future university satellites. A basic architecture of the single existing system and the benefits of its adaptability to be included in GENSO are discussed. Details of the software tools and their applicability to tracking, monitoring and processing are also provided as used by students and researchers performing GS operations.

Among other open-source software, HRD is very common and popular among Amateur and students involved in GS operations for university class small satellites. One limitation of HRD- Satellite Track is that it does not have a function to switching automatically to approaching satellites available in the satellites' list. Free software SatPC32 (SatPC32 2011) can replace it with this built-in capability. The scenario of its use here is to allow remote operation, i.e. to operate with SatPC32 using computer when the hardware (Radio, Antenna and Rotator) is not residing locally.

This software along with voice operated switch (VOX) function of TRX and/or any free trigger-sound recorder software forms a setup to perform automated TUG-GS operations. The TUGSat-1/LiNSAT-GS setup is shown in Figure 5-5 and Figure 5-6.

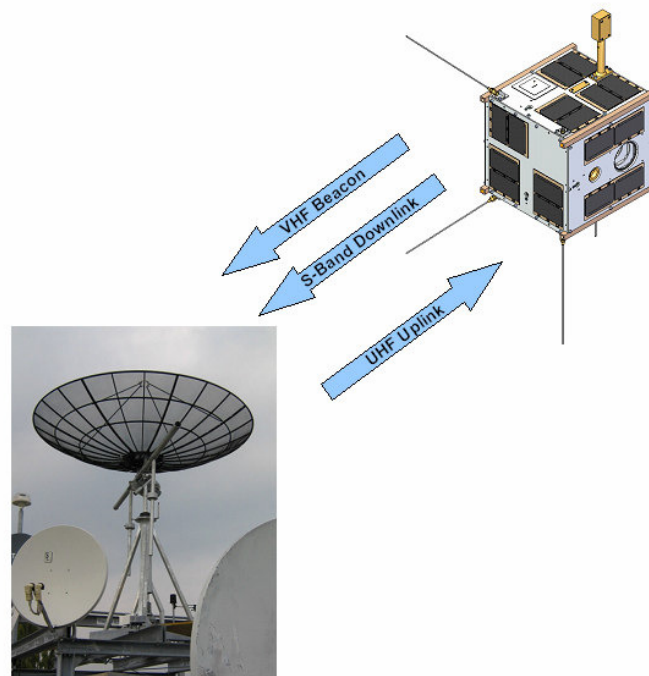


Figure 5-5: TUGSat-1/ LiNSAT-GS communication bands

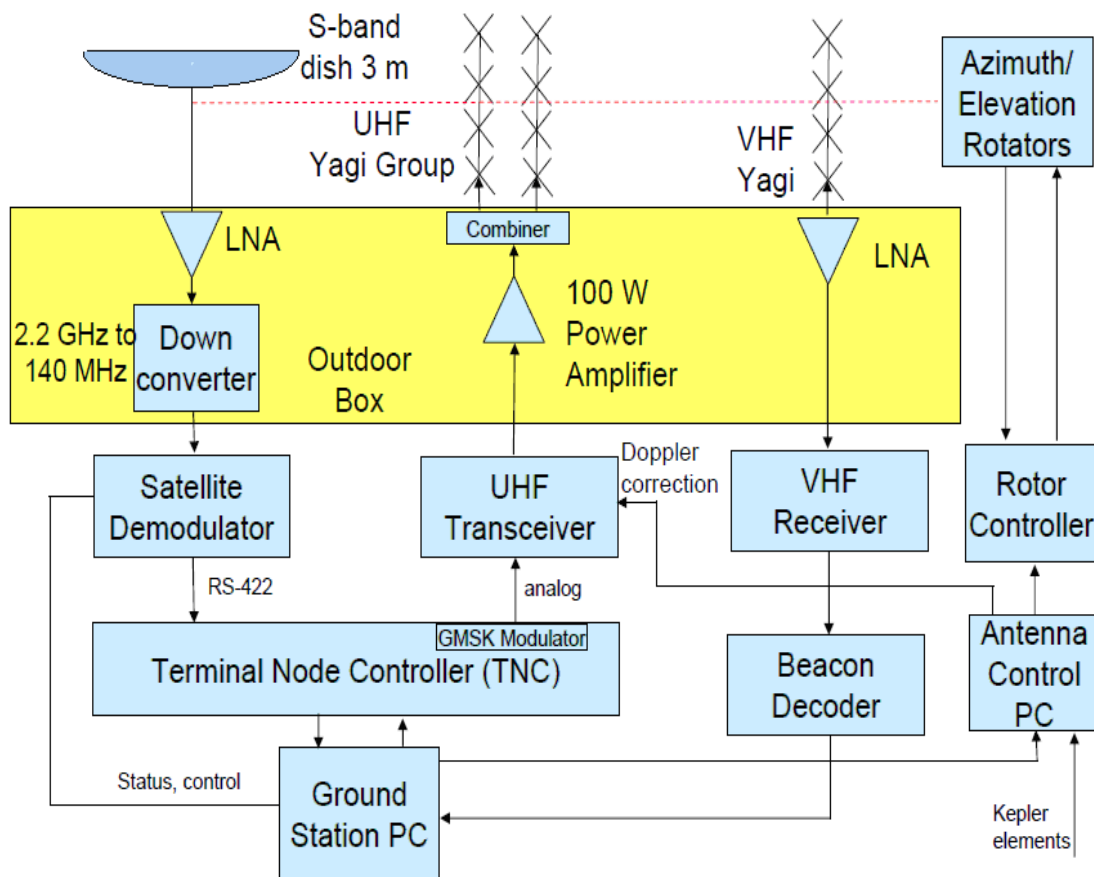


Figure 5-6: Block diagram of TU Graz GS (AR-TUG). Adopted from (Koudelka, Egger et al. 2009).

The recording of data for real-time or later processing and analysis is performed with VOX feature of Trx and/or trigger-sound recorder software to store AF signals with predetermined SNR.

5.6 AR-TUG Implementation

SatPC32 is tested with this setup. The CAT interface works perfectly for Doppler frequency compensation and antenna Azimuth-Elevation rotation and most important for remote operations; automatic satellite reception in queue. AF

decoding process starts with VOX and other sound-trigger software using pre-defined SNR.

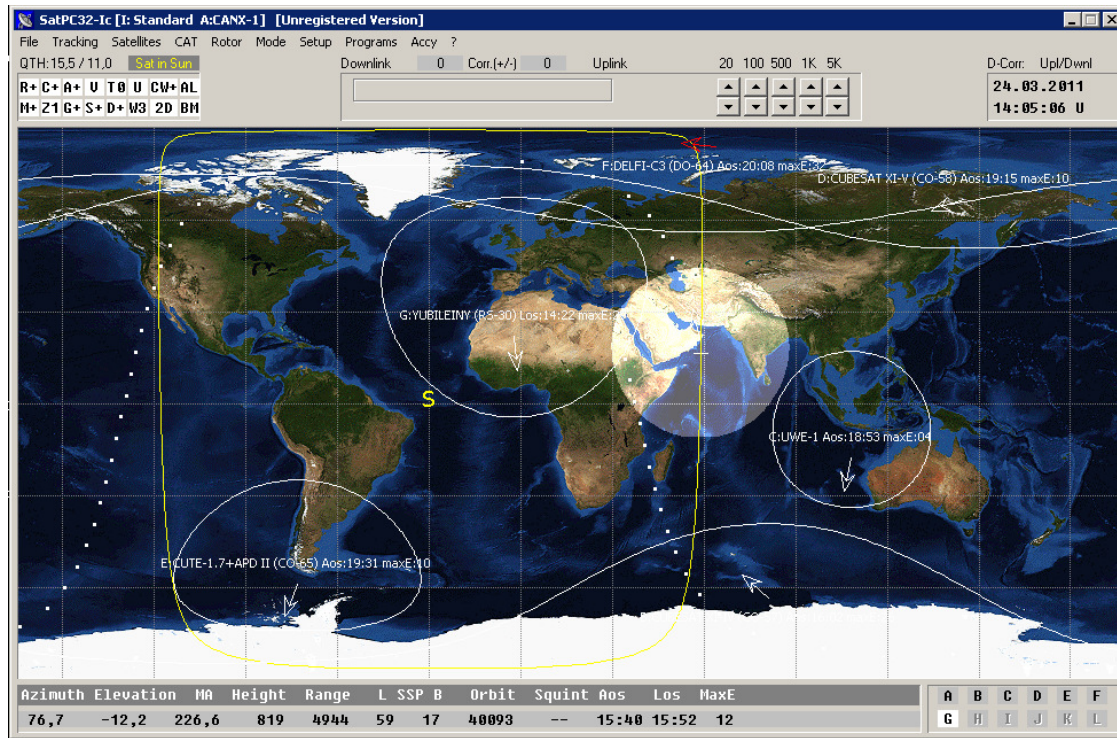


Figure 5-7: SatPC32 screenshot

To perform automated remote operations, the program can control over a virtual serial port (SatPC32 2011). The output of the CAT control is sent directly to a (physical or virtual) serial port (it can also be sent to the Kansas City Tracker (KCT)/Tuner thus the radio can be steered via the serial ports of the KCT/Tuner.

The results obtained with this setup indicate that Satpc32 readily can transform a real GS into an "autonomous virtual GS". By using a scheduler for automated GS that will work at the user end and current studies help support a future autonomous mode. A software for automation and/or adapt HRD-SatPC32 for this purpose will need to be developed.

5.7 Amateur License Requirement

Authorized GS can collect scientific/engineering data and command any one of the spacecraft's subsystems, not destined for the ordinary user. The most important requirement for mode Beta and Gamma is to hold an Amateur license (ARRL 2011). The Hermes GS will also be able to upload updates of on-board software to the nano-satellites. The relevant information is incorporated in Table 5-1.

Table 5-1: Information about all four modes of satellite operations

Issues/Modes	Alpha	Beta	Gamma	Delta
Modulation	CW, USB	CW, FM	FM	AM, FM
Data reception	Telemetry AF Receive-only	HDX Data Tx, Rx FDX (dual mode)	HDX Analog AF Tx, Rx, FDX (dual mode)	Weather AF receive only
Amateur License	No	Yes	Yes	No
Sync. Loss	No	No	No	Yes
Network Latency	Yes	Yes	Yes	No/Yes
Satellite Tracking	Yes	Yes	Yes	No/Yes
Doppler Shift (Detectable at AF)	Yes	Yes	Yes	No
Accomplished	Yes	Yes	No (API: future task)	Yes

The most important requirement for all remote users participating in the space operations is to hold the license to transmit on Amateur entitled bands (e.g. 2 m, 70 cm band), where most of the AMSAT or/and university class nano-satellites

are/will be communicating with their satellites like TUGSat-1 and LiNSAT. The Hermes accepts all transmissions encapsulated in AF.

The advantage of both receive-only modes, Delta and Alpha, is that there is no requirement for obtaining Amateur license for all remote users participating in the project Agora. Furthermore, as a redundant confirmation, remote users were all times in contact with local operators in Ecuador who were responsible to turn off the system if required (as per US, Ecuadorian, Austrian and Japanese law). For mode "Alpha and Delta", certainly, anyone can receive without a license.

5.8 Chapter Summary

The existing GS infrastructure to be used for university-class nano-satellite missions is investigated and an online I-2-O gateway is selected to serve LiNSAT as a potential remote GS for transmission and reception of its constellation.

Hermes/Minotaur is the first I-2-O-gateway in S-America region. Hermes DFCCs are automatic and do not need human intervention; however it embodies an excellent laboratory for high end space research and scientific outreach.

The I-2-O gateway is of great significance to use as a single-node command and control station for the satellites in a constellation, such as the planned LiNSAT is comprised of three identical nano-satellites for global coverage. To test and verify Hermes as a potential GS for TUGsat-1 and LiNSAT, the Amateur satellite community has introduced "a free access paradigm" to the whole world.

The functional capability of the I-2-O gateway "Hermes" as LiNSAT GS is detailed with the outcomes of tracking and commanding by remote users as well as real-time data processing from many satellites in orbit. The ground segment is of

utmost significance to use as a single-node command and control station for the satellites.

The other automated TU Graz GS (AR-TUG) is proposed and implemented as cost efficient operations: implementation with open source/free software and in this way its adaptability to GENSO/other networks becomes feasible. Online GS network for real-time reception and command/control of constellation and formation flights and moreover online and real-time data availability as well as real-time troubleshooting becomes evident for its effective usability in real-time.

Chapter 6 Ground Segment Performance

Verification

6.1 Introduction

Experiments were carried out to verify the technical capabilities of the Hermes GS by testing it for all four modes of Hermes operations (Alpha, Beta, Gamma and Delta) remotely (synchronous round-the-world test) to verify its capabilities to use as a potential command GS for nano-satellite missions. To avoid any noticeable latency in remote connection to the GS, a 512 kbps Internet connection was found to be good enough for clear reception. Multi-user test runs were verified where each participant was able to track the satellite, control the GS, and receive telemetry from a NOAA satellite. The configuration setup is elaborated in 0. Their Internet connections was found to be capable of handling the AF input load. All remote users decoded received AF signals

1. APT with WxtoImg (WxtoImg 2011)
2. Telemetry/housekeeping data using software-TNC

The software used for NOAA decoding included WxtoImg, a fully automated weather satellite recording, decoding, editing and post processing software with

the enhanced features like map overlays, 3-D imaging, animations, projection transformation etc. Its automatic processes featured the ability to decode and create images, anaglyphs, animations and movies. The software-TNC, MixW has an advantage over HRD- DM780 to use its notch filter feature for easy processing.

6.1.1 Virtual GS Implementation

The PC running this tracking program determines azimuth/elevation angles of antennas versus time and drives antenna rotators to compensate for spacecraft movement. As a result, the antenna points correctly to the spacecraft and follows its movement in the orbital velocity vector above horizon, from AOS till LOS.

The tracking system also compensates for Doppler shift on transmit and receive frequencies due to the significant relative movement between spacecraft and GS. These frequencies are shown on the HRD-Radio software as VFO-B and VFO-A respectively.

Satellite tracking, remote controlling of communication radio, acquisition of data and post processing are generally too complicated to be processed and displayed by one or two computers alone. The remote users have generally distributed processing of the entire setup using several PCs with multiple displays. While this setup has been run on a single laptop, a common distribution is as follows.

The 1st PC performs communications control using HRD-Radio and Hermes web interface IP antennas on-board and external cameras and antenna polarity selection. The interface is shown in Figure 6-1.

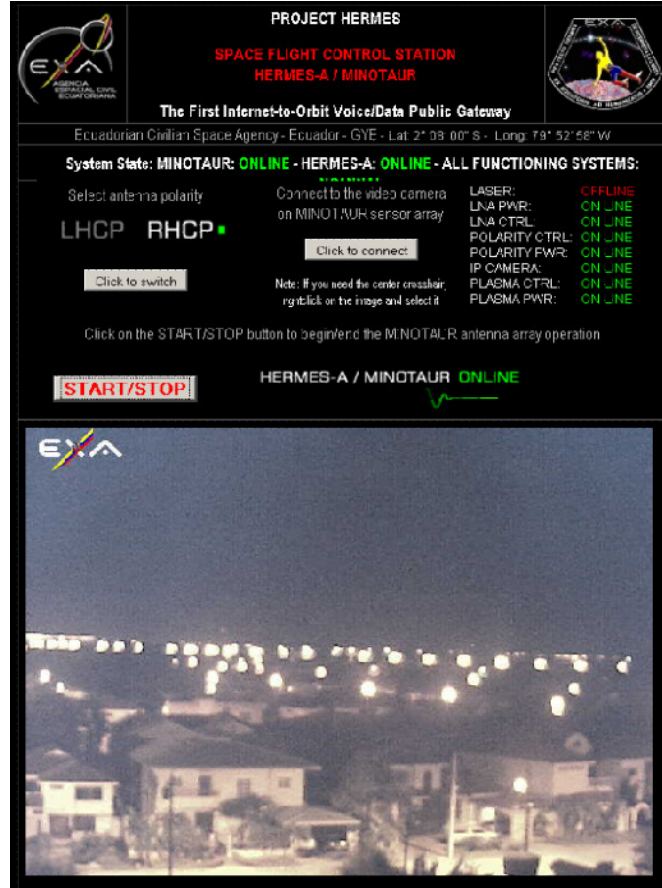


Figure 6-1: The communications control using Hermes Web Interface to run/stop, antenna polarity selection and on-board IP camera. An important interface for remote users

The 2nd PC functions orbital control using HRD-Sat Track, HRD-Antenna Rotator (AlphaspidRAS; working on local PC at EXA results shown remotely at user end) on 1st monitor display and Google Earth on the other. The 3rd PC carries out decoding/data processing using HRD-DM 780 or MixW, as a network client of the 1st and 2nd PC, so the decoding program can track the frequency changes. The 4th PC performs orbital simulation running STK simulation of the current NOAA satellite showing the orbital mechanics data in real-time. The STK real-time simulations are well synchronized. Initial setup for weather decoding and processing can be found on the Project Agora website (Agora 2011). If a faster PC is

used, then both HRD-Radio and HRD-Sat Track can be run on a single computer. A real-time STK simulation is shown in Figure 6-2

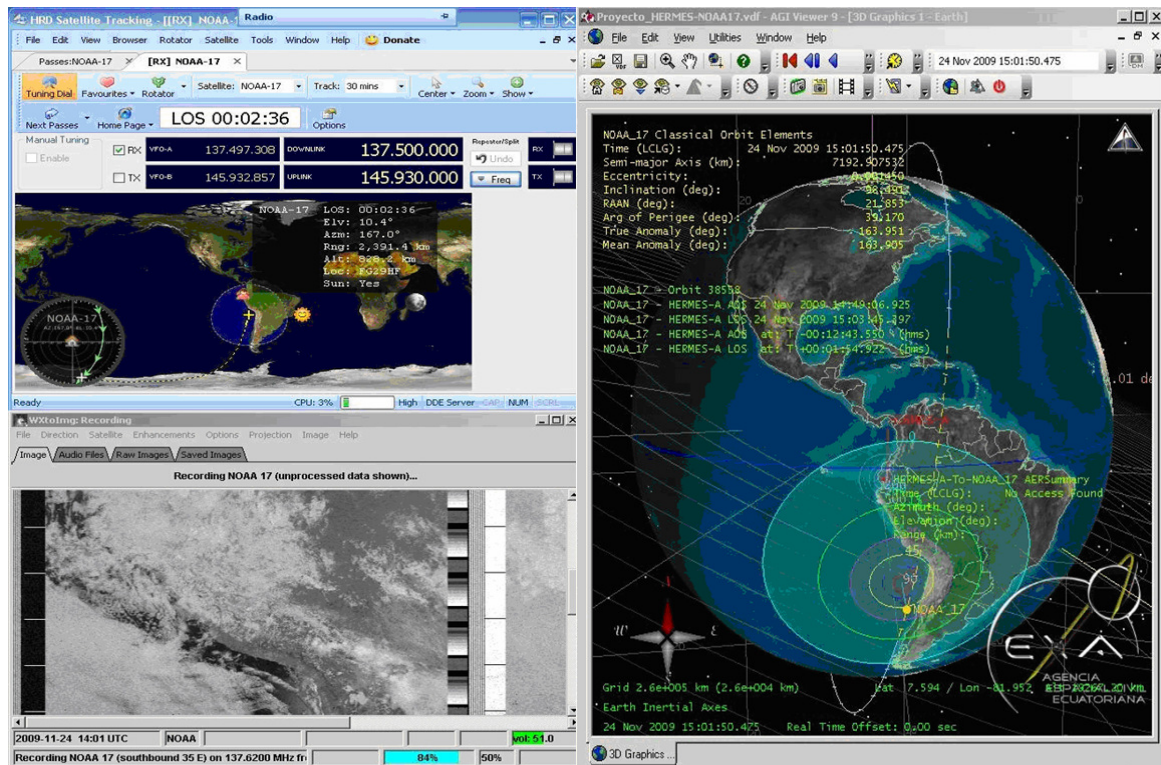


Figure 6-2: A real-time STK simulation while capturing NOAA-17 in mode delta operation. The simulation shows the orbital data.

The Minotaur array has 2 IP cameras, one on-board and one outside, pointing to the array. Figure 6-3 (Minotaur 2011) shows both camera views.

Using only one node at the remote user end to connect through Hermes with all satellites in a constellation is an advantage. Moreover, expansion of the Hermes network will allow us to connect to satellites for more than 1 hour uninterrupted instead of an average communication window of 10-15 min. in case of LEO satellites.

The multifold benefit of automating and scheduling this network through end user is foreseen. As Hermes is an OSI model gateway, a remote user can use any

compatible technology for automating the programs at the user end PC. Hermes will wait for the scheduled program to follow. Therefore, scheduling and automating is all about user end OS (Microsoft Windows, etc), not Hermes itself. It is designed to give the user total agility and flexibility.

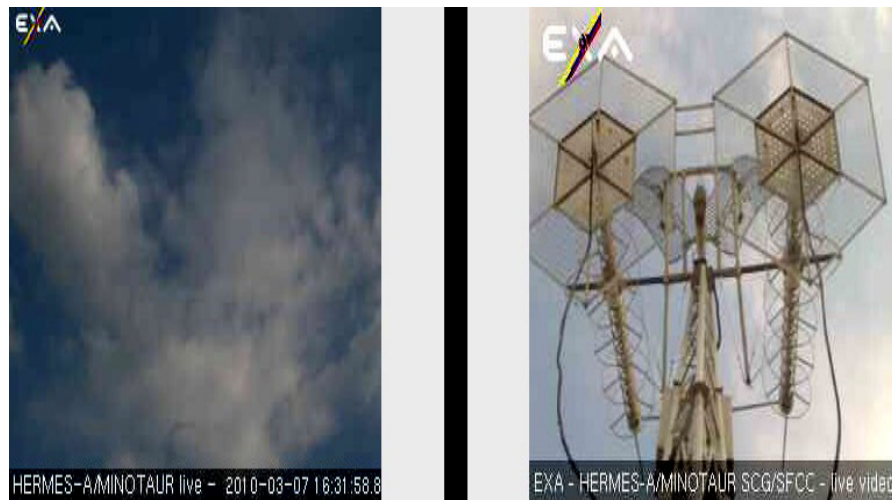


Figure 6-3: The Minotaur Array on-board and external camera view: Important for VGS user to see live tracking

One proposed setting could be to have a combination of SatPC32 and HRD as a future task, the reason to use a dual setup is the need to put the satellites in queue (SatPC32) and Dynamic Data Exchange (DDE) on HRD connected to Hermes.

From the bandwidth perspective, around 1200 remote users can connect simultaneously using VRS-RM to download operational NOAA and/or Amateur satellites. Therefore, selective universities worldwide can be facilitated (Nader, Carrion et al. 2010a). All other virtual GS in all four modes are shown in Figure 6-4, Figure 6-5 and Figure 6-6.

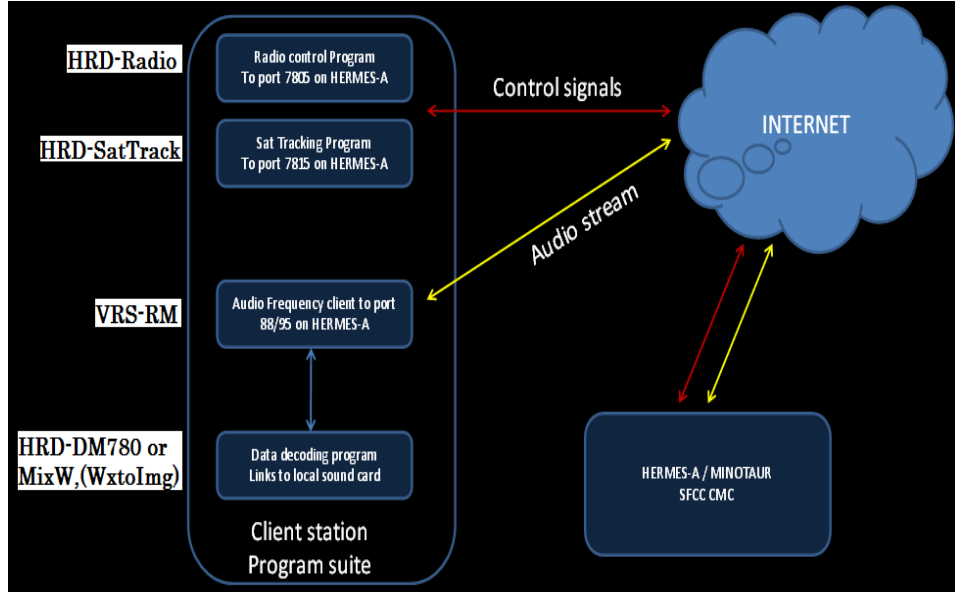


Figure 6-4: VGS for Data RX/TX: Hermes Client station implementation.

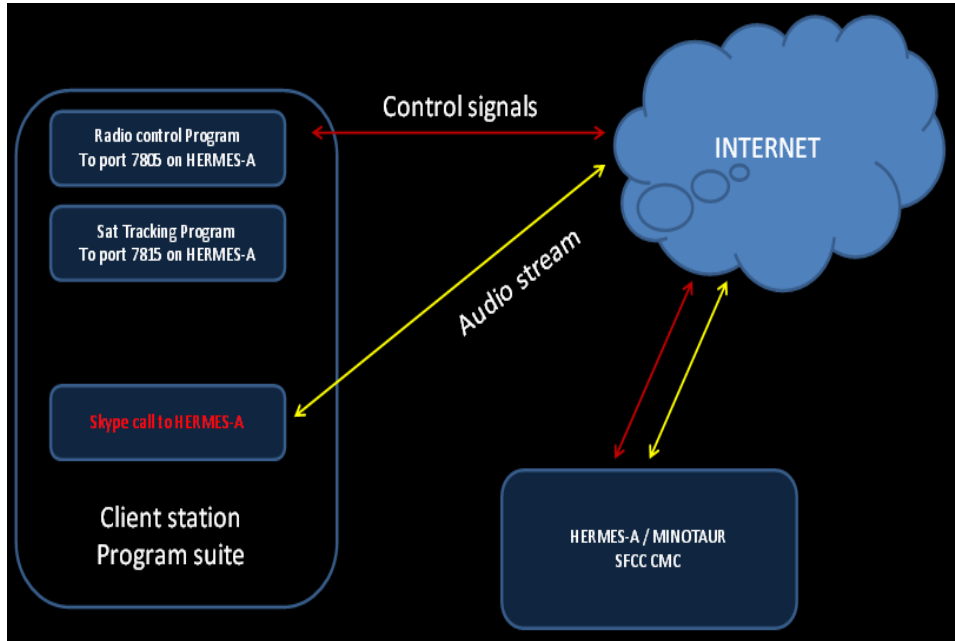


Figure 6-5: 2-Way Voice RX/TX: Client station implementation

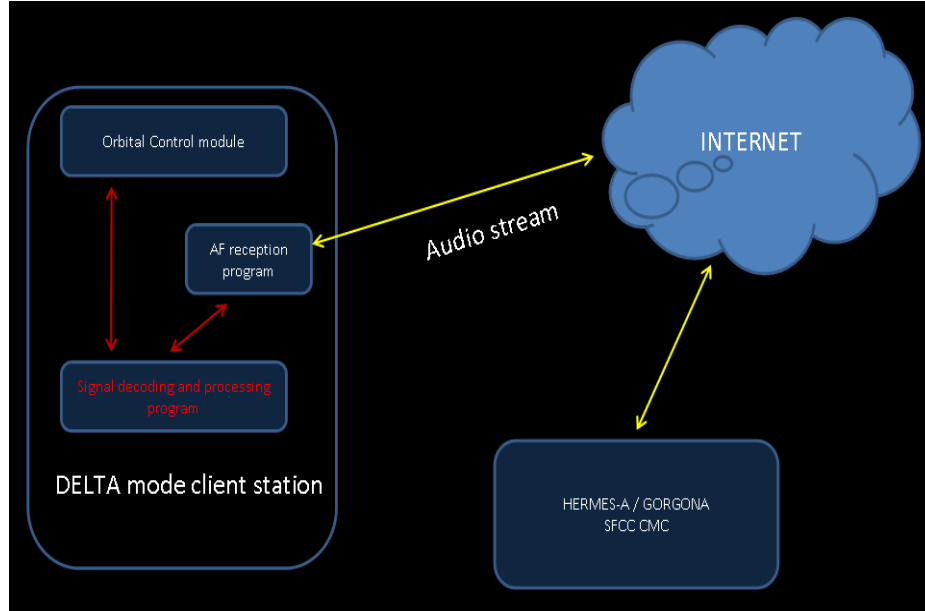


Figure 6-6: Hermes Delta mode client station. The APT from NOAA is received and relayed to remote users in real-time through Internet

6.2 Operational Modes: Results

6.2.1 Alpha Mode: Data Receiving Only

In this mode of operation, the user only receives the AF input of the target spacecraft (i.e. RS-30). The HRD - Sat Track program is an automated Doppler compensation program. It lets the remote user to select target satellite and commands Hermes-A to track the satellite accordingly and manage the Doppler frequency shift. After the satellite is acquired through Hermes, the remote user receives the satellite AF on VRS-RM channel 1 or 2 from the PC soundcard via Internet. The soft-TNC transforms this AF into the required data. The Hermes saves the AF as a sound file for accessing and processing it later.

6.2.1.1 ODR Experiment

To test Hermes reliable communication, it was used in Omni Directional Reception (ODR) state and the low noise amplifier (LNA) was shut down. The ODR is a state of Minotaur array at MEL (90° elevation, looking zenith direction). The telemetry from RS-30, CO-58 and AO-51 with acceptable SNR were received. From all of our experiments, it was evident that even in the worst cases signals from even faintest satellites were received. The suite of free software used to accomplish this and other modes of operation are shown in Figure 6-7 and Figure 6-8.

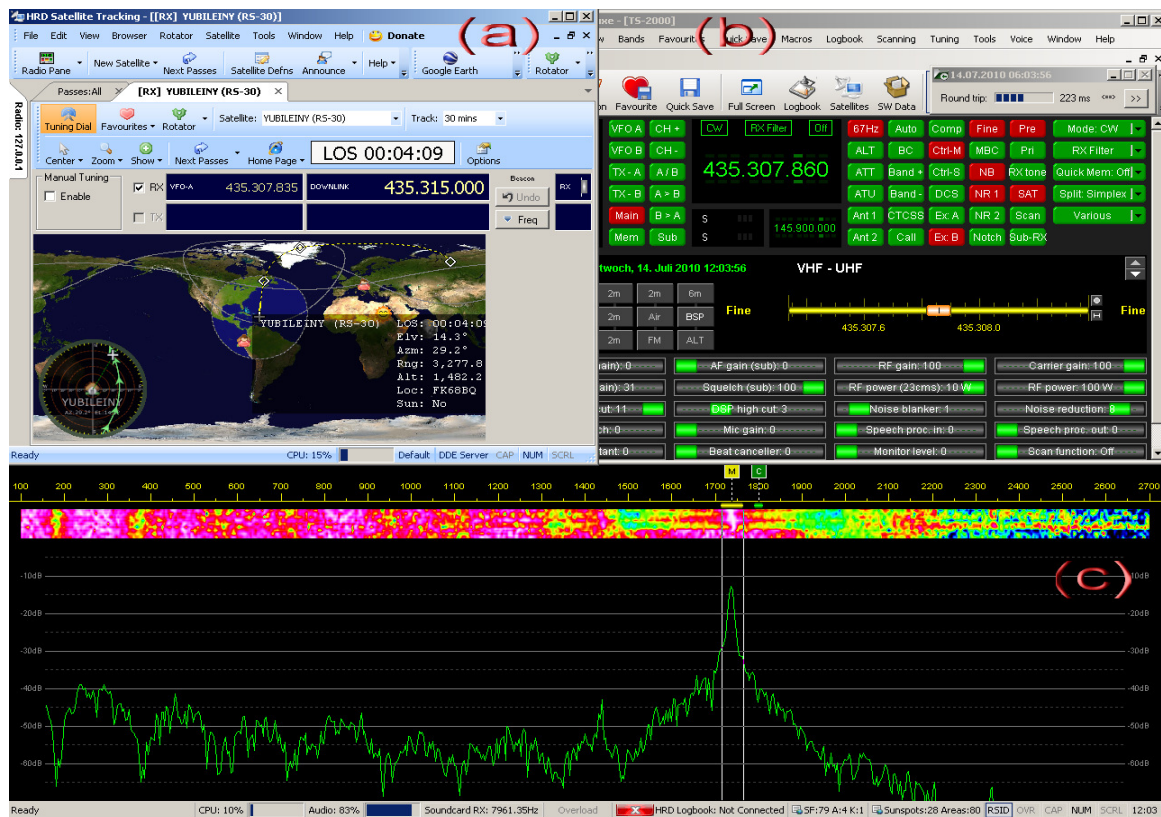


Figure 6-7: Alpha mode with Russian satellite RS-30, Yubileiny, tracked and received TLM beacon, (a): a screenshot of HRD-Sat track, (b): HRD-Radio engine as proxy of Kenwood TS 2000 Trx and (c): the received and analyzed telemetry beacon with HRD-DM780 in real-time

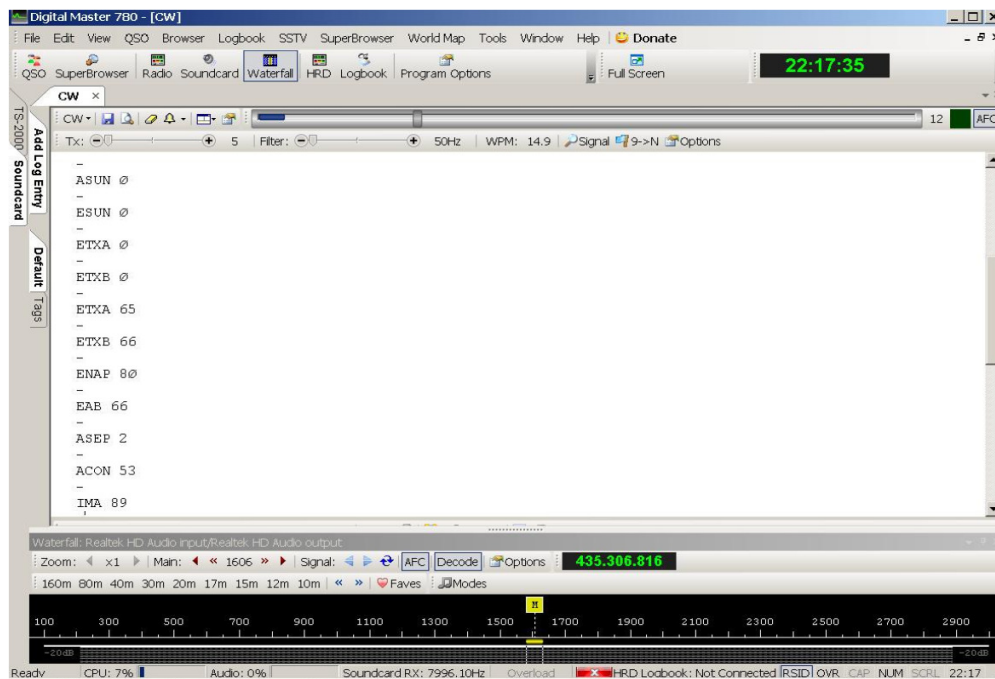


Figure 6-8: Russian satellite Yubileyne (RS-30) received and decoded in real-time

6.2.1.2 SwissCube Rotation Rate

As compared to AR-TUG, the spin rate determined by Hermes was low due to its location near the equator. On 29 June 2010, at AR-TUG, the received noise beeps were repeating every 4 sec, so satellite was spinning ~ 15 rpm. DK3WN (DK3WN 2011) calculated history of spin rate in 2009 as under: Apr 26 => 21 rpm, Mar 12 =>26 rpm, Feb 06 => 28.5 rpm, Sep 28 => 37 rpm.

Due to magnetic field variations, the SwissCube appears to function normally over Ecuador (above Equatorial region) and spins wildly over higher latitudes i.e. in Austria, Germany, Switzerland and Netherland.

6.2.1.3 SwissCube Near-Miss Event

On February 5, 2010 at 05h20.23 -5:00 UTC, the Hermes-A/Minotaur monitored the pass of SwissCube-35932 an Iridium-33DB-34891 that could pose a threat of

collision. The pass occurred without incident, however the only GS in view of SwissCube and able to monitor it was Hermes-A.

The live signal was routed via Internet to the EPFL Space Center and the Space Operations Division (SOD) crew at EXA could receive the SwissCube signal loud and clear from AOS till LOS at a range of 3115km N-bound. Signal analysis indicated the distance between the objects was 1058 m at the closest approach.

The EXA-SOD continued to monitor the objects when within range for the next few days and found that SwissCube remained safe. The STK simulation created at EPFL shown in Figure 6-9 was verified by Hermes results.

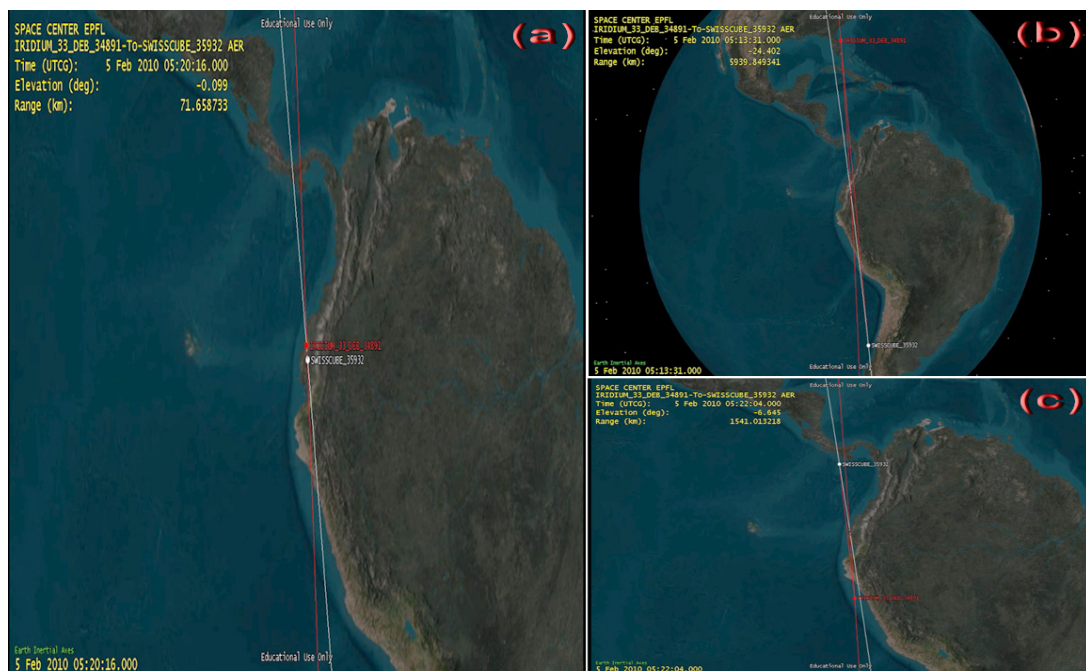


Figure 6-9: February 5th, 2010 a near-miss collision between Iridium-33/COSMOS 34891 debris and the SwissCube occurred. (a), angle between the two orbiting/approaching bodies ~ 0.09 degree (b), objects approaching (c), post-event

The near miss event made evident the need of this online and real-time tracking and monitoring as the Hermes-A/Minotaur team did by tracking the satellite

signal over the Internet in real time to monitor if the collision was to happen. In coordination with EPFL, remote users were able to watch the pass in real-time.

6.2.2 Beta Mode: Data Transceiving

In this mode of operation the user is able to receive the AF input of the target spacecraft in range and transmits to it as well. A half duplex communication is established if the spacecraft is operating in one band only, but full duplex communication can be established if the spacecraft operates in mixed modes like Mode U/V or Mode J. Many Amateur satellites in beta mode use Audio Frequency Shift Keying (AFSK) packets to transmit housekeeping data. These packets data can be decoded using either the TNC along with a radio transceiver or sound card of a PC and decoding software like MixW. For this mode, Compass1 was commanded with specific sequence of dual tone multi-frequency tones (DTMF) to activate its transponder for transmission of CW telemetry beacon and AFSK housekeeping data. At the user end, the data were analyzed in real-time, shown in Figure 6-10. The transmission link is somehow tricky to send DTMF tones through Skype, requires proper isolation from the receiving link.

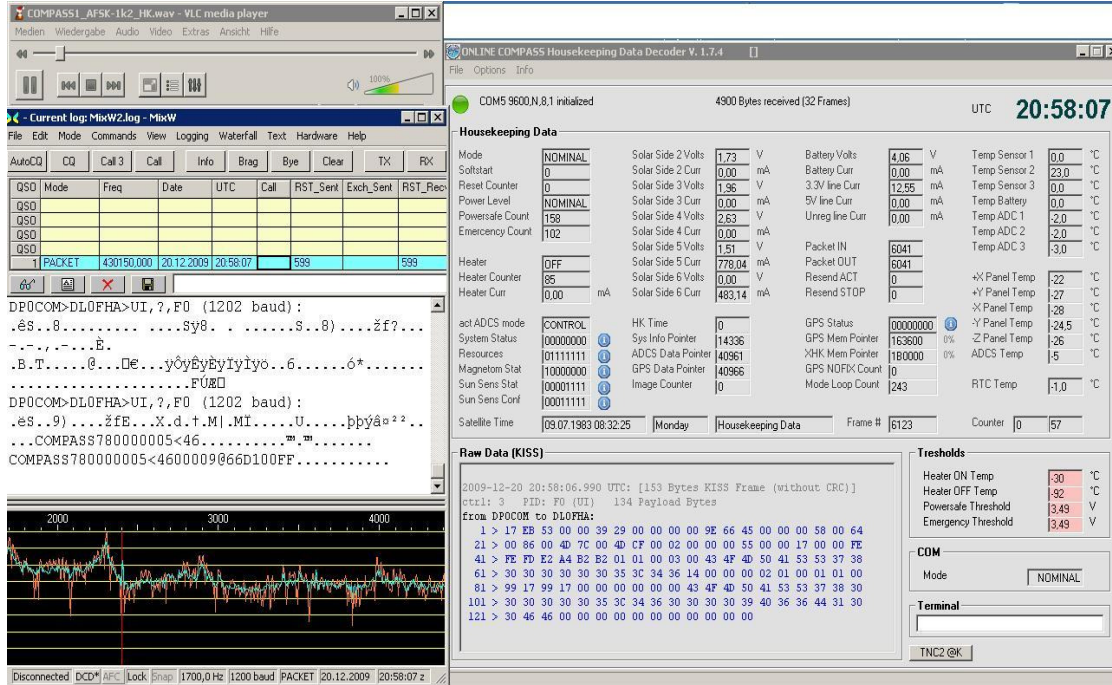


Figure 6-10: Mode Beta: Compass-1 tracked, commanded with activation codes and housekeeping data was analyzed in real-time

6.2.3 Gamma Mode: Voice Transceiving

This mode of operation is used to establish a half duplex voice communication with a manned spacecraft in orbit. (e.g. AR-ISS, AO 51, HO-68 etc). The relevant information is out of the scope of this dissertation.

6.2.4 Delta Mode: Weather Satellite Data Receiving

In this operating mode, a user receives the AF input from a passing NOAA satellite transmitting an APT signal and decodes it to translate into an image as the

spacecraft passes over Hermes-A gateway. APT data is transmitted continuously as an analogue signal using AM with a 2400 Hz sub-carrier on an FM carrier.

The lightning is a natural hazard, can trigger forest fire and also is closely associated with volcanic eruption. By using NOAA APT along with LiNSAT, the lightning detection and possible effects of lightning can be investigated using multi-sensor remote sensing techniques.

Among other findings, two captured and post processed images are shown in Figure 6-11 and Figure 6-12. The first image is a composition of images from NOAA 15, 18 and 19, received by Hermes from the satellites directly during the heavy South American rainfall of March 2010. It is a thermal enhancement. The high temperatures can be seen on Atacama Desert of Chile and in Venezuela that stresses the problems of blackouts due to dependence on hydroelectric power. The second image is enhanced using scheme 'MCIR-with precipitation' during the thunderstorm season. The cloud charging effect can be easily seen. In the third figure, some enhancements and color palette to differentiate cloud, ground, surface etc are shown that were applied at the virtual GS during image processing. Other features are extracted like regional temperatures (blue to red) and 3D anaglyph to get insight cloud structure.

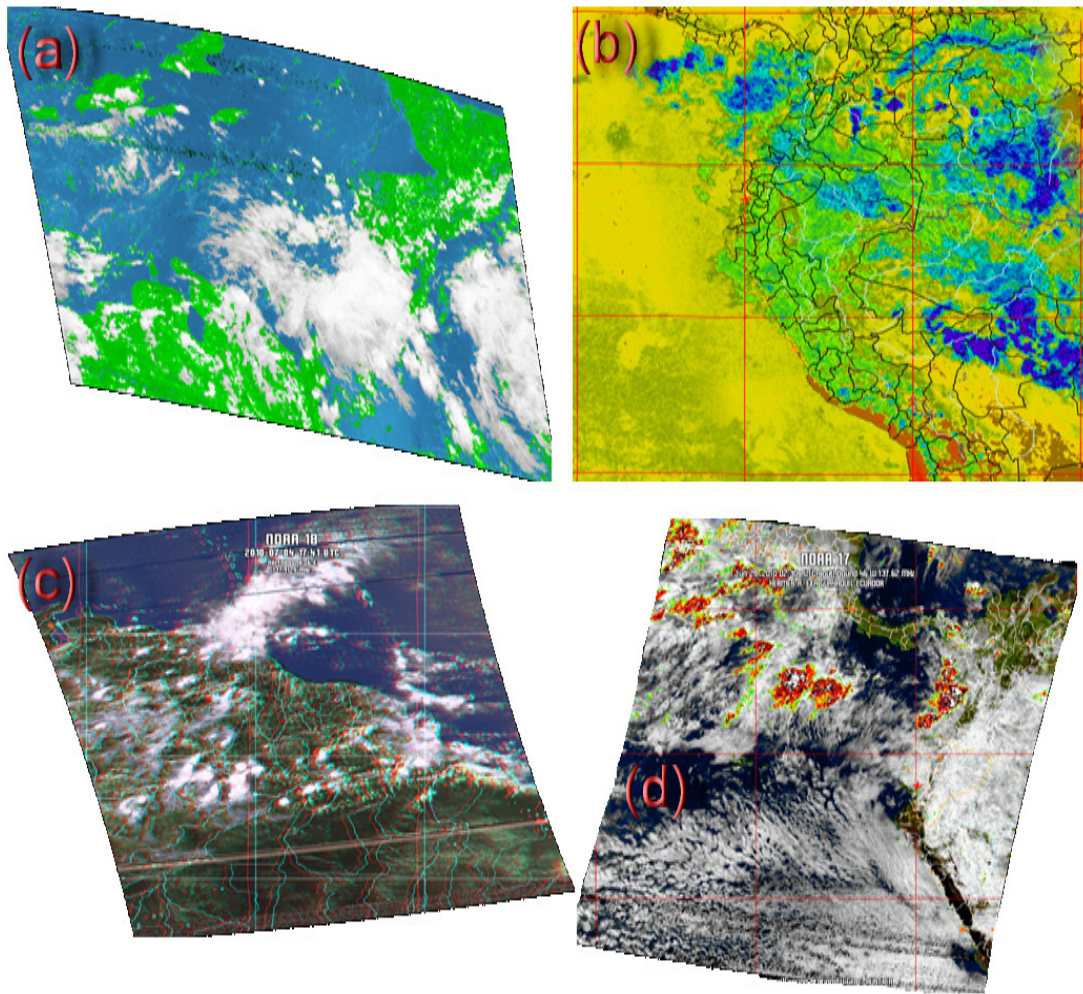


Figure 6-11: Enhancements used at virtual GS: (a): Color palette to differentiate cloud, ground, surface etc, (b): Composite image from NOAA 15, 18 and 19 with Thermal enhancement showing regional temperatures (blue to red), (c): 3D anaglyph to get insight cloud structure, (d): Enhancement showing precipitation

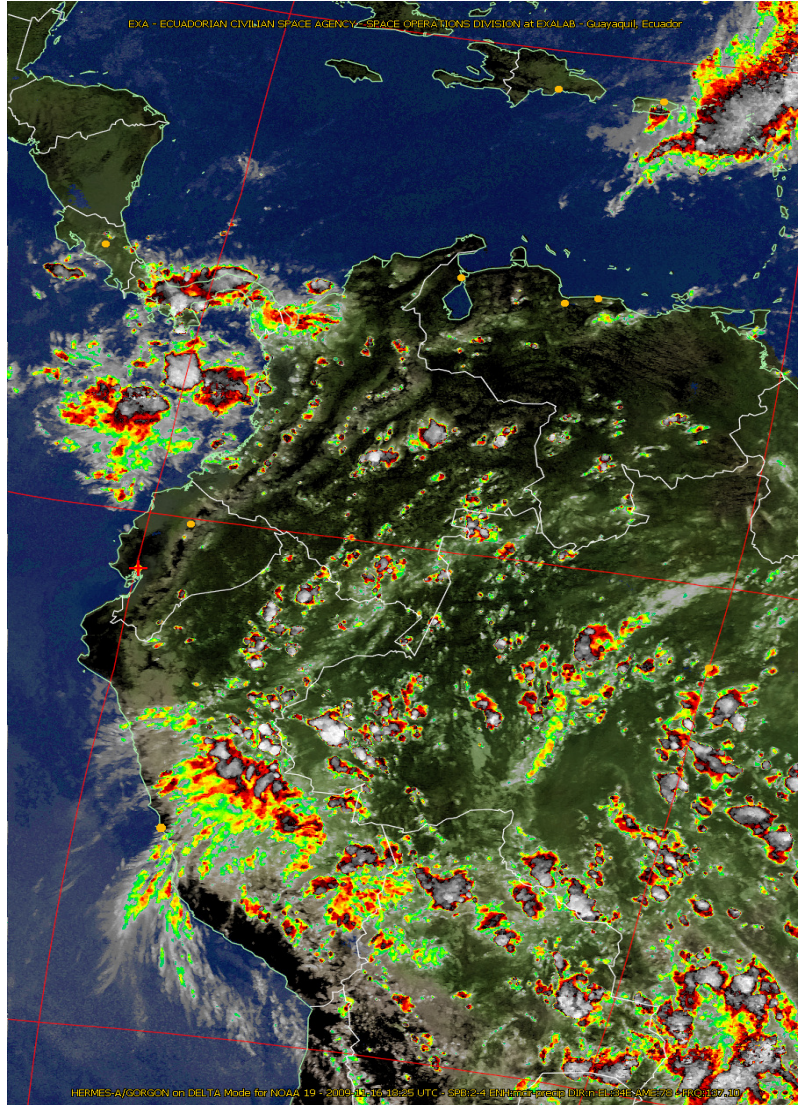


Figure 6-12: Multi Spectral Analysis (MSA) - with precipitation enhancement showing cloud charging during high thunderstorm activity in Ecuador. With this enhancement, high cold cloud tops are colored to indicate the probability and intensity of precipitation.

6.3 Online Monitoring of Real-Life Events

In our daily life, an increasing frequency of natural disasters can be observed due to rapid change in anthropogenic activities. Meteorological studies of our planet require atmospheric data available through space agencies like NASA, ESA and/or from freely available NOAA weather satellites. The APT data from NOAA can be received throughout the world using low-cost equipment and a wideband receiver operating in the 137 MHz frequency range FM mode. By times, NOAA satellites are already being used in remote sensing applications to monitor almost all types of natural disasters. The accuracy of analyzed data can be used in forecasting, monitoring and damage assessment caused by eruptions.

The event dealt in this section happened on May 28, 2010. A large ash cloud emanating from Tungurahua volcano was captured in the Andean region along with a large ash cloud from the Pacaya volcano in Guatemala by using far infrared images from NOAA-18 satellite with overlaid geo-reference coordinates. Both events were analyzed with remote sensing tools and image enhancement schemes e.g. 'thermal', 'hvct' and 'fire', available in the weather decoding software. The images were received due to unique location of Hermes GS which remarks the importance of having this kind of stations around the world and the scientists have remote access via Hermes GS. The processed image using virtual GS and the same image captured by Geostationary Operational Environmental Satellite (GOES 13) is shown in Figure 6-13.

Tungurahua is considered to be a dangerous volcano which threatens the tourist town of Baños, as well as the Agoyan dam that is used for hydroelectric power

generation. The eruptions of Tungurahua threaten this dam and reservoir, the second most important in Ecuador (Hall, Robin et al. 1999).

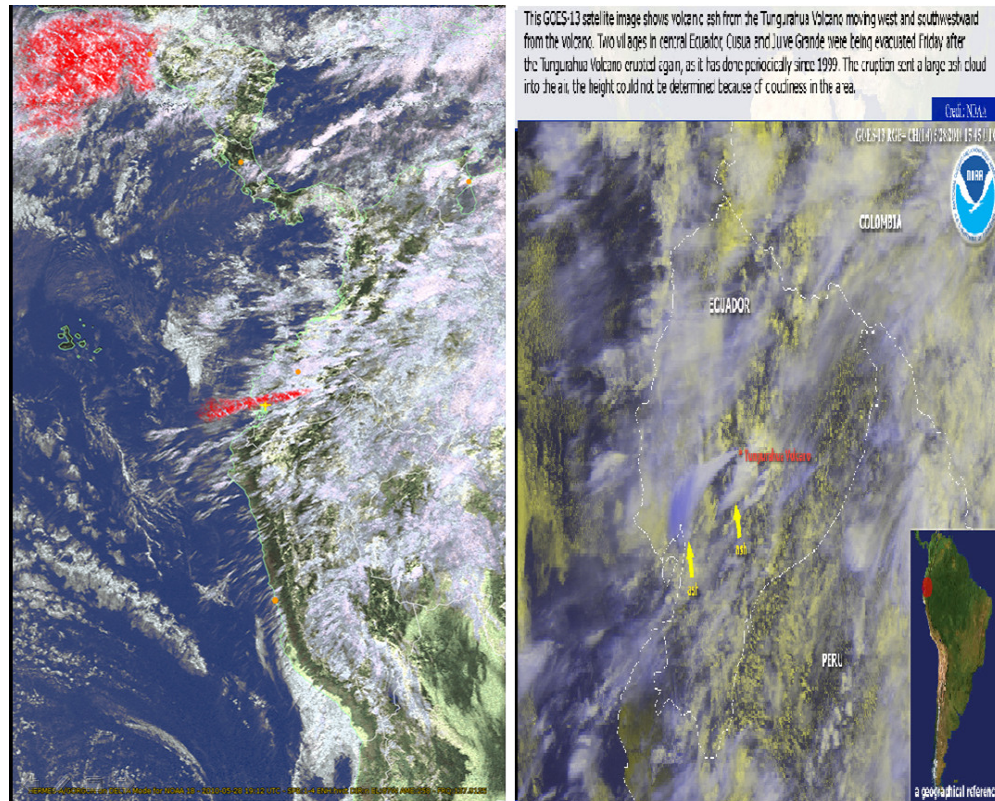


Figure 6-13: Tungurahua volcanic eruption captured by NOAA 18 using APT on May 28th 2010, processed with WXtoImg using 'hvct' false color enhancement. The same event monitored by GOES 13 satellite, (Courtesy of NOAA).

The second event of NOAA application is of Andean mountain area in Ecuador that is being affected by high temperatures over 30° C located over 3000 m high. From May 15 - 20, 2010, the images were received from NOAA-18 and NOAA-19 using the Hermes GS and processed with Surface Temperature (ST) remote sensing tool. Additionally, measured results were validated by the local meteorological stations network records. The volcanic eruption caused melting of glaciers due to high temperatures (30 °C). The regional temperatures are shown in Figure 6-14 and that of the affected region is indicated in Figure 6-15. The Figure 6-14 is a

composition of images from NOAA 15, 18 and 19, received by Hermes from the satellites directly during the heavy South American rainfall of March 2010 and processed with thermal enhancement.

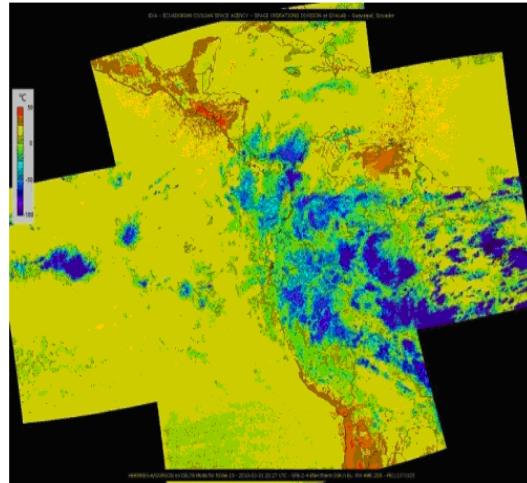


Figure 6-14: Regional temperatures: received images from NOAA-18 and NOAA-19 using Hermes GS and processed at user virtual GS using WXtoImg.

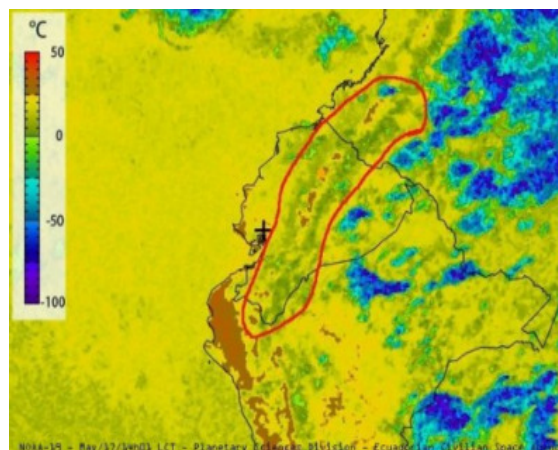


Figure 6-15: High temperature variations (up to 30° C) at Andean mountain region observed on May 15 through May 20, 2010. The image was received from NOAA-18 and NOAA-19 using Hermes GS and processed at user VGS. The after effects in the form of glaciers receding were visually observed.

Another captured event of interest was a twin-storm in Caribbean Sea on June 25, 2010. The image required multi-pass satellites data to make composition of these images and is shown in Figure 6-16.

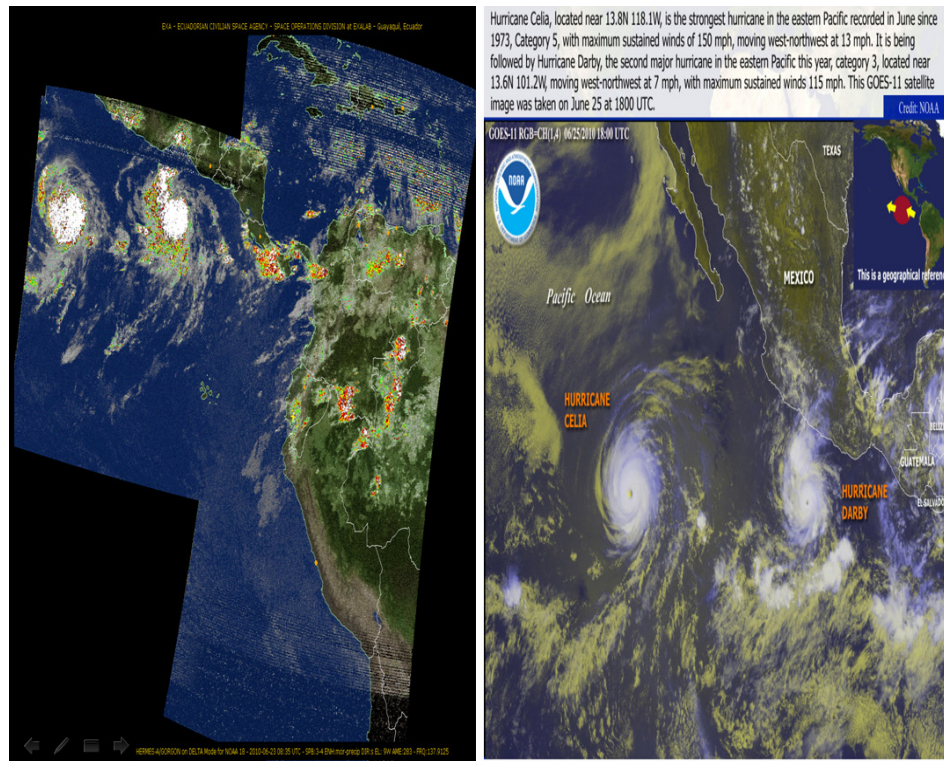


Figure 6-16: Images received and analyzed remotely with WxtoImg at user end, June 2010 (a) Twin-storms in the Pacific ocean (b): Tungurahua volcanic eruption

6.4 Constraints

There were a few constraints found in the execution of this project.

6.4.1 VRS-RM/Port Blocking/Firewall

It has been observed that VRS-RM freezes due to saturation and requires a reset every few months. Secondly, one remote user in Japan had an issue with port blocking due to firewall security at their organization. Because of this, they could not access Hermes remotely.

To resolve these problems at both ends and as a redundant protocol, called 'broadwave interface' was created as an alternative to VRS-RM but not a complete replacement. Hermes typically allows access through the 'Hermes broadwave interface', meant to be used over port 80, when access to port 264 is not possible due to firewall issues. It requires a static IP (authenticated by Hermes).

Another option is to use Skype for delta mode only when using Minotaur. It works in all modes but as stated earlier, VRS-RM is the first option in all cases.

To avoid further issues, a web interface was created on (Hermes-A 2011) for availing all channels like VRS-RM. The remote users can get AF signals by accessing a remote interface on port 94 to process the images after the pass is completed. The AF .wav of all NOAA satellites for the previous seven days passes are available on the EXA server.

6.4.2 Network Latency

A good Internet connection with Round Trip Time (RTT) < 50 ms was assumed to be required for remote operations, but many ISPs between a remote user node and Hermes are not offering up-to-the-mark connections as revealed by 'traceroute' and observed in all four modes of operations. It was found that the RTT is usually

greater than 300 ms which impairs links to Hermes. The RTT and is shown in Figure 6-17 and 'traceroute' in Figure 6-18.

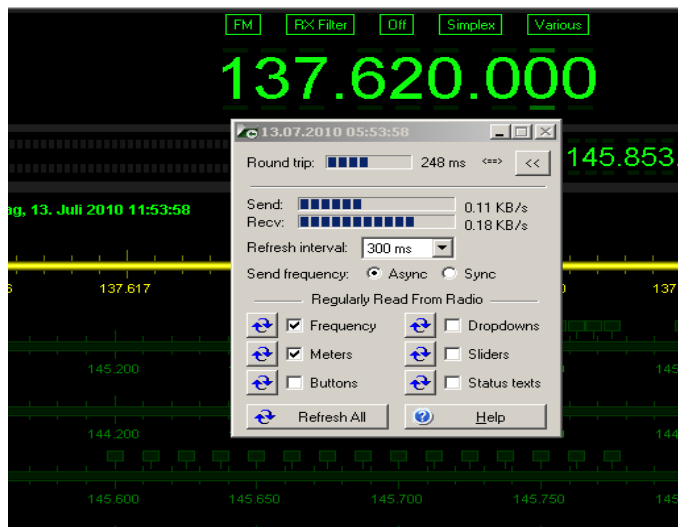


Figure 6-17: The round trip time on July 13, 2010 (Graz to Hermes, EXA).

A frequency shift during ± 3 min of maximum elevation (MEL) was found to be so high that HRD-Sat Track could not provide its automated Doppler compensation properly, as a result manual frequency adjustment was necessary. The network latency problem lasts only 3 - 4 min during the 14 - 18 min pass.

The Internet speed is never constant and results will always vary. Additionally the number of router hops will change to get to Ecuador, so it is likely to have changes in the latency. The immediate effect is seen with freezing HRD during satellite pass acquisition. From a command and control point of view, Hermes is tested for Alpha and Beta mode with excellent results, but voice mode (Gamma) is the real hard one to accomplish with such an issue for remote operations. None of the participating users was able to reduce the RTT to less than 150 ms (50 ms requirement). The 'traceroute' points out that the bottleneck is somewhere just before Ecuador. The Internet infrastructure is better in Europe. The HRD, 'ping' and 'traceroute' all validate that the RTT is ~ 250 ms, even when the Internet usage

is not so high here in Graz, Austria and other remote users' site. High RTT does not allow tracking any satellite using the synchronous option in HRD settings, causing freezing of the PC.

```

C:\WINDOWS\system32\cmd.exe
Microsoft Windows XP [Version 5.1.2600]
(C) Copyright 1985-2001 Microsoft Corp.

C:\>tracert hermes-a.exa.ec

Tracing route to hermes-a.exa.ec [200.24.192.105]
over a maximum of 30 hops:

  0  <1 ms    <1 ms    <1 ms    129.27.140.1
  1  <1 ms    1 ms     <1 ms    rtzid0.tu-graz.ac.at [129.27.1.41]
  2  1 ms     1 ms     1 ms     gigabitEthernet9-1.graz1.aco.net [193.171.21.41]
  3  2 ms     1 ms     1 ms     vlan323.graz2.aco.net [193.171.15.26]
  4  5 ms     5 ms     5 ms     vlan322.wien21.aco.net [193.171.15.21]
  5  5 ms     5 ms     4 ms     212.73.203.17
  6  57 ms    5 ms     5 ms     ae-11-11.car1.Vienna1.Level3.net [4.69.135.29]
  7  16 ms    16 ms    16 ms    ae-6-6.ebr1.Frankfurt1.Level3.net [4.69.135.34]
  8  26 ms    25 ms    25 ms    ae-46-46.ebr2.Paris1.Level3.net [4.69.143.138]
  9  26 ms    25 ms    26 ms    ae-2-52.edge4.Paris1.Level3.net [4.69.139.234]
 10  48 ms    48 ms    48 ms    213.242.111.10
 11  129 ms   130 ms   129 ms   Xe0-0-0-0-grtwaseq3.red.telefonica-wholesale.net.126.142.94.in-addr.arpa [94.142.126.85]
 12  188 ms   170 ms   156 ms   So6-1-0-0-grtniabr4.red.telefonica-wholesale.net [213.140.36.49]
 13  213 ms   199 ms   219 ms   So-6-1-0-0-grtluren2.red.telefonica-wholesale.net [213.140.43.157]
 14  221 ms   205 ms   220 ms   OTECEL-3-2-0-1000-grtsaltw1.red.telefonica-wholesale.net [84.16.6.42]
 15  *        *        *        Request timed out.
 16  204 ms   204 ms   226 ms   200.24.193.250
 17  238 ms   207 ms   207 ms   200.24.193.249
 18  242 ms   *        *        200.24.193.249
 19  237 ms   209 ms   *        200.24.192.105
 20  249 ms   282 ms   237 ms   200.24.192.105

Trace complete.

```

Figure 6-18: The current 'traceroute' as per June 14, 2010 (Graz to Hermes, EXA)

6.5 Chapter Summary

Hermes embodies an excellent laboratory for space operations and research worldwide through the Internet. It is a useful tool for educating students in the development of a small satellite program as the success of these missions depends on the post launch space operations.

A synchronous round-the-world test of the Hermes by a distributed team was demonstrated by tracking, controlling and decoding a NOAA and Amateur satellites transmissions using a suite of free software. Among many constraints, synchronization loss was addressed and network latency issues were discussed.

The SwissCube near-miss event was only possible to detect through the use of this gateway for a live relay to the satellite owners and the determination of the SwissCube rotation rate was also possible.

The VGS provided many users to get an insight into real-time monitoring of volcanic eruption and sea-storms in the Caribbean Sea. The application has direct impact on disaster management efforts. Also, other applications provided evidence that it can be a key to acquire most of the data related knowledge in space/satellite science/engineering.

The experiments and hardware simulations performed has verified that I-2-O-gateway make the mission feasible.

The reliability of the gateway was tested with support of current operational satellites by commanding them remotely using the Internet node and receiving the telemetry and housekeeping data, and analysing them in real-time. Although, the satellite owners have imposed some restrictions (i.e. authorization to command the satellite). But on the whole, the ground system can be used to command with a sequence encapsulated in AF. Within the constraints by satellite owners, the reliability of the GS was extremely high. Therefore, it is concluded that Hermes is a verified potential GS for LiNSAT.

Chapter 7 Conclusions and Suggestions for Future Work

7.1 Conclusions

A feasibility study of LiNSAT for lightning detection, geo-location and characterization as part of atmospheric research was presented with low-cost scientific mission was carried out in the framework of this PhD thesis. To perform scientific investigations, the LiNSAT is proposed to fly in a constellation of three identical nano-satellites. The GPS will be used for synchronization of the constellation to achieve μs accuracy in lightning geo-location experiments. In order to overcome the mass, volume and power constraints of the nano-satellite, it is planned to use the gravity gradient boom as a receiving antenna for lightning Sferics and to enhance the satellite's directional capability.

The lightning detection results in simulated and real terrestrial environment are presented. Lightning signals reception at MF, HF and VHF on ground is observed. The lightning detector is proposed to work in the HF/VHF range. The lightning transients (and on-board noise/ artifacts channel) will be digitized with 3 channels low power ADC 200 MS/s (over-sampling) for broadband reception without scanning.

To avoid false signals detection (false alarm), pre-selectors on-board LiNSAT are part of the Sferics detector. Adaptive filters are formulated and will be developed to differentiate terrestrial electromagnetic impulsive signals from ionospheric or magnetospheric signals. The noise-removed signal was found to be similar to the real lightning signal. Therefore, the signal will be used for fine trigger on-board the LiNSAT.

Operational and experiment modes on-board LiNSAT are optimized with telemetry/ memory requirements by mode-switching either autonomous or commanded from the ground station.

To support the planned LiNSAT mission, an online remote ground station, "Hermes-A/Minotaur" built by EXA was tested. The I-2-O gateway is of great significance to be used as a single-node command and control station for the satellites in a constellation, such as the planned LiNSAT. The Hermes-A has proved to be a useful tool for educating students in the development of a small satellite program as the success of these missions depends on the post launch space operations. The students in Space/Satellite research including the author of the dissertation used the virtual ground station (VGS) within a collaborative effort for a synchronous round-the-world test of the Hermes-A. International students' participation was developed for online and real-time data access that is freely available by Space Agencies.

The functional capability of the I-2-O gateway and the VGS provided evidence as a key to acquire data for small satellite missions at low cost. By testing most of the operational modes, Hermes-A was verified as a potential GS for American satellite RAX, SwissCube and LiNSAT. The SwissCube near-miss event was monitored and this was only possible through the use of this gateway for a live relay to satellite owners due to its unique location.

Another GS at TU Graz (AR-TUG) was used for test purposes. It is automated to reduce cost of space operations, as it requires no manual operators and is implemented with open source/free software. The advantage is the adaptability to GENSO and other networks. It can be integrated into an online GS network for real-time reception and command/control of constellation and formation flights. The online and real-time data availability and real-time troubleshooting makes it an economical platform for current and future university class nano-satellites like TUGSat-1 and LiNSAT.

7.2 Suggestions for Further Work

Here are a few suggestions to realize the conceptual study:

- The development of adaptive filters for on-board LiNSAT to differentiate terrestrial electromagnetic impulsive signals from ionospheric or magnetospheric origin.
- Also, use of existing lightning data from previous missions to validate the accomplished results.
- As Hermes is a pure gateway, it has remote GS capabilities but is not a remote GS like GENSO or MGSN, so scheduling a satellite would be implemented at the user end as Hermes will provide the API/Gateway interface according to the OSI model. Hermes has a deferred application layer for the users to upgrade its features. After having developed, this capability will be used to schedule the HRD- Sat Track program to run and automatically connect to the Hermes-A.

Appendix: Hermes-A: I-2-O Gateway: Remote Client Station Setup Procedures

The first station on the planned Hermes network is the Hermes-A/Minotaur gateway complex, based on Guayaquil, Ecuador with coordinates Lat: 2° 08' 02" S, Long: 79° 52' 58" W.

It can handle the following range of frequencies:

2m:	118 to 172 MHz	RHCP/LHCP
70cm:	320 to 500 MHz	RHCP/LHCP
33cm:	915 to 935 MHz	RHCP/LHCP
23cm:	2.2 to 2.6 GHz	RHCP
QHA:	137 MHz	

In order to connect to Hermes-A/Minotaur gateway the user needs to setup a client station to receive AF input from the target satellite or spacecraft, this appendix describes such setup procedures and basic operation of the system for its four modes of operation:

Mode Alpha: Satellite Tracking and AF Receiving

Requirements: Following programs installed on remote client/PC

- Windows XP/Vista
- HRDv5. (Full Suite)
- VRS Remote Monitor
- Java, latest version
- Internet Explorer/Firefox, latest version
- Any MCP/TNC (Soft-TNC e.g. MixW or HRD- DM780)

-

HRDv5 Radio Engine

- Start HRDv5 and Sat- Track program
- Home location: Guayaquil, Ecuador
- Company: Kenwood
- Radio: TS2000
- COM port: Remote
- Speed: 57600

- Flow Control: CTS and RTS
- Connection: Remote
- Address: hermes-a.exa.ec
- Port: 7805 (default)
- Username and Password
- Com port: COM7
- Enable 'Optional PTT(TX) configuration' and select COM8, only RTS, save settings

HRD Radio Console

- Tools menu=> IP server => Port => 7809
- Start server when HRD starts' and 'Same PC connections only'

-

HRD- Sat Track

Radio => Radio Connection, Address: 127.0.0.1, User and Password, Port 7809, automatically connect, Update speed: Fast

Connect => DDE Remote Server that will drive the Minotaur sensor array robot on Hermes-A:

Tools menu: DDE Server => DDE remote server: Enable NOVA, Address: hermes-a.exa.ec, Port 7815 (default), Password, Save

Browser: <http://hermes.exa.ec>, User and Password, Start/Stop, Camera view and Antenna polarity

Important: Update Keplerian elements (TLEs) regularly using Satellite Defns => Kepler data

Audio Stream/VRS Remote Monitor

- User and Password => Connect
- Ch-1: Main transceiver output
- Ch-2: Sub Transceiver output
- Ch-3: (NOAA) Weather satellite (APT) reception

Mode Beta: Satellite Tracking And Data Transceiving

All software required for Mode Alpha and additionally

- MixW v2.1x
- MCP/soft-TNC

- Skype, latest version

All configurations in Mode Alpha and additionally

- On HRD v5 => Tools and select 'N8VB VCOM configuration
- Define a COM port bridge, using a non physical com port, let's call it 'COMx', as the new local port on slot 1, where x can be any number, whenever it doesn't match a physical port on user computer.
- Define a bridge port as COMy, whenever it doesn't match a physical port on user computer. Install or Update as needed.
- On HRD v5 => Tools and select 3rd Party Serial Port, Port: COMx,
- Mode: Default, Speed: 57600, Enable and Connect when HRD starts
- PTT/CAT COM port on Software-TNC

-

MixWv2.1x (soft-TNC)

- Menu layout 2: Hardware, CAT settings: CAT Kenwood, model TS-2000
- PTT&CAT interface: Details, virtual COM port: HRD v5 COMy: Baud rate 57600, Data bits: 8, Parity: none, Stop bits: 1, RTS: PTT, DTR: Always Off

Continue setting up the MCP to Radio interface and select the following options:

- Save frequency on exit
- PTT via CAT command

- Other options as required
- Sound card interface setup => 'Hardware' tab: choose 'Sound device settings', then select the device as 'sound card' and the 'Input' and 'Output' as 'Preferred sound card'

-

Skype

The Hermes-A/Minotaur complex uses Skype as an audio Internet bridge. The remote user must setup a Skype account and add the Hermes-A ID to be able to use it for space operations.

- Add the identity Hermes-A to your contacts list and get approved by the system
- To connect with the gateway: Audio setup on Skype
- Audio input and output: 'Stereo MIX'
- Windows audio option: 'Stereo Mix'

-

HRD- Sat Track

- 'Satellite' => Home location: Guayaquil, Ecuador
- 'Radio' => 'Radio Connection': 127.0.0.1
- User and Password

- Port: 7809
- 'Automatically connect'
- 'Update speed': 'Fast'

Connect: DDE Remote Server

- 'DDE Server' option => 'DDE remote server' tab
- Enable NOVA
- Address: hermes-a.exa.ec
- Port: 7815 (default)
- User and password

Web-Interface/Browser

- <http://hermes.exa.ec>
- Hermes-A: User and password
- Options => Camera view: Antenna polarity

Mode Gamma: Satellite Tracking And Voice /Audio '*HDX*' Transceiving

All software required for Mode Alpha and Beta, additionally

- Skype => Audio input: 'Microphone'
- Audio output: 'Stereo MIX'
- To connect to the gateway, remote user needs to press the 'Call' button on Skype. The gateway will answer shortly and the Internet-to-Orbit communication is established.

Mode Delta: Weather Satellite Tracking and APT Data Receiving

All software required for Mode Alpha, additionally

- WXtoImg APT image decoding and WX satellite tracking program

WXtoImg

- Install the WXtoImg program

- Follow the calibration procedures (image quality relies on it)
- Home location: Guayaquil, Ecuador
- Update the Keplers from the 'File' menu, 'Update Keplers' option.
- 'Options' menu => 'Active APT Satellites' (NOAA: 137MHz)

VRS Remote Monitor

- Host address: hermes-a.exa.ec
- User and password
- Connection speed: 256

List of Acronyms

ADC	Analog to Digital converter
ADCS	Attitude Determination and Control System
AdF	Adaptive Filtering
AF	Audio Frequency
AFC	Automatic Frequency Control
AFSK	Audio Frequency Shift Keying
ALDF	Advanced Lightning Direction Finder
ALDIS	Austrian Lightning Detection and Information System
ALEXIS	Array of Low Energy X-ray Imaging Sensors. A satellite launched in April of 1993 to study soft X-rays and broadband radio signals. Also, the name of the primary payload on the satellite
AMSAT	Group/Corporation of Amateur Satellite Operators
ANC	Adaptive Noise Cancellation
AOS	Acquisition Of Satellite/Signal

API	Application Program Interface is a set of routines, protocols, and tools for building software applications.
APT	Automated Picture Transmission
ARGOS	Advanced Radio Signal Gathering from Orbiting Spacecraft
AR-ISS	Amateur Radio on International Space Station
AR-TUG	Automated Remote GS at TU Graz
ATD	Arrival Time Difference
AVHRR	Advanced Very High Resolution Radiometer
Blackbeard	A broadband radio receiver on the ALEXIS satellite. Blackbeard provided the first observations of TIPP events
BRITE	BRIght Target Explorer
CASSINI-HUYGENS	Is a joint NASA/ESA/ASI robotic spacecraft mission currently studying the planet Saturn and its many natural satellites
CCD	Charged Coupled Device
C-G	Cloud to Ground
C-GR3	Cloud-Ground Ratio
Changes	J, F and K changes. Lightning specific current flow
CID	Compact Intracloud Discharge. A powerful source of radio signals in thunderstorms that produces NPBPs, TIPPs, and SIPPs
CMC	Command and Control Centre

COTS	Commercial-Of-The-Shelf
CW	Continuous Wave
DAQ	Data Acquisition System
DC	Direct Current
DDE	Dynamic Data Exchange
DE	Detection Efficiency
DGSN	Distributed GSs Network
DMSP	Defense Meteorological Satellite Program
DPU	Data Processing Unit
DTMF	Dual Tone Multi-Frequency
EIRP	Effective Isotropic Radiated Power
ELF	Extremely Low Frequency (30 to 300 Hz)
EM	Experiment Modes
EMC	Electromagnetic Compatibility
EME	Earth-Moon-Earth
EMI	Electromagnetic Interference
EMP	Electromagnetic Pulse
EPFL	Swiss Ecole Polytechnique Fédérale de Lausanne
ESA	European Space Agency

EUCLID	European cooperation on Lightning Detection
EXA	Ecuadorian Civilian Space Agency
FFT	Fast Fourier Transform
FM	Frequency Modulation
FORTE	Fast On-orbit Recording of Transient Events
FSPL	Free Space Path Loss
GE	Google Earth
GENSO	Global Educational Network for Satellite Operations
GEO	Geostationary Earth Orbit
GGB	Gravity Gradient Boom
GGB-LA	Gravity Gradient Boom integrated into Lightning Antenna
GGG	Gravity Gradient Stabilization
GHz	Giga Hertz
GMSK	Gaussian Minimum Shift Keying
GNB	Generic Nano-satellite Bus
GOES	Geostationary Operational Environmental Satellite
GOES-13	Geostationary Operational Environmental Satellite-13.
GPC	Ground-based Preliminary estimation as preselector Co-efficients for AdF
GPS	Global Positioning System

GS	Ground Station
GSN	GS Network
HASI	HUYGENS Atmospheric Structure Instrument
HEO	Highly Elliptical Orbit
HF	High Frequency (3 to 30 MHz).
HRD	Ham Radio Deluxe (HRD, -Radio, -Sat Track, -DM 780), Suite of free software used for implementation of virtual GS
HRPT	High Resolution Picture Transmission
HV-PSU	High Voltage Power Supply Unit
Hz	Hertz
I-2-O	Internet to Orbit
I-C	Inter-/Intra Cloud
IP	Internet Protocol
IR	Infrared
ISM	Industrial, Scientific and Medical
ISS	International Space Station
ISS-B	Ionospheric Sounding Satellite-B
ITU	International Telecommunication Union
JAXA	Japan Aerospace Agency
KCT	Kansas City Tracker

L	Leader
LA2	2 nd Lightning Antenna
LA3	3 rd Lightning Antenna
LANL	Los Alamos National Laboratory
Lat	Latitude
LEMP	Lightning Electromagnetic Pulse
LEO	Low Earth orbit. An Earth orbit between about 300 and 2000 km
LF	Low Frequency (30 to 300 kHz).
LHCP	Left Hand Circular Polarization
LiNSAT	<u>Aus</u> <u>Trian</u> <u>L</u> <u>ightning</u> <u>N</u> <u>ano</u> - <u>S</u> <u>atellite</u> , a follow-up mission of Austrian first Astronomical satellite TUGSat-1/BRITE
LIS	Lightning Imaging Sensor
LLP	Lightning Location and Protection
LLS	Lightning Location System
LMS	Least Mean Square
LNA	Low Noise Amplifier
Long	Longitude
LOS	Loss Of Satellite/Signal
LPATS	Lightning Positioning and Tracking System
LRPT	Low-Rate Picture Transmission

MEL	Maximum Elevation
MGSN	Mercury GS Network
MHz	Mega Hertz
MO	Mission Modes of Operation
MSA	Multi Spectral Analysis
MSG	Meteosat Second Generation
NALDN	North American Lightning Detection Network
NASA	National Aeronautic and Space Administration
NLDN	National Lightning Detection Network (USA)
NLSI	National Lightning Safety Institute
NOAA	National Oceanic and Atmospheric Administration
NORAD	North American Aerospace Defense Command
OBC	On-Board Computer
ODR	Omni Directional Reception
OLS	Optical Lightning Sensor (on FORTE)
ONERA	Office National d'Etudes et de Recherches Aérospatiale
OS	Operating System (Microsoft Windows, etc)
OSI	Open System Interconnection
OTD	Optical Transient Detector

PB	Preliminary Breakdown
PC	Personal Computer
PCB	Printed Circuit Board
PLL	Phase Locked Loop
POES	Polar Earth Orbiting Satellites
QHA	Quadrifilar Helical Antenna
RAX	Radio Aurora Explorer
RF	Radio Frequency
RHCP	Right Hand Circular Polarization
RS	Return Stroke
RTT	Round Trip Time
Rx	Receiver
SAA	Southern Atlantic Anomaly
SAFIR	Surveillance et Alerte Foudre par Interférométrie Radioélectrique
SEE	Single Event Effects
SEU	Single Event Upset
SFCC	Space Flight Control Centre
Sferics	Atmospheric Electromagnetics, A term used to describe VLF/LF/HF radio pulses from lightning
SNR	Signal to Noise Ratio

SOD	Space Operations Division
S-PA	S-band Patch Antenna
SSB	Single Side Modulation
SST	Sea Surface Temperature
ST	Surface Temperature
STK	Satellite Toolkit
TCP	Transmission Control protocol
TIPP	Trans-ionospheric Pulse Pair. A paired pulse recorded by the Blackbeard satellite instrument. The events are produced by CIDs and possibly by other singular, elevated, transient RF sources.
TLE	Two Line Elements
TLM	Telemetry
TNC	Terminal Node Controller
TOA	Time of Arrival
TRMM	Tropical Rainfall Measurement
TRX	Transceiver
TTC&M	Telemetry, Tracking, Command and Monitoring
TU Graz	Graz University of Technology
TUGsat1	Graz University of Technology, Graz, Austria's first Nano-Satellite
Tx	Transmitter

UESS	Universidad Espiritu Santo
UHF	Ultra High Frequency (300 to 3000 MHz).
ULF	Ultra Low Frequency
U-MP	UHF Monopole Antenna
UTC	Coordinated Universal Time.
VFO-A	Variable-Frequency Oscillator (Rx Frequency at HRD)
VFO-B	Variable-Frequency Oscillator (Tx Frequency at HRD)
VGS	Virtual GS
VHF	Very High Frequency (30 to 300 MHz).
VHFDX	VHF DiXing
VIS	Visible
VLf	Very Low Frequency (3 to 30 kHz).
V-MP	VHF Monopole Antenna
VOX	Voice Operated Switch
VRS-RM	VRS-Remote Monitor
VSWR	Voltage Standing Wave Ratio

List of Publications

The following papers were contributed during this thesis and published in international congresses/workshops, refereed conferences and journals. The publications with the author of the thesis as lead author are subsequently presented in chapters 3 - 6. Additionally, few papers were co-authored by the author of this thesis.

Ghulam Jaffer, Cmdr. Ronnie Nader, Prof. Otto Koudelka, (2011). Online and real-time space operations using Hermes-A I-2-O gateway, in: 1st IAA Conference On University Satellites Missions, Rome, Italy, 24 - 29 Jan.

Ghulam Jaffer, Hans U. Eichelberger, Konrad Schwingenschuh, Otto Koudelka, (2010). Lightning detector on-board Austrian nano-satellite (LiNSAT), in: American Geophysical Union (AGU) Fall meeting 2010 in San Francisco, California, 13 - 17 Dec.

Ghulam Jaffer, Ronnie Nader, Otto Koudelka, (2010). NOAA/APT satellite data for online and real time monitoring of Tungurahua volcanic eruption and temperature profile in Ecuador, in: American Geophysical Union (AGU) Fall meeting 2010 in San Francisco, California, 13 - 17 Dec.

Ghulam Jaffer, Dr. Andrew Klesh, Cmdr. Ronnie Nader, Prof. Otto Koudelka, (2010). Using a virtual GS as a tool for supporting higher education, IAC-

10.E1.4.11, in: 61st International Astronautical Congress (IAC), Prague, Czech Republic, 26 Sep. – 1 Oct.

Ghulam Jaffer, Cmdr. Ronnie Nader, Dr. Andrew Klesh, Prof. Otto Koudelka, (2010). Project Agora: Simultaneously downloading a satellite signal around the world, in: 61st International Astronautical Congress (IAC), IAC-10.B2.5.12, Prague, Czech Republic, 26 Sep. – 1 Oct.

Ronnie Nader, Hector Carrion, **Ghulam Jaffer**, (2010). Hermes-A Delta: The Use Of The Delta Operation Mode Of The Hermes-A/Minotaur I-2-O Gateway To Turn A Laptop In To A Virtual EO GS, in: 61st International Astronautical Congress (IAC), IAC-10.B1.711, Prague, Czech Republic, 26 Sep. – 1 Oct.

Ronnie Nader, Prof. Patricio Salazar, **Ghulam Jaffer**, (2010). The Ecuadorian Civilian Space Program: Near-future manned research missions in a low cost, entry level space program, IAC-10.B3.1.6, in: 61st International Astronautical Congress (IAC), Prague, Czech Republic, 26 Sep. – 1 Oct.

Ghulam Jaffer, Cmdr. Ronnie Nader, Prof. Otto Koudelka, M. Tahir Mushtaq, (2010). An online and real-time virtual GS for small satellites, in: UN/Austria/ESA Symposium on Small Satellite Programmes for Sustainable Development: Payloads for Small Satellite Programmes Graz, Austria, 21 - 24 Sep.

H. U. Eichelberger, G. Prattes, K. Schwingenschuh, **G. Jaffer**, Ö. Aydogar, I. Jernej, B.P. Besser, M. Stachel, T. Tokano, P. Falkner:, (2010). Acoustic measurements of atmospheric electrical discharges for planetary probes, in: EGU General Assembly Vienna, Austria, 2 – 7 May.

- G. Jaffer**, O. Koudelka, K. Schwingenschuh, H. Eichelberger, (2008). The detection of sferics by a nano-satellite, in: 59th International Astronautical Congress (IAC), IAC-08.B4.2.12, Glasgow, UK, 29 Sep. – 3 Oct.
- Schwingenschuh, Konrad; **Jaffer, Ghulam**; Koudelka, O.; Khan, S.; Grant, C.; Unterberger, M.; Lichtenegger, Herbert; Macher, W.; Hausleitner, W., (2008). Feasibility study for a future Austrian lightning nano-satellite, in: 37th COSPAR Scientific Assembly, p.2794, Montreal, Canada, 13 - 20 Jul.
- Schwingenschuh, Konrad; Lichtenegger, Herbert; Simoes, Fernando; Tokano, T.; Hofe, R.; Besser, B. P.; Eichelberger, H. U.; **Jaffer, Ghulam**; Macher, W.; Jernej, I, (2008). Electric discharges in the lower atmosphere of Titan: HUYGENS acoustic and electric observations, in: 37th COSPAR Scientific Assembly, Montreal, Canada, p.2793a, 13 - 20 Jul.
- K. Schwingenschuh, B.P. Besser, R. Hofe, T. Tokano, J.J. Lopez-Moreno, R. Gard, P. Falkner, R. Trautner, M. Hamelin, F. Simoes, I. Jernej, **G. Jaffer**, G.J. Molina-Cuberos, M. Fulchignoni, F. Ferri, (2007). HUYGENS in-situ observations of Titan's atmospheric electricity, in: European Geophysical Union (EGU) General Assembly Vienna, Austria, 15 - 20 Apr.
- Jaffer, G.** and Schwingenschuh, K, (2006). Lab experiments of corona discharges, Technical Report in: Space Research Institute, Austrian Academy of Sciences (IWF) Graz, Sep.
- Ghulam Jaffer** and Konrad Schwingenschuh, (2006). Lab experiments of corona discharges, in: ISSI workshop, Bern/Switzerland about the PWA HUYGENS, 20 Nov.
- G. Jaffer**, (2006). Measurements of electromagnetic corona discharges, in: Educational workshop, Lehrerfortbildung des Pädagogischen Institutes des Bundes in Steiermark: von Monden, Kometen und Planeten im Sonnen-

system, Space Research Institute, Austrian Academy of Sciences Graz, Austria 23 Dec.

K. Schwingenschuh, R. Hofe, T. Tokano, J.J. Lopez-Moreno, R. Grard, P. Falkner, R. Trautner, M. Hamelin, F. Simoes, I. Jernej, **G. Jaffer**, G.J. Molina-Cuberos, M. Fulchignoni, F. Ferri, (2006). In-situ observations of electric field fluctuations and impulsive events during the descent of the HUYGENS probe in the atmosphere of Titan, in: European Planetary Science Congress Berlin, Germany, p.690, 18 - 22 Sep.

Schwingenschuh, K.; Hofe, R.; Tokano, T.; Lopez-Moreno, J. J.; Grard, R.; Falkner, P.; Trautner, R.; Hamelin, M.; Simoes, F.; Jernej, I.; **PWA/HASI Team***, (2006). Electric field observations during the descent of the HUYGENS probe: evidence of lightning in the atmosphere of Titan, in: 36th COSPAR Scientific Assembly Beijing, China, 16 - 23 Jul.

ACCEPTED/ IN PRESS

Ghulam Jaffer, Otto Koudelka, (2011). Lightning detection on-board nano-satellite (LiNSAT), in: International Conference on Atmospheric Electricity (I-CAE), Rio de Janeiro, Brazil, 8 - 12 Aug.

H. U. Eichelberger, G. Prattes, K. Schwingenschuh, **G. Jaffer**, Ö. Aydogar, I. Jernej, B.P. Besser, M. Stachel, T. Tokano, P. Falkner, (2011). Acoustic outdoor measurements with a multi-microphone instrument for planetary atmospheres and surfaces, in: EGU General Assembly Vienna, Austria, 3 - 8 Apr.

Ghulam Jaffer, (2011). Austrian Lightning Nano-satellite (LiNSAT): Space and Ground Segments, in: 3rd International Conference on Advances in Satellite

and Space Communications (SPACOMM 2011), Budapest, Hungary, 17 - 22 Apr.

Ghulam Jaffer, Ronnie Nader, (2011). Virtual GS and NOAA: Online tool for real-time monitoring of volcanic eruption, in: 3rd International Conference on Advances in Satellite and Space Communications (SPACOMM 2011), Budapest, Hungary, 17 - 22 Apr.

Ghulam Jaffer, Cmdr. Ronnie Nader, Prof. Otto Koudelka, (2011). Online and real-time space operations using Hermes-A I-2-O gateway, in: International Journal - Actual Problems of Aviation and Aerospace Systems

Ghulam Jaffer, Prof. Otto Koudelka, (2011). Automated remote GS for Austrian lightning nano-satellite (LiNSAT), in: 8th IAA Symposium on Small Satellites for Earth Observation, Berlin, Germany, 4 - 8 Apr.

Ghulam Jaffer, Cmdr. Ronnie Nader, Prof. Otto Koudelka, (2011). Using a virtual GS as a tool for supporting higher education, in: Acta Astronautica

Ghulam Jaffer, Otto Koudelka, Hans U. Eichelberger, Konrad Schwingenschuh, (2011). A LEO nano-satellite mission for the detection of lightning VHF sferics, Book Chapter in: Adaptive Filtering, ISBN 978-953-307-442-9, InTech Publishers

Ghulam Jaffer, Ronnie Nader, Otto Koudelka, (2011). Online and real time monitoring of volcanic eruption in Ecuador using NOAA APT, in: NOAA Satellite Direct Readout Conference, Miami, Florida, USA, 4 - 8 Apr.

Ghulam Jaffer, Ronnie Nader, (2011). A virtual GS for satellites formation flights, in: 28th International Symposium on Space Technology and Science (ISTS), Okinawa, Japan, 5-12 Jun.

UNDER REVIEW

Ghulam Jaffer, Ronnie Nader, Otto Koudelka, (2011). Online virtual GS for real-time multi-satellite communications, in: 4th International Conference on Spacecraft Formation Flying Missions & Technologies (SFFMT), St-Hubert, Québec, Canada, 18 - 20 May

Ghulam Jaffer, Ronnie Nader, Otto Koudelka, (2011). Online monitoring of real-life environmental events using NOAA APT and virtual GS, in: International Conference on Space Science & Communication (IconSpace2011), Genting Highlands, Pahang, Malaysia, 12 - 13 Jul.

Ghulam Jaffer, Ronnie Nader, Otto Koudelka, (2011). Online virtual ground station: A tool for space/satellite research and scientific outreach, in: Einsteins in the City conference, the City University of New York, USA, 13 - 15 Apr.

*** PWA/HASI Team:**

T. Tokano, J.J. Lopez-Moreno, R. Grard, P. Falkner, R. Trautner, M. Hamelin, F. Simoes, I. Jernej, **G. Jaffer**, G.J. Molina-Cuberos, M. Fulchignoni, F. Ferri
<http://www.cosis.net/members/meetings/team.php?team=2805&PHPSE>

*** ESA: EPSC2006-A-00690; p. 19 Team**

R. Hofe, T. Tokano, J.J. Lopez-Moreno, R. Grard, P. Falkner, R. Trautner, M. Hamelin, F. Simoes, I. Jernej, **G. Jaffer**, G.J. Molina-Cuberos, M. Fulchignoni, F. Ferri
http://esamultimedia.esa.int/docs/science/programme_book.pdf

Bibliography

- Agora (2011). <https://sites.google.com/site/projagora/instructions/image-translation>.
- AMSAT (2011). "<http://www.amsat.org/amsat-new/satellites/status.php>."
- Anderson, R., H. Van Niekerk, et al. (1979). "Improved lightning flash counters." Electra **66**: 85-98.
- ARRL (2011). "<http://www.arrl.org/>."
- ATS (2011). "<http://nasascience.nasa.gov/missions/ats/>."
- AX.25 (2011). "http://www.tapr.org/pr_intro.html#AX.25".
- Barillot, C. and P. Calvel (2002). "Review of commercial spacecraft anomalies and single-event-effect occurrences." Nuclear Science, IEEE Transactions on **43**(2): 453-460.
- Beasley, W. H. and B. C. Edgar (2004). "Early coincident satellite optical and ground-based RF observations of lightning." Geophysical Research Letters **31**(7): -.
- Berthelier, J. J., M. Godefroy, et al. (2006). "ICE, the electric field experiment on DEMETER." Planetary and Space Science **54**(5): 456-471.
- Berthelier, J. J., M. Malingre, et al. (2008). "Lightning-induced plasma turbulence and ion heating in equatorial ionospheric depletions." Nature Geoscience **1**(2): 101-105.
- Betz, H. D., U. Schumann, et al. (2008). Lightning: Principles, Instruments and Applications: Review of Modern Lightning, Springer.
- Blanc, E., F. Lefeuvre, et al. (2007). "TARANIS: A microsatellite project dedicated to the study of impulsive transfers of energy between the Earth atmosphere, the ionosphere, and the magnetosphere." Advances in Space Research **40**(8): 1268-1275.
- Boccippio, D. J., W. Koshak, et al. (2000). "The Optical Transient Detector (OTD): Instrument characteristics and cross-sensor validation." Journal of Atmospheric and Oceanic Technology **17**(4): 441-458.

- Bondiou-Clergerie, A., P. Lalande, et al. (2004). "'ORAGES': a dedicated sensor for detection, localisation and fine analysis of lightning flashes from space." Acta Astronautica **55**(3-9): 245-254.
- Borgeaud, M., N. Scheidegger, et al. (2010). "SwissCube: The First Entirely-Built Swiss Student Satellite with an Earth Observation Payload." Small Satellite Missions for Earth Observation: 207-213.
- Burr, T., A. Jacobson, et al. (2004). "A global radio frequency noise survey as observed by the FORTE satellite at 800 km altitude." Radio Science **39**(4): -.
- Burr, T., A. Jacobson, et al. (2005). "A dynamic global radio frequency noise survey as observed by the FORTE satellite at 800 km altitude." Radio Science **40**(6): -.
- Cecil, D. J., S. J. Goodman, et al. (2005). "Three years of TRMM precipitation features. Part I: Radar, radiometric, and lightning characteristics." Monthly Weather Review **133**(3): 543-566.
- Celestrak (2011). <http://celestrak.com/NORAD/elements/>.
- Christian, H. (2010). Lightning Sensing from Space: Early Observations to the Geostationary Lightning Mapper (Invited).
- Christian, H. J., R. J. Blakeslee, et al. (2003). "Global frequency and distribution of lightning as observed from space by the Optical Transient Detector." Journal of Geophysical Research-Atmospheres **108**(D1): -.
- Christian, H. J., R. J. Blakeslee, et al. (1989). "The detection of lightning from geostationary orbit." Journal of Geophysical Research **94**(D11): 13329.
- Christian, H. J. and J. Latham (1998). "Satellite measurements of global lightning." Quarterly Journal of the Royal Meteorological Society **124**(549): 1771-1773.
- Cooray, V. (2003a). The lightning flash, Iet.
- Cooray, V. (2003b). "The mechanism of the lightning flash." The Lightning Flash: 144-159.
- Cooray, V. (2007). "Propagation effects on radiation field pulses generated by cloud lightning flashes." Journal of Atmospheric and Solar-Terrestrial Physics **69**(12): 1397-1406.
- Cooray, V. (2010). "Horizontal Electric Field Above- and Underground Produced by Lightning Flashes." Ieee Transactions on Electromagnetic Compatibility **52**(4): 936-943.
- Cooray, V., M. Fernando, et al. (2000). "Propagation of lightning generated transient electromagnetic fields over finitely conducting ground." Journal of Atmospheric and Solar-Terrestrial Physics **62**(7): 583-600.
- Coustonis, A. (2006). "Titan and the Cassini-Huygens mission." Recent Advances in Astronomy and Astrophysics **848**: 23-40, 954.
- Coustonis, A. and M. Hirtzig (2009). "Cassini-Huygens results on Titan's surface." Research in Astronomy and Astrophysics **9**(3): 249-268.
- DA-RP (2011). <http://www.moonraker.com.au/techni/discs&cones.htm>.

- Davis, S. M., D. M. Suszcynsky, et al. (2002). "FORTE observations of optical emissions from lightning: Optical properties and discrimination capability." Journal of Geophysical Research-Atmospheres **107**(D21): -.
- de Carufel, G. (2009). Assembly, Integration and Thermal Testing of the Generic Nanosatellite Bus. M.Sc., University of Toronto.
- Diendorfer, G., W. Schulz, et al. Comparison of correlated data from the Austrian lightning location system and measured lightning currents at the Peissenberg tower.
- Diendorfer, G., W. Schulz, et al. (2002). "Lightning characteristics based on data from the Austrian lightning locating system." Electromagnetic Compatibility, IEEE Transactions on **40**(4): 452-464.
- DK3WN (2011). "<http://www.dk3wn.info/>."
- Eichelberger, H., G. Prattes, et al. (2010). Acoustic measurements of atmospheric electrical discharges for planetary probes. European Geosciences Union (EGU). Vienna, Austria.
- Eichelberger, H., G. Prattes, et al. (2011). Acoustic outdoor measurements with a multi-microphone instrument for planetary atmospheres and surface. European Geosciences Union (EGU). Vienna, Austria.
- Elvidge, C. D., K. E. Baugh, et al. (1997). "Mapping city lights with nighttime data from the DMSP operational linescan system." Photogrammetric Engineering and Remote Sensing **63**(6): 727-734.
- EXA (2011). "<http://www.exa.ec/>."
- Falkner, P. (1999). Permittivity and Altimeter Wave Analyzer for the ESA / NASA Project Cassini-Huygens. PhD, Graz University of Technology.
- Finke, U. and O. Kreyer (2002). "Detect and locate lightning events from Geostationary Satellite observations." ReFort Part I: Review of existing lightning location systems, Sept~ nber: 3-17.
- Fiser, J., J. Chum, et al. (2010). "Whistler intensities above thunderstorms." Annales Geophysicae **28**(1): 37-46.
- Fulchignoni, M., F. Ferri, et al. (2005). "In situ measurements of the physical characteristics of Titan's environment." Nature **438**(7069): 785-791.
- GE (2011). "<http://earth.google.com/>."
- GENSO (2011). "<http://www.genso.org/>."
- Graybill, R. and R. Melhem (2002). Power aware computing, Plenum Pub Corp.
- Hall, M. L., C. Robin, et al. (1999). "Tungurahua Volcano, Ecuador: structure, eruptive history and hazards." Journal of Volcanology and Geothermal Research **91**(1): 1-21.
- Hayenga, C. O. (1979). "Positions and movement of VHF lightning sources determined with microsecond resolution by interferometry."
- Hayenga, C. O. and J. W. Warwick (1981). "Two-Dimensional Interferometric Positions of Vhf Lightning Sources." Journal of Geophysical Research-Oceans and Atmospheres **86**(Nc8): 7451-7462.

- Haykin, S. (1996). Adaptive Filter Theory, Prentice Hall.
- Hermes-A (2011). "<http://hermes-a.exa.ec/>".
- Hofe, R. (2005). Signal Analysis of the Electric and Acoustic Field Measurements by the Huygens Instrument HASI/PWA. Diploma Thesis, Graz University of Technology.
- Holden, D., C. Munson, et al. (1995). "Satellite Observations of Transionospheric Pulse Pairs." Geophys. Res. Lett. **22**(8): 889-892.
- Holle, R. H., R. E. López, et al. (1993). Overview of real-time lightning detection systems and their meteorological uses, US Dept. of Commerce, National Oceanic and Atmospheric Administration, Environmental Research Laboratories, National Severe Storms Laboratory.
- Hoots, F. R. and R. L. Roehrich (1988). "Spacetrack Report No. 3-Models for Propagation of NORAD Element Sets." Project Spacetrack Reports, Peterson.
- HRD (2011). "www.ham-radio-deluxe.com/".
- Huang, C. Y. and W. J. Burke (2004). "Transient sheets of field-aligned current observed by DMSP during the main phase of a magnetic superstorm." Journal of Geophysical Research-Space Physics **109**(A6): -.
- Inan, U. S., D. Piddiyachiy, et al. (2007). "DEMETER satellite observations of lightning-induced electron precipitation." Geophysical Research Letters **34**(7): -.
- Jacobson, A., S. Knox, et al. (1999). "FORTE observations of lightning radio-frequency signatures: Capabilities and basic results." Radio Sci. **34**(2): 337-354.
- Jacobson, A. R., S. O. Knox, et al. (1999). "FORTE observations of lightning radio-frequency signatures: Capabilities and basic results." Radio Sci. **34**(2): 337 - 354.
- Jacobson, A. R. and T. E. L. Light (2003). "Bimodal radio frequency pulse distribution of intracloud-lightning signals recorded by the FORTE satellite." Journal of Geophysical Research-Atmospheres **108**(D9): -.
- Jaffer, G. (2011a). Austrian Lightning Nanosatellite (LiNSAT): Space and Ground Segments. 3rd International Conference on Advances in Satellite and Space Communications (SPACOMM 2011). Budapest, Hungary, (*in Press*).
- Jaffer, G., A. Klesh, et al. (2010c). Using a virtual ground station as a tool for supporting higher education. 61st International Astronautical Congress (IAC). Prague, Czech Republic. **73**: 178-183.
- Jaffer, G. and O. Koudelka (2011b). Lightning detection onboard nano-satellite (LiNSAT). International Conference on Atmospheric Electricity (ICAE). Rio de Janeiro, Brazil, (*in Press*).
- Jaffer, G. and O. Koudelka (2011d). Automated remote ground station for Austrian lightning nanosatellite (LiNSAT). 8th IAA Symposium on Small Satellites for Earth Observation. Berlin, Germany, (*in Press*).

- Jaffer, G., O. Koudelka, et al. (2011c). A LEO nano-satellite mission for the detection of lightning VHF sferics. Adaptive Filtering. Vienna, Intech. **2**, (*in Press*).
- Jaffer, G., O. Koudelka, et al. (2010a). A Lightning Detector Onboard Austrian Nanosatellite (LiNSAT). American Geophysical Union, Fall Meeting.
- Jaffer, G., O. Koudelka, et al. (2008). The detection of sferics by a nano-satellite. 59th International Astronautical Congress (IAC). Glasgow, UK 8.
- Jaffer, G., R. Nader, et al. (2010d). Project Agora: Simultaneously downloading a satellite signal around the world. 61st International Astronautical Congress (IAC). Prague, Czech Republic. **74**: 145-148.
- Johnson Jr, H. L., R. D. Hart, et al. (1977). "Measurements of radio frequency noise from severe and nonsevere thunderstorms." Monthly Weather Review **105**(6): 734-747.
- Kikuchi, H., T. Morimoto, et al. (2010). "Wideband Radio Wave Observations of Lightning Discharge by Mado-1 Satellite." Ieice Transactions on Communications **E93b**(8): 2226-2227.
- Koshak, W. J. (2010). "Optical Characteristics of OTD Flashes and the Implications for Flash-Type Discrimination." Journal of Atmospheric and Oceanic Technology **27**(11): 1822-1838.
- Kotaki, M. and C. Katoh (1983). "The Global Distribution of Thunderstorm Activity Observed by the Ionosphere Sounding Satellite (Iss-B)." Journal of Atmospheric and Terrestrial Physics **45**(12): 833-&.
- Kotaki, M., I. Kuriki, et al. (1981). "Cosmic Radio Noise at High-Frequencies as Observed with Iss-B." Journal of the Radio Research Laboratory **28**(125-): 35-48.
- Kotaki, M., I. Kuriki, et al. (1981). "Global Distribution of Thunderstorm Activity Observed with Iss-B." Journal of the Radio Research Laboratory **28**(125-): 49-71.
- Koudelka, O., G. Egger, et al. (2009). "TUGSAT-1/BRITE-Austria-The first Austrian nanosatellite." Acta Astronautica **64**(11-12): 1144-1149.
- Krider, E., C. Weidman, et al. (1979). "The Temporal Structure of the HF and VHF Radiation Produced by Intracloud Lightning Discharges." J. Geophys. Res. **84**(C9): 5760-5762.
- Kummerow, C., W. Barnes, et al. (1998). "The tropical rainfall measuring mission (TRMM) sensor package." Journal of Atmospheric and Oceanic Technology **15**(3): 809-817.
- Lange, R. D. (2008). "Cassini-Huygens mission overview and recent science results." 2008 Ieee Aerospace Conference, Vols 1-9: 247-256.
- Le Vine, D. M. (1987). "Review of measurements of the RF spectrum of radiation from lightning." Meteorology and Atmospheric Physics **37**(3): 195-204.
- Lefeuvre, F., E. Blanc, et al. (2008). "TARANIS - A satellite project dedicated to the physics of TLEs and TGFs." Space Science Reviews **137**(1-4): 301-315.

- Lefeuvre, F., E. Blanc, et al. (2009). "TARANIS - a Satellite Project Dedicated to the Physics of TLEs and TGFs." Coupling of Thunderstorms and Lightning Discharges to near-Earth Space **1118**: 3-7.
- Lehtinen, N. G., P. W. Gorham, et al. (2004). "FORTE satellite constraints on ultrahigh energy cosmic particle fluxes." Physical Review D **69**(1): -.
- Light, T. E. L. and A. R. Jacobson (2002). "Characteristics of impulsive VHF lightning signals observed by the FORTE satellite." Journal of Geophysical Research-Atmospheres **107**(D24): -.
- MacGorman, D. R. and W. D. Rust (1998). The electrical nature of storms, Oxford University Press, USA.
- Mackerras, D., M. Darveniza, et al. (1998). "Global lightning: Total, cloud and ground flash estimates." Journal of Geophysical Research-Atmospheres **103**(D16): 19791-19809.
- Massey, R. and D. Holden (1995). "Phenomenology of transionospheric pulse pairs." Radio Sci. **30**(5): 1645-1659.
- Massey, R., D. Holden, et al. (1998). "Phenomenology of transionospheric pulse pairs: Further observations." Radio Sci. **33**(6): 1755-1761.
- Massey, R. S. and D. N. Holden (1995). "Phenomenology of Transionospheric Pulse Pairs." Radio Science **30**(5): 1645-1659.
- Massey, R. S., D. N. Holden, et al. (1998). "Phenomenology of transionospheric pulse pairs: Further observations." Radio Science **33**(6): 1755-1761.
- Mathworks (2011). <http://www.mathworks.com/>
- Matson, D. L., J. P. Lebreton, et al. (2005). "Cassini/Huygens mission to Saturn: Results and prospects." Highlights of Astronomy, Vol 13 **13**: 904-904.
- Matson, D. L., J. P. Lebreton, et al. (2004). "The Cassini-Huygens mission to the Saturnian system." Proceedings of the International Conference Titan: From Discovery to Encounter: I-Xvi, 412.
- Matuura, N., M. Kotaki, et al. (1981). "Iss-B Experimental Results on Global Distributions of Ionospheric Parameters and Thunderstorm Activity." Acta Astronautica **8**(5-6): 527-548.
- McNutt, S. R. and E. R. Williams (2010). "Volcanic lightning: global observations and constraints on source mechanisms." Bulletin of Volcanology **72**(10): 1153-1167.
- MGSN (2011). <http://mgsn.sourceforge.net/index.php>
- Minotaur (2011). <http://minotaur.exa.ec/>.
- MixW (2011). <http://mixw.net/>.
- Miyazaki, S., E. Sagawa, et al. (1980). "Observational Results of the Nighttime Ion Temperatures in the Topside Ionosphere by Iss-B." Journal of the Radio Research Laboratory **27**(124): 187-194.
- Molina-Cuberos, G. J., J. J. Lopez-Moreno, et al. (2001). "Capability of the Cassini/Huygens PWA-HASI to measure electrical conductivity in Titan." Io, Europa, Titan and Cratering of Icy Surfaces **28**(10): 1511-1516.

- Molina-Cuberos, G. J., J. Porti, et al. (2004). "Shumann resonances and electromagnetic transparency in the atmosphere of Titan." Mercury, Mars and Saturn **33**(12): 2309-2313.
- Morimoto, T., H. Kikuchi, et al. (2009). Broadband VHF observations for lightning impulses from a small satellite SOHLA-1 (Maido 1).
- Nader, R., H. Carrion, et al. (2010a). HERMES Delta: The use of the DELTA operation mode of the HERMESA/ MINOTAUR Internet-to-Orbit gateway to turn a laptop in to a virtual EO ground station. 61st International Astronautical Congress (IAC). Prague, Czech Republic
- Nag, A. and V. A. Rakov (2010). "Compact intracloud lightning discharges: 1. Mechanism of electromagnetic radiation and modeling." Journal of Geophysical Research-Atmospheres **115**: -.
- Nag, A. and V. A. Rakov (2010). "Compact intracloud lightning discharges: 2. Estimation of electrical parameters." Journal of Geophysical Research-Atmospheres **115**: -.
- Nanevicz, J. E., E. F. Vance, et al. (1987). "Observation of lightning in the frequency and time domains." Electromagnetics **7**(3): 267-286.
- NASA (2011a). <http://thunder.msfc.nasa.gov/data/query/mission.png>.
- Oetzel, G. and E. Pierce (1969). "VHF Technique for Locating Lightning." Radio Sci. **4**(3): 199-202.
- Parrot, M., J. J. Berthelier, et al. (2008). "DEMETER observations of EM emissions related to thunderstorms." Space Science Reviews **137**(1-4): 511-519.
- Parrot, M., U. Inan, et al. (2008). "HF signatures of powerful lightning recorded on DEMETER." J. Geophys. Res. **113**(A11): 1-7.
- Parrot, M., U. S. Inan, et al. (2009). "Penetration of lightning MF signals to the upper ionosphere over VLF ground-based transmitters." J. Geophys. Res. **114**(A12): 1-12.
- Petersen, W. A., S. W. Nesbitt, et al. (2002). "TRMM observations of intraseasonal variability in convective regimes over the Amazon." Journal of Climate **15**(11): 1278-1294.
- Platino, M., U. S. Inan, et al. (2006). "DEMETER observations of ELF waves injected with the HAARP HF transmitter." Geophysical Research Letters **33**(16): 16101.
- Popov, A. S. (1896). "Instrument for detection and registration of electrical fluctuations." Journal or Russian Physics and Chemistry Society **28**: 1-14.
- Quakesat (2011). <http://www.quakefinder.com/joomla15/index.php>.
- Rakov, V. A. and A. Uman (2003). Lightning, Physics and Effects, Cambridge University Press, Cambridge, U. K
- Ramirez, S. I. (2006). "Electric activity on Titan before and after Cassini-Huygens arrival." Origins of Life and Evolution of the Biosphere **36**(3): 333-334.

- Rawashdeh, S. A. and J. E. Lumpj Jr (2010). "Nano-Satellite Passive Attitude Stabilization Systems Design by Orbital Environment Modeling and Simulation."
- RAX-UoM (2011). <http://rax.engin.umich.edu/>.
- Richard, P. and G. Auffray (1985). "Vhf-Uhf Interferometric Measurements, Applications to Lightning Discharge Mapping." Radio Science **20**(2): 171-192.
- Rittner, D. (2003). A to Z of Scientists in Weather and Climate, Facts on File.
- Roussel-Dupre, R. A., A. R. Jacobson, et al. (2001). "Analysis of FORTE data to extract ionospheric parameters." Radio Science **36**(6): 1615-1630.
- Russell, C. T., R. S. Zuelsdorf, et al. (1998). "Identification of the cloud pulse responsible for a trans-ionospheric pulse pair." Geophysical Research Letters **25**(14): 2645-2648.
- Sandau, R. (2006). International study on cost-effective earth observation missions, Taylor & Francis.
- SatPC32 (2011). <http://www.dk1tb.de/indexeng.htm>
- Schulz, W., K. Cummins, et al. (2005). "Cloud-to-ground lightning in Austria: A 10-year study using data from a lightning location system." J. Geophys. Res. **110**(D9): 1-20.
- Schulz, W. and G. Diendorfer (1999). Lightning Characteristics as a function of altitude evaluated from lightning location network data, SOC AUTOMATIVE ENGINEERS INC.
- Schulz, W. and G. Diendorfer (2004). Lightning peak currents measured on tall towers and measured with lightning location systems.
- Schwingschuh, K. (2006). In-situ observations of electric Field fluctuations and impulsive events during the Descent of the HUYGENS Probe in the atmosphere of Titan.
- Schwingschuh, K., B. P. Besser, et al. (2007). HUYGENS in-situ observations of Titan's atmospheric electricity. European Geosciences Union (EGU) General Assembly. Vienna, Austria.
- Schwingschuh, K., G. J. Molina-Cuberos, et al. (2001). "Propagation of electromagnetic waves in the lower ionosphere of Titan." Adv. Space Res. **28**(10): 1505-1510.
- Schwingschuh, K., R. Hofe, et al. (2006). In-situ observations of electric field fluctuations and impulsive events during the descent of the HUYGENS probe in the atmosphere of Titan. European Planetary Science Congress. Berlin, Germany. **37**: 2793.
- Schwingschuh, K., H. Lichtenegger, et al. (2008b). Electric discharges in the lower atmosphere of Titan: HUYGENS acoustic and electric observations. 37th COSPAR Scientific Assembly. Montral, Canada. **37**: 2793.
- Schwingschuh, K., T. Tokano, et al. (2010). Electric field transients observed by the HUYGENS probe in the atmosphere of Titan: Atmospheric electricity

- phenomena or artefacts? 7th International Workshop on Planetary, Solar and Heliospheric Radio Emissions (PRE VII) Graz, Austria
- Shao, X.-M. and A. R. Jacobson (2002). "Polarization observations of lightning-produced VHF emissions by the FORTE satellite." J. Geophys. Res. **107**(D20): ACL 7-1-ACL 7-16.
- Shao, X., D. Holden, et al. (1996). "Broad band radio interferometry for lightning observations." Geophysical Research Letters **23**(15): 1917-1920.
- Shao, X., P. Krehbiel, et al. (1995). "Radio interferometric observations of cloud-to-ground lightning phenomena in Florida." Journal of Geophysical Research **100**(D2): 2749-2783.
- Shao, X. M. (1993). The development and structure of lightning discharges observed by VHF radio interferometer, New Mexico Institute of Mining and Technology.
- Shriver, P. M., M. B. Gokhale, et al. (2002). A power-aware, satellite-based parallel signal processing scheme, Power aware computing, Kluwer Academic Publishers, Norwell, MA.
- Smith, D. A. (1998). Compact intracloud discharges, University of Colorado.
- Suszcynsky, D., M. Kirkland, et al. (2000). "FORTE observations of simultaneous VHF and optical emissions from lightning: Basic phenomenology." J. Geophys. Res. **105**(D2): 2191-2201.
- Suszcynsky, D. M., M. W. Kirkland, et al. (2000). "FORTE observations of simultaneous VHF and optical emissions from lightning: Basic phenomenology." Journal of Geophysical Research-Atmospheres **105**(D2): 2191-2201.
- Suszcynsky, D. M., T. E. Light, et al. (2001). "Coordinated observations of optical lightning from space using the FORTE photodiode detector and CCD imager." Journal of Geophysical Research-Atmospheres **106**(D16): 17897-17906.
- SwissCube (2011). <http://swisscube.epfl.ch>.
- Takayabu, Y. N. (2006). "Rain-yield per flash calculated from TRMM PR and LIS data and its relationship to the contribution of tall convective rain." Geophysical Research Letters **33**(18): -.
- Taylor-Univ (2011). http://www.css.taylor.edu/~physics/picosat/technical_specs/mechanical/sum_from_pap.htm.
- Taylor-University (2011). GGB Design Document.
- Taylor, W. L. (1973). "Electromagnetic radiation from severe storms in Oklahoma during April 29-30, 1970." Journal of Geophysical Research **78**(36): 8761-8777.
- Thomson, E. M. (1980). "The Dependence of Lightning Return Stroke Characteristics on Latitude." Journal of Geophysical Research-Oceans and Atmospheres **85**(Nc2): 1050-1056.

- Tierney, H. E., A. R. Jacobson, et al. (2001). "Determination of source thunderstorms for VHF emissions observed by the FORTE satellite." Radio Science **36**(1): 79-96.
- Tierney, H. E., A. R. Jacobson, et al. (2002). "Transionospheric pulse pairs originating in maritime, continental, and coastal thunderstorms: Pulse energy ratios." Radio Sci. **37**(3).
- TUGSat-1 (2011). <http://www.tugsat.tugraz.at/tugsat-1>.
- Turman, B. N. (1978). "Analysis of Lightning Data from Dmsp Satellite." Journal of Geophysical Research-Oceans and Atmospheres **83**(Nc10): 5019-5024.
- Uman, M. A. (2001). The Lightning Discharge. Toronto, General Publishing Co.
- Unterberger, M. (2007). Simulation of Data Throughput of a LEO Satellite System. M.Sc. Academic, Graz University of Technology.
- Unterberger, M. (2008). Communication Systems Design: Critical Design Document.
- Ushio, T., S. J. Heckman, et al. (2001). "A survey of thunderstorm flash rates compared to cloud top height using TRMM satellite data." Journal of Geophysical Research-Atmospheres **106**(D20): 24089-24095.
- Ushio, T., Z. I. Kawasaki, et al. (1997). "Broad band interferometric measurement of rocket triggered lightning in Japan." Geophysical Research Letters **24**(22): 2769-2772.
- Volland, H. (1995). Handbook of atmospheric electrodynamics, CRC.
- Vorpahl, J. A., J. G. Sparrow, et al. (1970). "Satellite Observations of Lightning." Science **169**(3948): 860-&.
- VRS-RM (2011). <http://www.nch.com.au/vrs/remote.html>.
- Weber, M. E., L. Laboratory, et al. (1998). An assessment of the operational utility of a GOES lightning mapping sensor, Massachusetts Institute of Technology, Lincoln Laboratory.
- Wertz, J. R. (1978). Spacecraft attitude determination and control, Kluwer Academic Pub.
- Wertz, J. R. and W. J. Larson (1996). Reducing space mission cost, Microcosm Press Torrance, CA.
- Wertz, J. R. and W. J. Larson (1999). "Space mission analysis and design."
- Williams, E. R. (2005). "Lightning and climate: A review." Atmospheric Research **76**(1-4): 272-287.
- Williams, E. R. (2009). "The global electrical circuit: A review." Atmospheric Research **91**(2-4): 140-152.
- Williams, E. R., M. E. Weber, et al. (1989). "The Relationship between Lightning Type and Convective State of Thunderclouds." Journal of Geophysical Research-Atmospheres **94**(D11): 13213-13220.
- WxtoImg (2011). <http://www.wxtoimg.com/>.

- Yokoyama, C. and Y. N. Takayabu (2008). "A Statistical Study on Rain Characteristics of Tropical Cyclones Using TRMM Satellite Data." Monthly Weather Review **136**(10): 3848-3862.
- Zlotnicki, J., F. Li, et al. (2010). "Signals recorded by DEMETER satellite over active volcanoes during the period 2004 August-2007 December." Geophysical Journal International **183**(3): 1332-1347.